Chapter 8

General pathology in the Circle: biocultural insights into population health, trauma and care in Neolithic Malta

Ronika K. Power, Bernardette Mercieca-Spiteri, Jess E. Thompson, Rowan McLaughlin, Jacinta Carruthers, Hannah Vogel, Laura T. Buck, Jaap Saers, Margery Pardey, Jay T. Stock & John S. Magnussen

8.1. Introduction

As with other components of this volume, this chapter builds on the original observations established in Malone *et al.* (2009d), with particular reference to the co-authored paper by Stoddart, Barber, Duhig, Mann, O'Connell, Lai, Redhouse and Malone on the osteological inventory, introductory analyses, and isotopic pilot study of the human and animal remains of the Circle. The primary report (Stoddart *et al.* 2009a) provided invaluable initial insights into local Maltese and regional Mediterranean prehistoric population profiles and mortuary behaviour via their presentation of osseous representation by element (including fragments and exfoliated teeth); preliminary observations of general pathologies and 'dental attrition' (Stoddart *et al.* 2009a, 315, 318); and (re)distribution patterns of elements across the site.

The 2009 volume records the people and processes responsible for extracting data from one of the most analytically challenging assemblages of human bones within the region for the Neolithic period. The challenge of the assemblage lies not only in its scale – an estimated minimum of 220,000 human elements – but also in its disarticulated, highly fragmented and commingled nature (Fig. 8.1). The seemingly unfathomable nature of this challenge is brought to bear when considering that almost 41,000 fragments (~19.0%) were in such a deteriorated state that they could not be identified to a skeletal element (Stoddart *et al.* 2009a, 317). Nevertheless, from 1988–1995, under the direction of Caroline Malone and Simon Stoddart, a devoted and resilient team comprised of Caroline Barker, Gary Burgess, Andrew Clarke, Corinne Duhig, George Mann and Cristina Sampedro undertook the painstaking process of attempting to identify each fragment to element, part of element and side. Further pathology observations were undertaken by George Mann, an Ear, Nose and Throat physician with further qualifications in biological anthropology, to whom this volume is dedicated. These activities resulted in a baseline profile of the Circle burial population, including key demographic indicators of age and sex (p.320–1), and other population descriptors such as stature (p.325). This data collection, in conjunction with relative and absolute dating activities, facilitated a broad overview of the individuals represented within the Circle and their experiences of health, disease, trauma, nutrition, congenital and behavioural variation and social inclusion. As a result, we have far greater understanding of the role of the space as an interment site for more than 1000 individuals of all biological sexes and ages across the life course, in which engagement continued between communities of the living and dead.

The greater focus of the initial report from Stoddart *et al.* (2009a) was to relay the demography, general taphonomic character and organization, and incidental osteological observations for each major context and chronological phase within the Circle. The original analysts commented on the general 'good health' of the population, noting the relative absence of osteological markers for chronic disease (Stoddart *et al.* 2009a, 318). When viewed through the perspective of the 'Osteological Paradox' (Wood *et al.* 1992; cf McFadden & Oxenham 2020), it is clear that the implied inference was that the causes of death for the majority of the initial Circle tudy sample appear to be of an acute nature, perhaps including those respiratory or gastrointestinal illnesses that modern medicine has since brought into submission for the Western world (Stoddart *et al.* 2009a, 321; cf Roberts & Manchester 2005). With the exception of occasional observations of localized periostitis, sinusitis, osteomyelitis and chronic

Figure 8.1. *A typical bag of disarticulated, fragmented and commingled human remains from the Xagħra Brochtorff Circle Cambridge Gozo Project excavations, under analysis as part of the ERC-funded FRAGSUS Project in the National Museum of Archaeology, Valletta, Malta. (Photo Ronika. K. Power).*

ear infections, mastoiditis and meningitis (p.325, 329), pathognomonic evidence for chronic infectious disease processes such as tuberculosis are absent from the initial Circle study sample, in contrast to contemporaneous populations elsewhere (for example, Canci *et al.* 1996; Formicola *et al.* 1987).

Stoddart *et al.* (2009a) attribute the most numerous pathological osseous changes to degenerative joint disease, mostly in the spine, hands and feet (overall attribution: 38% of pathology; Stoddart *et al.* 2009a, 318, 322, 323, 324, 325), and very occasionally elsewhere in the body, such as the shoulder (Stoddart *et al.* 2009a, 319), clavicle (Stoddart *et al.* 2009a, 323), temporomandibular joint (Stoddart *et al.* 2009a, 323, 328), tibia, fibula and patella (Stoddart *et al.* 2009a, 324). Higher incidences of degenerative joint disease are particularly noted in Context (1268) (Stoddart *et al.* 2009a, 328). Healed fractures are mentioned (but not described) on two ribs (Context 1241/6; Stoddart *et al.* 2009a, 324), a humerus (Context (1268); Stoddart *et al.* 2009a, 325), and an overall total of 40 observations are reported for the Tarxien deposits, including insults to the manual and pedal elements, teeth, clavicle, arm, leg, knee and nose (Stoddart *et al.* 2009a, 329). Neoplastic disease is also mentioned, as are congenital variations such as sutural ossicles (Stoddart *et al.* 2009a, 325), and developmental disturbances such as spina bifida (especially in Context (783); Stoddart *et al.* 2009a, 328). The authors make particular note of the relatively low occurrence of indicators of nutritional, environmental or psychological stress, such as *cribra orbitalia*, porotic hyperostosis or enamel hypoplasia (Stoddart *et al.* 2009a, 318, 322, 325, 329). Furthermore, other forms of dental pathology, including carious lesions and dental calculus (Stoddart *et al.* 2009a, 318, 322, 323, 324; overall attribution: 23% of pathology, Stoddart *et al.* 2009a, 325), presented low overall incidence rates.

Within the parameters of the *FRAGSUS Project*, significant advancements have been made to further characterize the experience of dental pathology amongst a sample of the Circle burial population. These findings are reported in Chapter 4 of this volume. The current chapter makes similar advancements in the description of other osseous pathologies, presenting an updated and detailed account of severe conditions and traumas experienced by individuals within the study sample.

8.2. Materials

All available human skeletal material pertaining to the 1987–1994 Circle excavations curated by Heritage Malta within the National Museum of Archaeology was subject to examination for this component of the study. As mentioned above, this amounts to approximately 220,000 human bone fragments which, although varying in size and preservation, are mostly in advanced stages of fragmentation. Analysis of >19,000 fragments from 16 contexts across the rock-cut tomb and cave complex, accounting for approximately 8.6% of the total assemblage, found that mean fragment size was between 21–50 mm in each context and most elements were between 25–49% complete (Chapter 12; cf Thompson 2020). Such high fragmentation is attributed to the process of successive deposition of

human remains, resulting in deep deposits which were frequently disturbed. However, bone preservation was qualitatively fair-to-good across many contexts, as conditions within the limestone cave environment were largely favourable. Bone surface preservation varied more strongly between contexts because of a complex interplay of factors including depositional methods, flow of water, duration of use, soil ecology and extent of post-depositional disturbance.

8.3. Methods

The 2009 report established a framework of close investigation of 'significant intact individuals' (Stoddart *et al.* 2009a, 321ff.) to shape inferences regarding the Circle burial population. In an assemblage such as this, our colleagues were right to draw upon the osteobiographies of individuals who, for various reasons, were subject to less *postmortem* disturbance than the majority of those interred in the Circle. From these profiles, we were able to gain great insight into the lived experiences of the Neolithic inhabitants of Gozo. Notwithstanding these achievements, it was not the mandate of the 2009 volume to present any of the reported pathologies in the form of complete scientific description including differential diagnoses. The current study seeks to bring further clarity to the known spectrum of health and disease for the Circle population by continuing the original focus on case studies of so-called 'extreme pathology', and to present them according to scientific recording and reporting convention (§8.5, below). We also present a methodological case study of how careful observation, description and contextual recording of pathological lesions can serve to reunite fragmentary individuals posthumously in commingled skeletal assemblages (§8.6, below).

As detailed in Chapter 2, the team undertaking the osteological analyses faced similar sampling strategy decisions as other archaeometric colleagues in order to produce novel work within the temporal and pecuniary parameters of the *FRAGSUS Project.* Mercieca-Spiteri has detailed this strategy for the Population History Workgroup both here and elsewhere (Mercieca-Spiteri 2016). In order to achieve meaningful population insights into this complex assemblage in our limited time, and to support parallel investigations into scientific dating, palaeodiet and geographical affinity, our activities focused on analyses of 'extreme' skeletal pathology determined by the investigators to be of greatest cultural and temporal significance.

The team developed a highly ambitious programme that aimed to examine the whole available collection (*c.* 220,000 fragmentary elements) in a series of five intensive seasons in the stores of the National Museum of Archaeology (henceforth, NMA), Valletta, with a two-stage mandate to 1) isolate; and 2) examine the remains requiring further study. These remains included all exfoliated dentition and all maxillae and mandibular elements, and all other elements of special interest, including those presenting 'extreme' pathology, such as healed or unhealed fractures, osteoarthritis to an expression of eburnation, activity- and/or entheseal changes to an expression of dysplasia, and periostitis. The logic here is that extreme presentations of pathology thereby also infer that lesser expressions were present amongst the assemblage. This was pertinent for various reasons, particularly that the expression of spinal degenerative joint disease was so prevalent in the assemblage that dedicated study of this pathology alone would have consumed the entire workgroup's resources for the duration of the project. Although unconventional, our approach was deemed to be the most efficient and effective way of characterizing the lived experiences of this population in light of the significant challenges posed by the disarticulated, highly fragmented and commingled nature of the assemblage.

Considering the size of the assemblage, the logistical scale of the *FRAGSUS* sorting, storage and analytical enterprise was immense. The managerial and archival processes required to ensure that every isolated tooth and bone fragment was traceable not only to its archaeological context but also to its curatorial context within the NMA are described in more detail in Chapter 2.

It is important to note that observations of pathology were significantly inhibited in some contexts because of adhering burial matrix (including dirt, mud and ochre); concretion and mineralization of the burial matrix; and severe taphonomic/diagenetic change (cf Stoddart *et al.* 2009a, 318). Once items of special interest were isolated, they were placed in laboratory-quality self-seal bags and clearly labelled with all available archaeological data transcribed from their original label, which continued to be curated with the remaining skeletal material from the find context. All archaeological and curatorial data of the isolated remains were entered into a Microsoft Excel spreadsheet to form a searchable digital database/inventory. All elements of special interest were photographed with a scale, and all photographs were curated using the Google Photos platform. Once a digital archive was created for every isolated element, the element was placed in a designated depository according to its category of study within the *FRAGSUS Project*, either dentition or pathology. Additionally, the depositories were also organized according to context reference to make them searchable and easily accessible for the research team.

The methodology and results of the dental pathology, modification and anthropology studies are presented in Chapters 4, 5 and 6 of this volume, respectively. Gross morphological analyses undertaken for this chapter took place in the NMA over the final two seasons of work in December 2016–February 2017, and April–June 2017, alongside all dental and taphonomic research, and the execution of the Population History Workgroup destructive sampling strategy for isotopic, chronometric and genetic research. For the present study, a sub-sample of elements were selected according to their novelty or significance within the assemblage, or their capacity to serve as case studies for particular biological or cultural phenomena. Pathological descriptions for each element (or fragment) were the collaborative effort of Power, Mercieca-Spiteri and Thompson. Our approach included the recording of inventory numbers; element identification; anatomical side; element preservation assessment; anatomical location of insult; lesion measurement/s; lesion preservation; lesion type; healing status; and description. Our general osteological analytical techniques are based on standard criteria described in Buikstra and Ubelaker (1994: specific references indicated alongside analyses, below). All surfaces were examined macroscopically and under magnification using a 10x hand lens. Within the study sample, selected items were identified as worthy of further examination via radiographic analyses. Eligibility included those of sufficient scientific interest that were also suitable for transport from Malta from a preservation perspective, and of a compatible size with the radiographic equipment.[1]

The results of these analyses are presented below. As with all endeavours pertaining to this site, it must be noted that the work presented here is a further strategic sub-sample of the overall assemblage achieved during the parameters of the *FRAGSUS Project*, rather than comprehensive documentation of the Neolithic population who employed the Circle for funeral and interment rites and practices from 2900–2350 BC. 'Comprehensive' knowledge of the complete preserved archaeological nature and scope of the Circle assemblage will require not only exhaustive excavation of the site, but also the synthesis of several scholars' lifetime of works, including those of the current authors.

8.4. Results: overview

The *FRAGSUS* Population History Workgroup identified 2,819 fragments of human remains of special interest from the Circle study sample (Fig. 8.2). This is slightly lower than the 2,891 reported pathological observations in Stoddart *et al.* (2009a, 325), however it must be noted that the 2009 data included dental pathology whereas the results presented here do not. In the earlier reports, dental disease and 'habitual activities' predominated within the sample, accounting for 1,218 observations or 42.1% (Stoddart *et al.* 2009a, 325), leaving 1,673 observations restricted to skeletal pathology. As mentioned above, the *FRAGSUS*

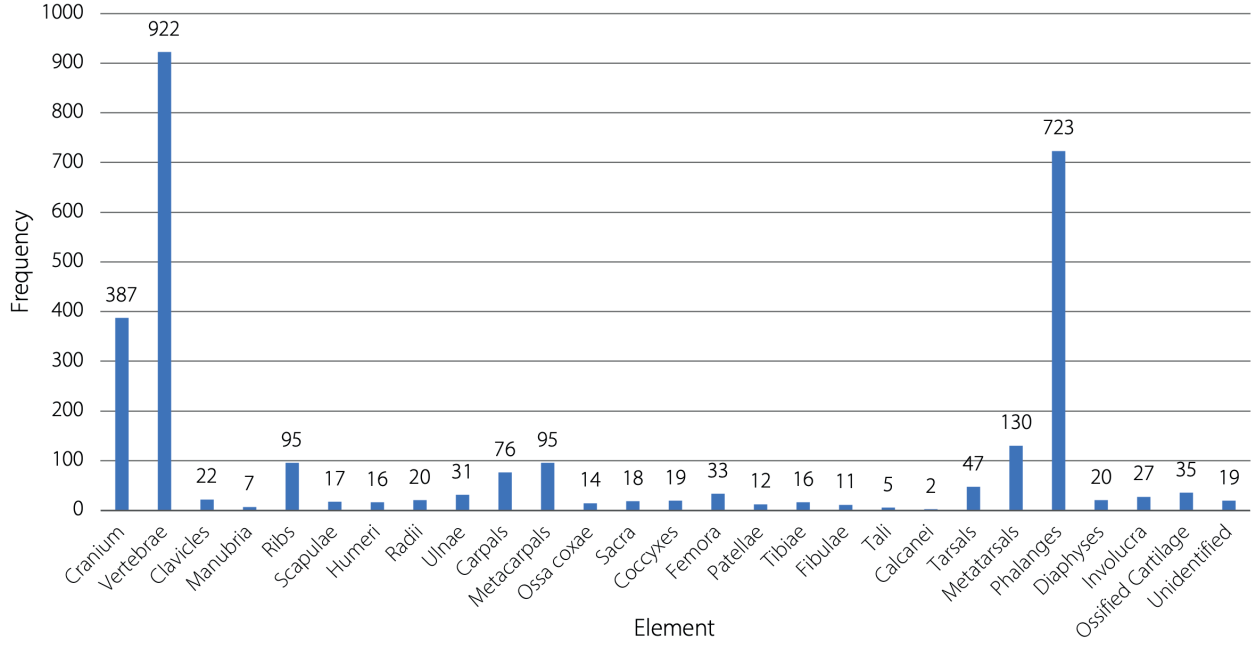

Figure 8.2. *Frequency distribution of human remains of special interest from the Circle (Σ=2819).*

observations of dental pathology and modification are recorded and reported separately (Chapters 4 & 5).

The current identification of 2,819 elements/fragments of special interest therefore represents a raw increase of 1,146 observations across the study sample, or 168.5% increase expressed proportionately. It is important to note that even though the current analyses were subject to tight temporal and pecuniary parameters, they took place under relatively controlled laboratory circumstances, which were far more conducive to systematic observations as opposed to the field conditions experienced by Stoddart *et al.* (2009a). Notwithstanding these logistical differences, the consonance between the respective findings is reassuring.

8.4.1. Spinal pathologies

As seen in Figure 8.2, the spinal column presented the most substantial observations of pathology, with 922 vertebral fragments isolated, accounting for 32.7% of all pathological observations. The majority of these observations were associated with osteoarthritis, including the remodelling and dysplasia of superior and inferior articular processes and facets of vertebrae of all regions (cervical, thoracic and lumbar), with a tendency towards unilateral presentation (i.e. one-sided, suggestive of bodily lateralization). Observations of spondylosis; osteophytosis; fractures; vertebral depression (a.k.a. 'codfish' vertebrae); scoliosis and Schmorl's nodes also featured amongst the assemblage (Fig. 8.3a-i). The majority of the preceding observations are indicative of quotidian, extraordinary, chronic stress and physiological loading of the spine, leading to degenerative change (Rogers 2000, 166), and can be exacerbated by other factors including age, malnutrition and genetic predisposition. The lived experiences of these stressors are described and considered in more detail via a small selection of case studies presented in §8.5.3, below. Further discussions of activity-related changes observed within the assemblage are presented by Parkinson and Stock in Chapter 7.

8.4.2. Extreme extremities

Another prevailing trend within the assemblage was the observation of severe osteoarthritis, enthesopathies, osteophytosis, dysplasia, fractures and *myositis ossificans traumatica* in the bones of the hands and feet. Figure 8.2 demonstrates that the manual and pedal phalanges (Σ=723; 25.6%), carpals (Σ=76; 2.7%), metacarpals (Σ=95; 3.4%); tarsals (Σ=47; 1.7%) and metatarsals (v=130; 4.6%) collectively account for 1,071 (or 38.0%) fragments of special interest within the sample. As with spinal pathologies, the observed manual and pedal pathologies indicate extreme, chronic stress and physiological loading of the extremities; however, these elements also present substantial evidence for single-event insults, such as trauma. A selection of images pertaining to manual and pedal pathology are presented in Figure 8.4a-m.

8.4.3. Notable absences

As always in bioarchaeology, what we *don't* see is as compelling and revealing as what we *do* see. In this case, the almost complete absence of extreme degenerative joint disease and so-called occupationally related change in the major weight- and stress-bearing joints of the shoulder, elbow, hip and knee is astonishing. This is not an artefact of fragmentation, as every observable joint surface was closely examined. Notwithstanding this fact, it is acknowledged that diaphyseal preservation is generally better than that of epiphyses and metaphyses, owing to their more robust structure. In tandem with the pathologies described above, this observation provides critical information regarding the type, frequency and severity of habitual physical behaviour/s carried out by those individuals represented within this assemblage. This is investigated further with biomechanical analyses carried out by Parkinson and Stock in Chapter 7.

Also of note is the relative absence of skeletal indicators of chronic or systemic nutritional, environmental, psychological or pathological stress, including porotic hyperostosis and *cribra orbitalia* (Goodman 1984; Goodman & Armelagos 1989; Goodman *et al.* 1988; Larsen 2015; McFadden & Oxenham 2020). Again, this is not an artefact of fragmentation or taphonomy, as every extant cortical surface was closely examined. Although there were some observations of enamel hypoplasia, these were generally not as severe, nor as frequent as might be expected for an ostensibly geographically isolated and environmentally constrained population of this period (Chapter 4). These observations suggest that, generally speaking, the majority of individuals appear to have had adequate access to subsistence strategies that addressed both their qualitative and quantitative dietary requirements and were only under acute stress for a restricted amount of time. Further commentary on Neolithic Maltese palaeodietary reconstructions is undertaken by McLaughlin *et al.* in Chapter 10; and individual case studies of potential nutritional deficiencies amongst the sample are presented in §8.5–8.6 and §8.7.6, below.

Observations regarding systemic stress also provide a human biocultural framework in which to situate environmental findings reported by colleagues in other *FRAGSUS* Workgroups. For example, Fenech *et al.* (Volume 1, Chapter 4) have identified specimens of *Bulinus* freshwater snails in core samples, including Xemxija 1, Marsa Core 2 and in the Salina Deep Core. This species is indicative of a variety of perennial

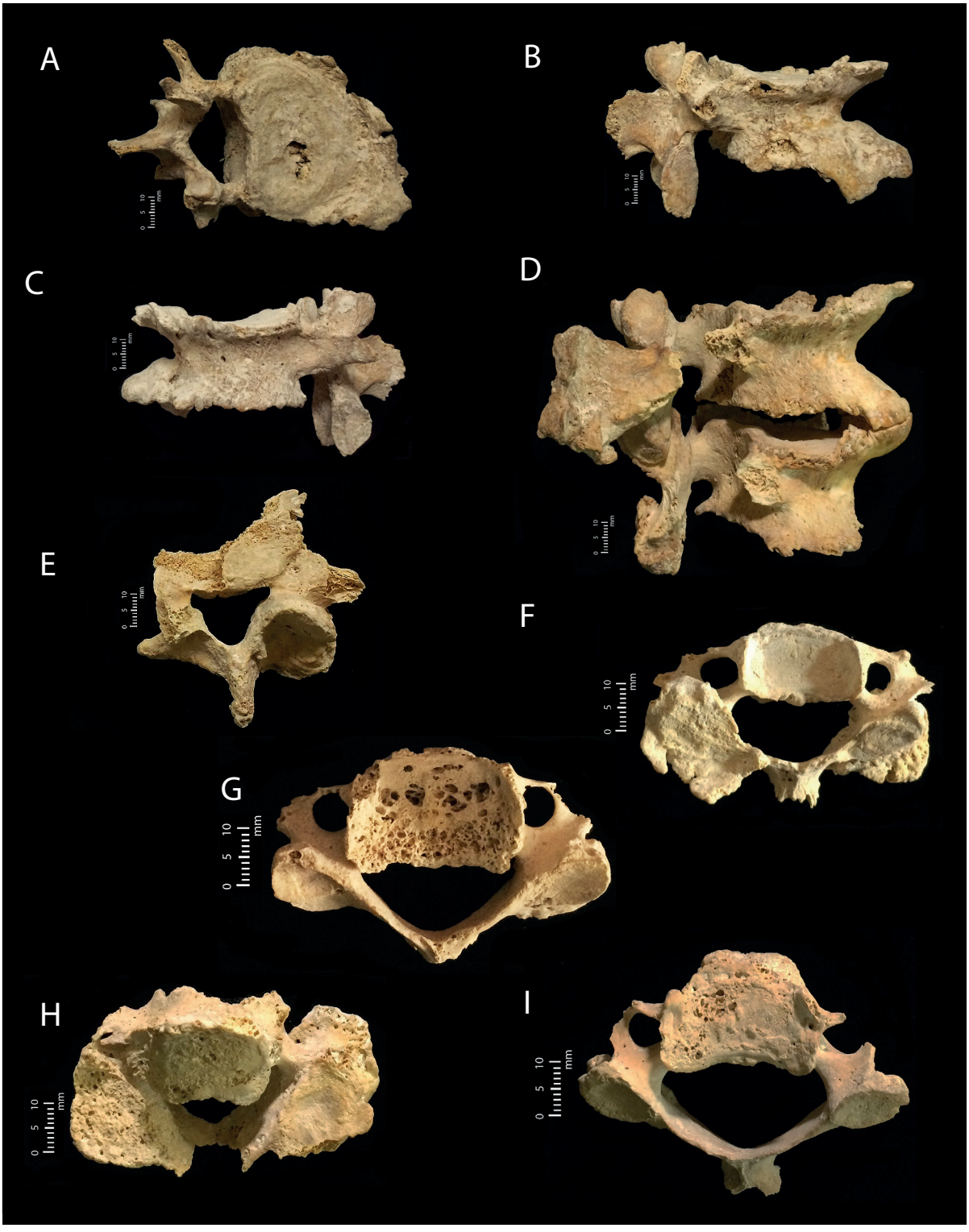

Figure 8.3. *A representative selection of vertebrae presenting extreme pathology including osteophytosis and degenerative joint disease from various contexts of the Circle sample: a–c) Context (1268) 99E/111N Spit 2, Unit 4; d) Context (1268) 99E/111N Spit 2, Unit 12; e) Context (1206) 100E/110N, Spit 4, Unit 2; f) Context (960) 98E/109N Spit 3; g) Context (1024) 98E/113N Spit 1; h) Context (783) 96E/110N; i) Context (783) 96E/110N Spit 1, No. 84. Scale bar: 1 cm. (Photos Ronika K. Power).*

Figure 8.4. *A representative selection of metacarpals, metatarsals and manual and pedal phalanges presenting extreme pathology including healed and* perimortem *fractures, myositis ossificans traumatica and degenerative joint disease from across various contexts of the Circle sample: a) Context (595) 100E/104N No. 320; b) Context (697); c) Context (1268) 101E/109N Spit 2; d) Context (1268) 100E/109N Spit 2, Unit 9; e) Context (1268) 99E/110N Spit 2, Unit 5; f) Context (1206) 100E/110N Spit 1, No. 1; g) Context (783) 96E/113N; h) Context (783) 95E/113N; i) Context (783) 94E/112N; j) Context (783) 95E/112N; k) Context (783) 94E/113N; l) Context (783) 96E/111N Spit 1; m) Context (783) 96E/110N Spit 1, No. 38. Scale bar: 1 cm. (Photos Ronika K. Power).*

flowing and standing water bodies, where it lives on the banks among vegetation and on stony beaches (Giusti *et al.* 1995; IUCN 2017). It was found in deposits pre-dating the end of the Temple Period in Xemxija 1 and in the upper half of the Salina Deep Core. In Marsa Core 2 it was last found in deposits dated to the Late Bronze Age/Early Phoenician Period. This species is extinct from the Maltese Islands today, which is of interest from a public health perspective, as it is an intermediate host for the schistosomiasis (bilharzia) parasite. This debilitating disease has been traced back to the Neolithic period in Chad and in Egypt, where it is likened to the '*Aaa*' disease (King & Bertsch 2015; cf Anastasiou *et al.* 2014; Kloos & David 2002). It is therefore possible that within the Maltese Islands *Bulinus truncatus* also acted as an intermediate host for

the parasites causing the disease (trematode worms of the genus *Schistosoma*), which could have negatively affected the local human and animal populations.

Humans and animals contract schistosomiasis when wading in warm freshwater, for such activities as bathing, swimming, crop irrigation, fishing, fowling or foraging, and coming into contact with the intermediate forms of the bilharzia parasite, cercariae, when they leave the *Bulinus* snail in free-swimming form (Nunn 1996, 68). The cercariae burrow into human or animal skin, from where they continue their life cycle and grow into adult worms, variably taking up residence in either the blood vessels of the bladder and kidneys (*S. haematobium*) or intestines (*S. intercalatum*) depending upon their species. Once established, they mate, reproduce, and their eggs are excreted in either the urine or the faeces, again depending on genus (Anastasiou *et al.* 2014). Although people across the ancient world may not have explicitly understood the cause of schistosomiasis, they would have been able to identify its symptoms. In the case of *S. haematobium*, bilharzia infestation leads to haematuria (blood in the urine), and ancient Assyrian medical texts dating to ~4000 BC describe diseases causing such symptoms (Adamson 1976); while more recently (and famously) Napoleon's troops reported that Egypt was the 'land of menstruating men' (Nunn 1996, 69). Considering both the life–cycle of the parasite and the pathogenesis of infestation, positive identification of schistosomes in bioarchaeological studies is either restricted to observations of the effects of the worms and/or their calcified eggs in preserved soft tissue via radiological analyses, such as in mummified Egyptian human remains (Sandison & Tapp 1998, 39–40); the worms themselves are dissolved by autolysis within twenty-four hours of the death of the host (Ghalioungui 1987). Alternatively, the eggs may be preserved in sediment excavated from the thoracic cavities of skeletonized human remains and later identified under light microscopy (Anastasiou *et al.* 2014); or the preserved human tissue samples may be subjected to schistosome circulating anodic antigen (Deedler *et al.* 1990; Miller *et al.* 1993; Nunn 1996).

Untreated, schistosomiasis brings a significant morbidity burden to affected populations, with sequelae including anaemia, lassitude, loss of appetite, kidney failure, bladder cancer, immunocompromise and, in up to 60% of cases, death (Anastasiou *et al.* 2014; Hicks 1983; Fenech *et al.* 2020; Nunn 1996, 69). Chronic infestations can lead to liver dysfunction, which in itself can produce gynaecomastia (breast glandular tissue development in males; Nunn 1996). In other cultural contexts, including ancient Egypt, scholars have argued that chronic schistosomiasis amongst the population may explain the representations of plump-breasted men in visual culture, including representations of the so-called heretic pharaoh Akhenaten (Ghalioungui 1973; Nunn 1996, 69). In light of Fenech *et al.*'s recent discoveries, perhaps similar considerations should also now be included in the long-standing debates surrounding the gender-fluid figurative art of Neolithic Malta? In the absence of current definitive identification of schistosome eggs, larvae or adult worms in reliable Maltese funerary contexts, we are unable to claim unequivocally that this parasite also imposed its notorious morbidity and mortality burden on the Neolithic population of Gozo. However, it seems unlikely that the Gozitans would have been able to avoid what many other contemporary regional populations suffered. Such a claim would need to justify a lack of engagement with freshwater sources at a time when we already have evidence for human manipulation of water sources for the purposes of proto–irrigation, such as at the nearby sites of Santa Verna and Ġgantija (Volume 1, Chapter 3, & Volume 2, Chapter 9). Despite the relatively low levels of biological stress reported for the Circle population, we are again called to reflect on the implications of the 'Osteological Paradox', and the necessity for further integrated archaeometric and palaeopathological research to articulate the nuances of traditional systemic stress indicators such as *cribra orbitalia*, porotic hyperostosis and enamel hypoplasia (McFadden & Oxenham 2020; Oxenham & Cavill 2010; Rivera & Lahr 2017; Temple & Goodman 2014).

8.4.4. Persons of interest

Although the current research was not focused on demographic analyses, it is nonetheless important to report observed evidence for age across the life course (Fig. 8.5a-g), including several cases of *hyperostosis frontalis interna* (§8.5.2 & §8.7.4, below), extreme pubic symphysis degeneration (x3; Fig. 8.5b-d) and ossified cartilage (Fig. 8.5e-g; Boylston *et al.* 2000, 51), indicating that some individuals lived to an advanced age in Neolithic Gozo. At the opposite end of the life-course, our team also examined the remains of many foetuses and perinates (Fig. 8.5a). The inclusion of individuals of all ages and stages of life is a significant point of discussion for the Population History Workgroup and is expanded upon by Thompson *et al.* in Chapter 12 of this volume and in §8.7.3, below.

8.4.5. Taphonomic considerations

Thompson *et al.* (Chapter 12; cf Thompson *et al.* 2018; 2020; Thompson 2020) explored some of the taphonomic phenomena observed while sorting the assemblage, including the extensive fragmentation of most elements, alongside the preservation of small and/or delicate elements such as auditory ossicles; hyoids;

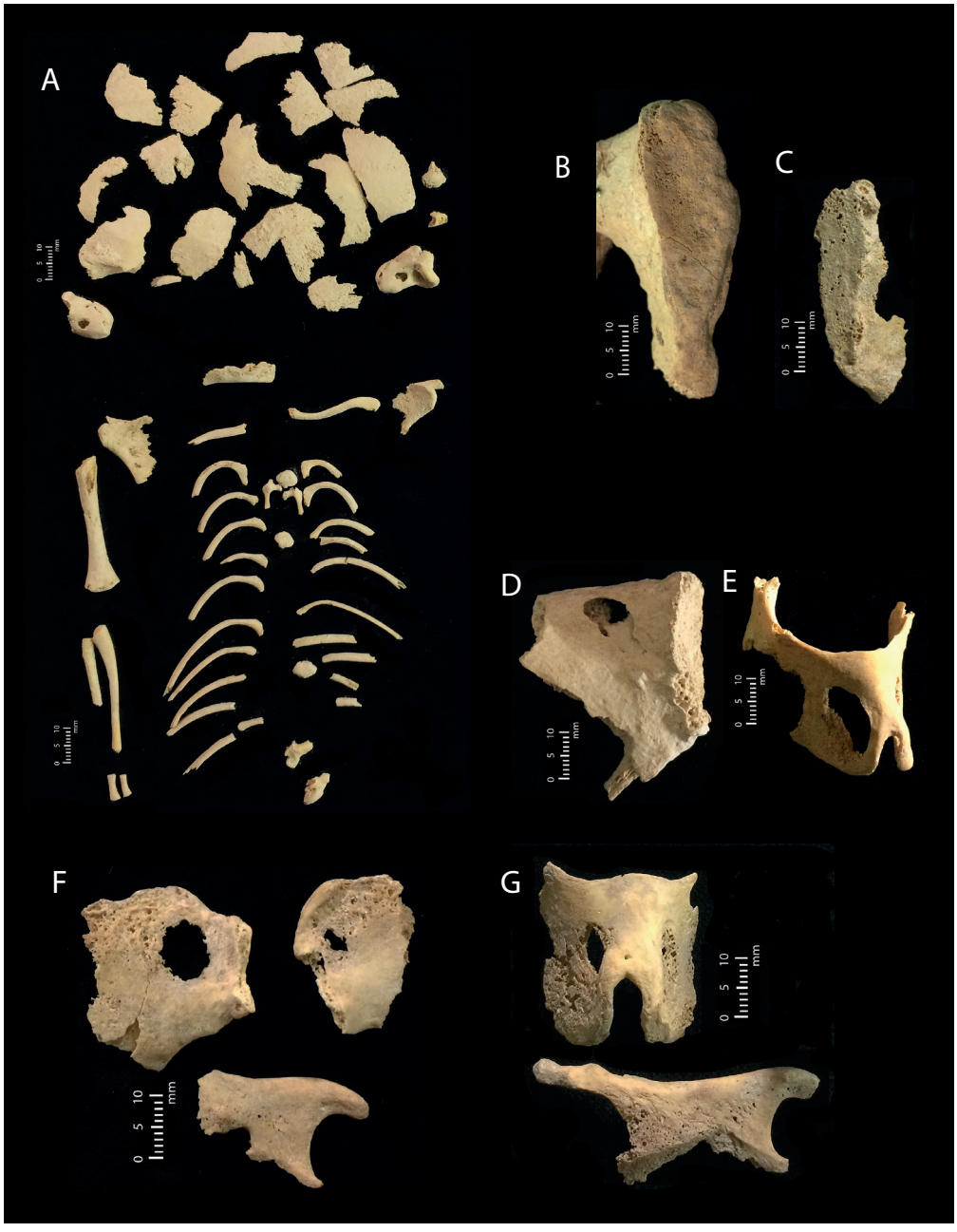

Figure 8.5. *A selection of indicators that the Circle was used as an interment space for individuals across the life course: a) from the partially articulated skeleton of a 24–26 week-old foetus from Context (831); to the markers of advanced age, including: b–d) eroded and eburnated pubic symphyseal fragments from Contexts (845), (1206) and (960), respectively; and f–g) ossified cartilage from Contexts (960), (960) and (783), respectively. Scale bar: 1 cm. (Photos Ronika K. Power).*

ossified cricoid and thyroid cartilage; vomers; styloid processes (of basicrania), phalanges, patellae, carpals and tarsals (especially pisiforms), sesamoids and foetal and neonatal bones. This may seem paradoxical but can be explained by the complex interaction between fair preservation conditions within the natural limestone geology and a long history of successive deposition incorporating substantial rearrangement of remains. Altogether, the burial deposits were likely quite turbulent, leading to the fragmentation of most of the larger skeletal elements, as well as the destruction of an unquantifiable number of bones. However, as

described in Chapter 12, while small bones are present and therefore indicate the largely primary nature of deposition, proportionately they are considerably under-represented across the full assemblage. It appears that the combination of natural taphonomic degradation and compaction because of sediment pressure particularly undermined the survival and preservation of less robust elements with a high proportion of trabecular bone. Movement and tumbling within deposits may have provided spaces for small and fragile elements to shift and therefore preserve.

8.5. Results: case studies

The remainder of this chapter is devoted to the presentation of case studies of skeletal changes or variations, providing insights into the spectrum of health issues experienced by the living Neolithic Maltese community before their eventual demise and deposition in the Circle. Considering the highly fragmented, disarticulated and commingled nature of the assemblage, the case studies are presented as individual extant elements grouped by bodily zonation – trauma of the cranium and mandible; other cranial pathology; and post-cranial pathology. The intention of this approach is to draw forth a small number of key reflections from the lived experiences of Gozo's ancient inhabitants and bring life to the extraordinary (and mundane) achievements represented (or invisible) in the Maltese prehistoric archaeological record. At all times, we must hold at the forefront of our minds that the temples, terraces and all manner of technological and artistic endeavours were made *by* real people, *for* real people. As such, the case studies presented below build into bigger conversations regarding the lived experiences of poor health, ageing and interpersonal violence across centuries, reinforcing the impact that considerations of the 'bioarchaeology of care' have on our reconstructions of past populations (§8.7.3, below; Tilley 2013, 2015, 2017; Tilley & Cameron 2014; Tilley & Oxenham 2011). Notwithstanding these important facts, what is presented here represents only a sub-sample of the extant pathological bone from the Circle, and the overall incidence and prevalence of all forms of skeletal pathology is relatively low across the assemblage.

In terms of data presentation, many excellent resources provide direction and frameworks for the reporting of pathology in bioarchaeology (for example, Roberts & Manchester 2005, 96ff.) and some offer further specialty in recording and description of trauma in fragmented assemblages (for example, Judd 2000, 2002a, 2002b). In agreement with Roberts and Connell (2004, 34; cf Buikstra & Ubelaker 1994; Lovell 2000; Ortner 2003), our own direction seeks to abide by the fundamental elements for recording skeletal pathology, namely unambiguous terminology; precise identification of the position of lesions in affected elements; and a descriptive summary of the morphology of the observed variation. The description is offered prior to any differential diagnoses, so that others may be resourced to evaluate each case as they see fit. Following the foundational intentions of Buikstra and Ubelaker (1994, 105) regarding palaeopathological analyses, our Workgroup goal is always to encourage further discussion, collaboration and scholarship.

8.5.1. Trauma: cranium and mandible

A selection of case studies featuring trauma to the cranium and mandible are presented below. Where available, radiological observations supplement macroscopic descriptions. Note that 'diameter' is expressed as: Ø; and 'no data' is expressed as: n/d.

8.5.1.1. FB0002: Mandible

Context:	(951)
Grid Ref.:	-
Year of Excavation:	BR93
Other Details:	Skull No. 15, E. Layer 2

Element identification and preservation:

Adult mandible, based on eruption and occlusion of right permanent mandibular third molar (FDI 48). Sex assessment is indeterminate because of element dysplasia. The element is ~90% complete and fragmented at both left and right ascending rami. Retained dentition includes the left permanent mandibular first and second premolars (FDI 34–35) and first and second molars (FDI 36–37); and the right permanent mandibular first, second and third molars (FDI 46–48). All absent dentition has been exfoliated *postmortem*. Extant element is in excellent condition. All damage is assessed as *postmortem*.

Macroscopic observations:

A complete fracture is observed comprising the left mandibular corpus and ascending ramus (Figs 8.6a-c, 8.7a-g). When viewed from the lateral aspect the fracture is located along the oblique line (Figs 8.6b, 8.7c); from the lingual aspect it is located immediately distal to the tooth-row, posterior to the retro-molar space and truncating the base of the left mylohyoid line (Fig. 8.6c, 8.7d). The fracture is not reduced; the element is dysplastic; the inferior border of the left mandibular corpus is laterally displaced at the level of the left ramus, which is offset in a lateral direction (Fig. 8.6a-c, 8.7c-g). There is a slight superior displacement of the ascending ramus. At the fracture site, the inferior

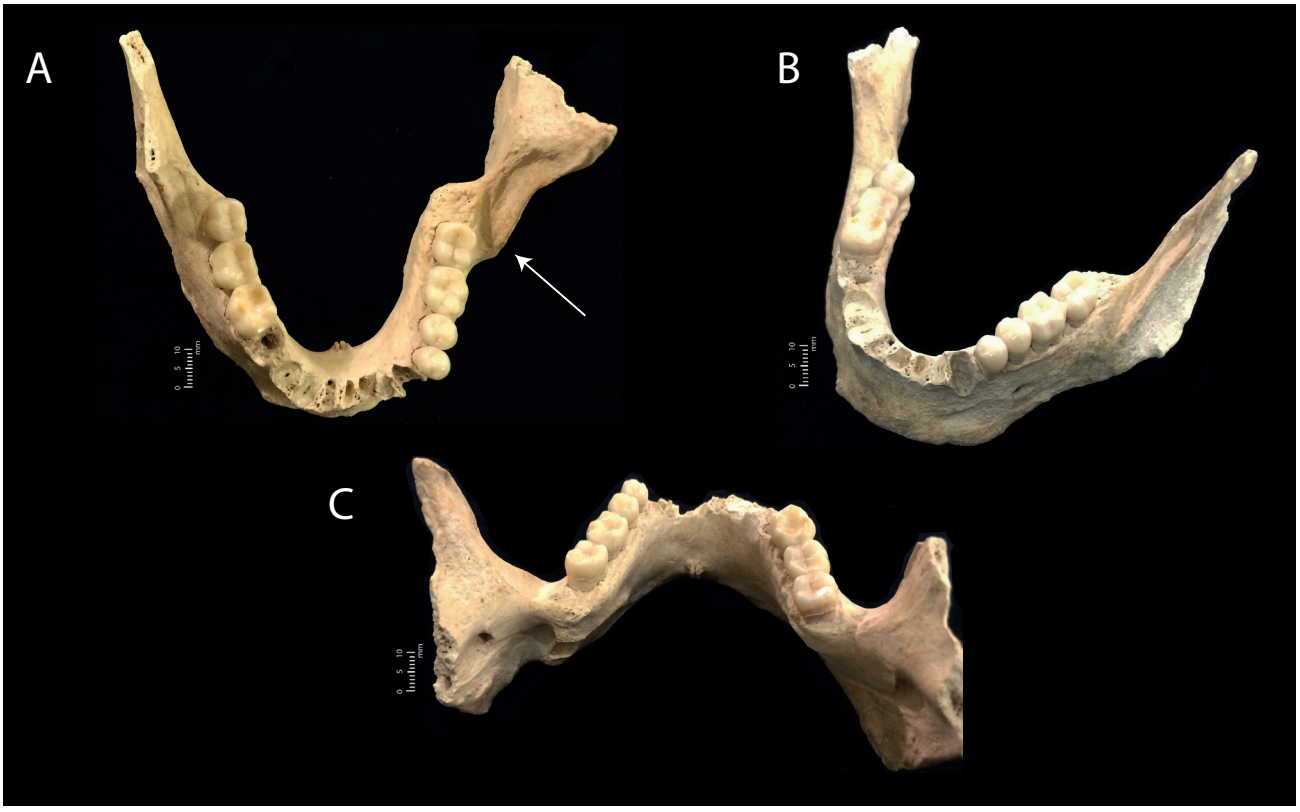

Figure 8.6. *A selection of photographic images pertaining to an adult mandible of indeterminate biological sex (FB0002) from Context (951) of the Circle sample, detailing healed fracture of the left mandibular corpus and ascending ramus, including: a) superior view; b) left supero-lateral view; c) supero-posterior view. Scale bar: 1 cm. (Photos Ronika K. Power).*

aspect of the left ramus is thicker than the opposing side. The left permanent mandibular third molar (FDI 38) is absent and there are no visible indications of peri-mortem tooth-loss or impaction. A small, smooth-walled cavity is observed in the lingual aspect of the corpus at the fracture line.

The left lateral aspect of the corpus is observed to be dysplastic (Figs 8.6a-c, 8.7c-d). The dysplasia presents as a slight elevation of the intermediate component of the left corpus in comparison with the opposing side. In this case, the intermediate component is comprised of the section of the mandibular corpus from the left tubercle of the mental trigone to the fracture margin described above, distal to the left retromolar space. This segment is approximately 51.8 mm in length.

The dysplasia is noted both at the inferior border of the mandibular corpus as well as in the alignment of the left dental arcade (Figs 8.6a-c, 8.7d-g); here, the intermediate segment of the mandibular corpus is superiorly and laterally displaced. When viewed inferiorly, the lingual aspect of the left dental arcade presents pronounced asymmetry, with the intermediate segment described above appearing to be displaced towards the midline. When the element is viewed anteriorly, the point at which the dysplasia commences is located just anterior to the left tubercle of the mental trigone, approximately 12.8 mm infero-lateral to the mental symphysis.

Radiological observations:
The mandible presents a significantly laterally and anteriorly displaced posterior fragment on the left side. Complete healing is evident across the fracture line, as is reestablishment of the cortical surface and trabeculae throughout the fracture site (Fig. 8.7e-g). No scarring is observed to indicate osteomyelitis was suffered *in vivo*, as the effects would have continued into the adjacent cortical bone on the lingual aspect of the mandible, and rarefaction of the trabeculae would be observed. The lingual surface at the posterior aspect of the anterior component of the fracture segment is less well-organized, which would be the expected location of the mesial margin of the third molar – appearing

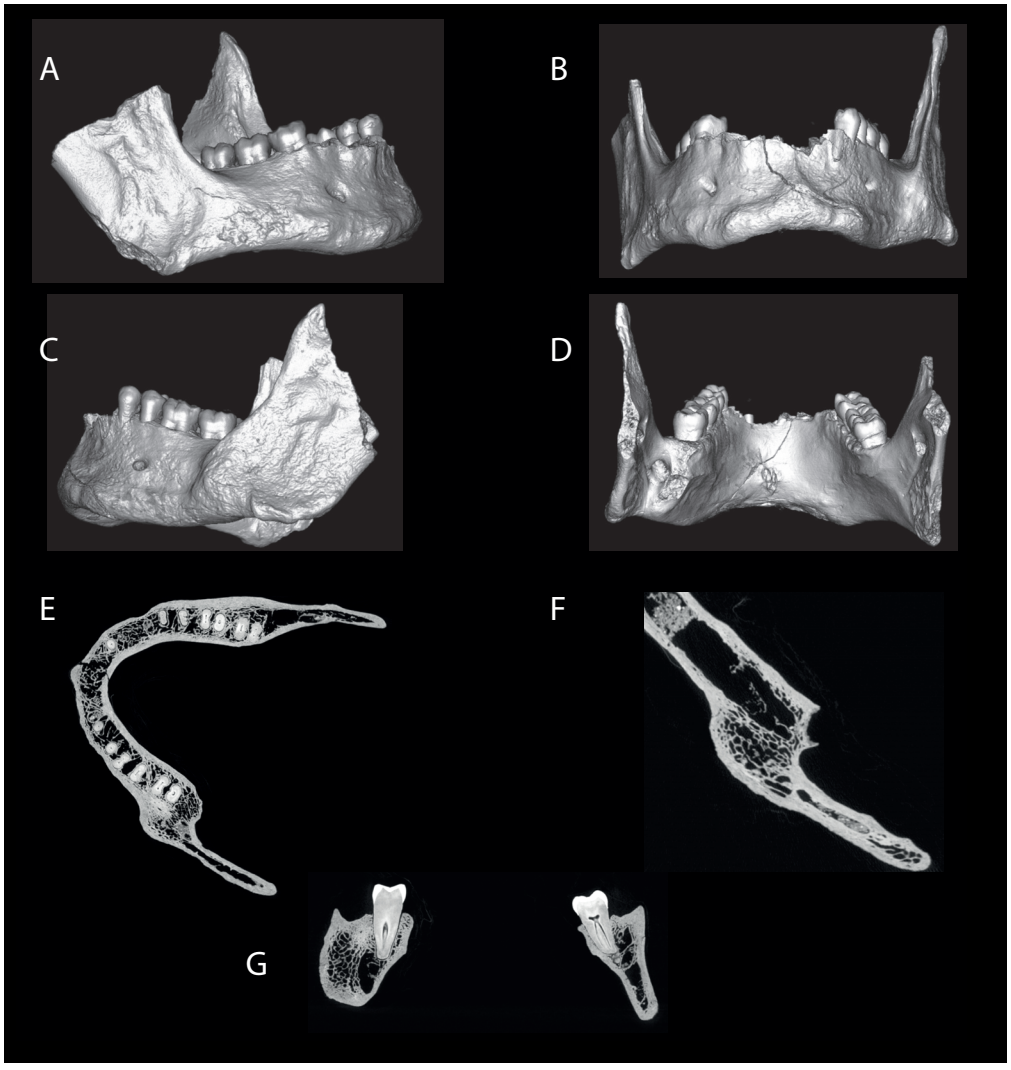

Figure 8.7. *A selection of radiological images pertaining to an adult mandible of indeterminate biological sex (FB0002) from Context (951) of the Circle sample, detailing healed fracture of the left mandibular corpus and ascending ramus, including: a) 3D render right lateral view; b) 3D render anterior view; c) 3D render left lateral view; d) 3D render posterior view; e) transverse cross-section detailing healed fracture; f) transverse cross-section close-up of left aspect of mandible, detailing healed fracture; g) sagittal cross-section detailing left and right mandibular corpora and permanent second molars* in situ *(FDI 37, 47), featuring healed fracture on left aspect. (Radiological images captured by L. Buck, Cambridge Biotomography Centre; processed by J. Magnussen & M. Pardey, Macquarie Medical Imaging).*

quite sharp and irregular (Figs 8.6c, 8.7d-f). Considering the inferior position of the feature in relation to the remainder of the arcade, it is possible that this was a cyst associated with an unerupted third molar. If this is the case, it would indicate that the individual was at least 14–16 years of age at the time of insult (White & Folkens 2005, 366–7). In clinical cases, fractures such as these present as a result of direct impact either onto the mental eminence, or lateral impact onto the corpus (Dreizin *et al.* 2016). It is common to see two points of fracture associated with these injuries, especially in the mandibular condyles (Dreizin *et al.* 2016); however, the element is fragmented and thus further pathological evidence may be absent.

The canal for the inferior alveolar nerve is filled with matrix. The fracture line has traversed the canal but has also partially overlapped as the affected segments resolved in a dysplastic position. It is possible that the dysplasia observed at the anterior aspect of the mandible is associated with the disuse and misuse of the element in association with the major fracture insult and subsequent healing.

In terms of the dentition, the occlusal surfaces present slightly more wear on the ipsilateral than contralateral side, almost to the extent of dentine exposure on the left permanent mandibular first molar (FDI 36). A root remnant is observed in the retromolar space deep within the trabeculae of the right arcade.

Lesion type and healing status: Trauma; Healed.
Lesion preservation: Excellent.
Differential diagnosis: Blunt-force trauma.

8.5.1.2. FB0014: Nasal Bone

Context:	(468)
Grid Ref:	99E/113N
Year of Excavation:	BR93
Other Details:	n/d

Element identification and preservation:
Fragmentary remains of an adult cranium, featuring partial frontal, left and right nasal and right temporal bones. Age estimation is based on size, robusticity, density of cortices and the commencement of sutural obliteration as observed in extant right coronal, sphenofrontal and sphenotemporal sutures. Sex assessment is possible male, based on evaluation of the extant sexually dimorphic traits presented in Buikstra and Ubelaker (1994, 20), including supraorbital margin (4/5) and supraorbital ridge/glabella (4/5). There is no extant dentition. The extant elements are assessed as representing ~30% of a complete cranium and are in very good condition. All damage is assessed as *postmortem*.

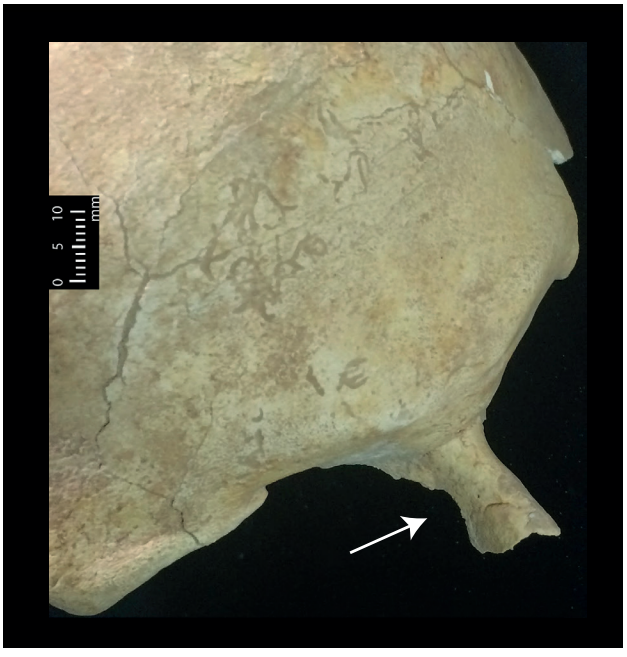

Figure 8.8. *Fragmentary remains of adult possible male cranium (FB0014) from Context (468) of the Circle, featuring healed fracture of the right nasal bone. Scale bar: 1 cm. (Photos Ronika K. Power).*

Macroscopic observations:
A healed fracture is observed on the ectocranial surface of the antero-medial aspect of the right nasal bone (Fig. 8.8). The nasal bone is fragmented at the most distal and lateral aspects. The feature presents as a canal-shaped trough; the inferior aspect of the fracture margin has smooth, rounded contours and slightly overlies the superior aspect of the fracture indicative of slight superior displacement. The superior aspect of the fracture margin is continuous with the surrounding cortical bone with no clearly defined margin. The character of the cortical bone within and across this feature is continuous with the surrounding elements. The maximum dimensions of the feature are 6.51 mm length and 0.5 mm width. The most superior aspect of the feature is located 2.0 mm inferior to the right nasal foramen; the most inferior aspect of the feature is located approximately at 14.2 mm inferior to nasion and meeting the internasal suture.

Lesion type and healing status: Trauma; Healed.
Lesion preservation: Excellent.
Differential diagnosis: Trauma.

8.5.2. Other cranial pathology
A selection of case studies featuring general cranial pathology is presented below. Where available, radiological observations supplement macroscopic descriptions.

8.5.2.1. FB0005: Frontal bone

Context:	(783)
Grid Ref.:	94E/111N
Year of Excavation:	BR94
Other Details:	Spit 4, Unit 8

Element identification and preservation:
Adult cranium, based on eruption and occlusion of left permanent maxillary third molar and fusion of the spheno-occipital synchondrosis. Sex assessment is possible male, based on evaluation of the sexually dimorphic traits presented in Buikstra and Ubelaker (1994, 20), including nuchal crest (5/5), mastoid process (4/5), supraorbital margin (4/5), and supraorbital ridge/glabella (4/5). The cranium is ~95% complete; there are small areas of *postmortem* damage to the palatine process of the left maxilla. Dentition exfoliated *postmortem*

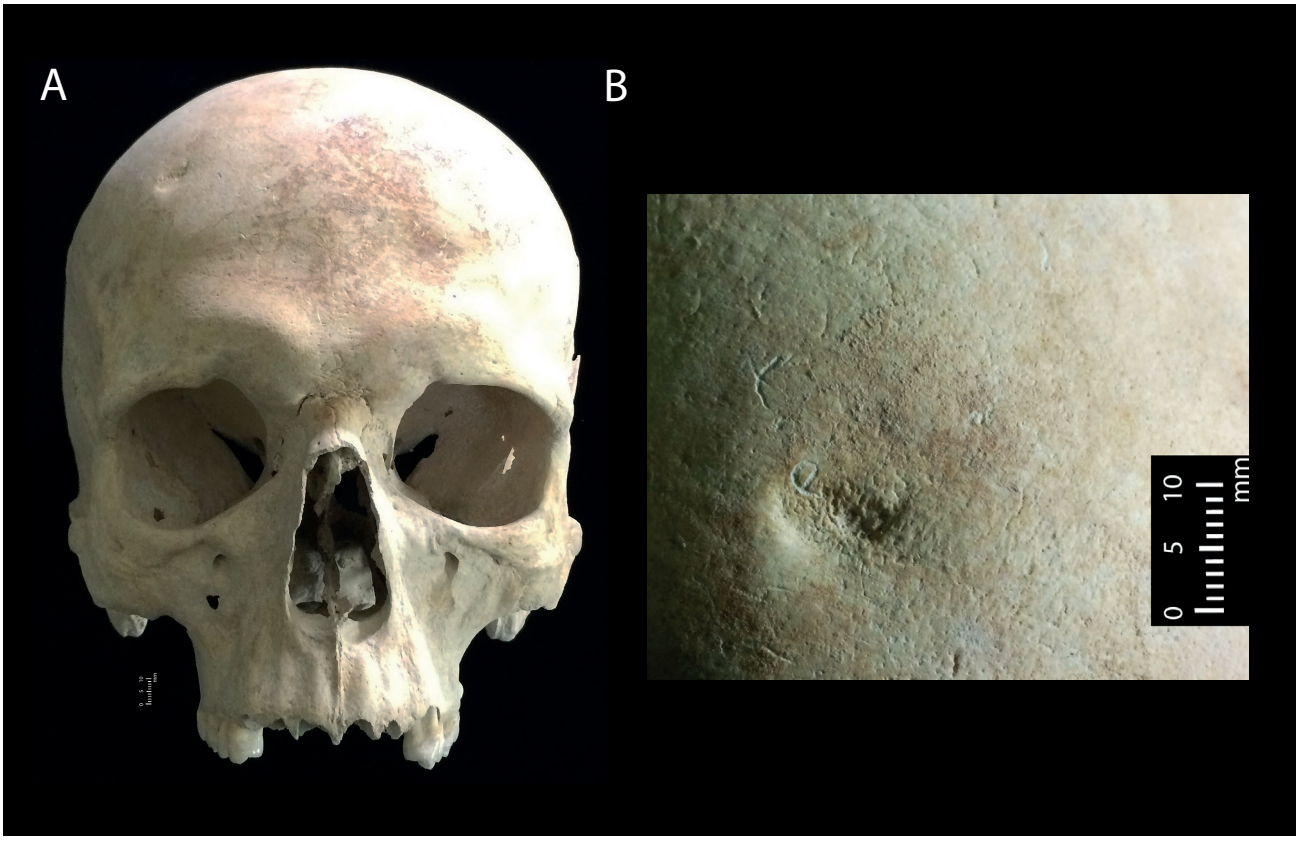

Figure 8.9. *a) Adult possible male cranium (FB0005) from Context (783) of the Circle; b) detailing focal depression on ectocranial surface of the right antero-lateral aspect of the frontal squama. Scale bar: 1 cm. (Photos Ronika K. Power).*

includes the right and left permanent maxillary central and lateral incisors and canine (FDI 11–13; 21–23), and the right permanent maxillary third molar (FDI 18). Extant element is in excellent condition. All damage is assessed as *postmortem*.

Macroscopic observations:
A focal depression is observed on the ectocranial surface of the right antero-lateral aspect of the frontal squama (Fig. 8.9a-b). The feature presents as an approximately crescent-shaped depression with smooth, rounded margins. The cortical bone within this feature presents a pitted surface when compared with the surrounding bone; the character of this pitting is smooth and is not suggestive of an active lesion. The maximum dimensions of the feature are 8.1 mm width and 5.6 mm length. The most inferior aspect of the feature is located 46.2 mm supero-lateral to the right supraorbital notch.

Lesion type and healing status: Erosive; Healed.
Lesion preservation: Excellent.
Differential diagnosis: Infection, Neoplasm.

8.5.2.2. FB0006: Frontal bone

Context:	(1238)
Grid Ref:	98E/114N
Year of Excavation:	BR94
Other Details:	Spit 1, Unit 4

Element identification and preservation:
Fragmentary remains of adult cranium, featuring partial frontal and left and right parietal bones. Age estimation is based on size, robusticity, density of cortices and the commencement of sutural obliteration as observed in extant left coronal and anterior sagittal sutures. Sex assessment is possible male, based on evaluation of the extant sexually dimorphic traits presented in Buikstra and Ubelaker (1994, 20), including supraorbital margin (5/5) and supraorbital ridge/glabella (5/5). Despite the strength of expression of these two extant traits, we remain conservative in our expression considering the absence of the majority of the cranium. There is no extant dentition. The extant elements are assessed as representing ~20% of a complete cranium. The elements are in very good condition. All damage is assessed as *postmortem*.

Macroscopic observations:
Two focal depressions are observed on the ectocranial surface of the left supero-lateral aspect of the left frontal squama (Fig. 8.10a-c). The most anterior aspect of the first of these two features is located 54.0 mm supero-lateral to the left supraorbital notch. The second depression, described below, is located 9.4 mm postero-lateral to the first depression.

The first depression presents as an approximately oval-shaped concavity with smooth, rounded margins. The cortical bone within this feature presents as a pitted and rugged surface when compared with the surrounding bone, with pronounced rugosity observed on the most superior and left lateral aspects of the feature. The character of this pitting is smooth and is not suggestive of an active lesion. The maximum dimensions of the feature are 9.4 mm width and 15.2 mm length.

The most anterior aspect of the second of these two features is located 66.0 mm supero-lateral to the left supraorbital notch. The first depression, described above, is located 9.4 mm supero-medial to the second depression. The second depression presents as an approximately trapezoidal-shaped concavity with smooth, rounded margins. The cortical bone within and across this feature is continuous in character with the surrounding bone. The maximum dimensions of the feature are 10.7 mm width and 14.0 mm length.

Radiological observations:
From a radiological point of view, the anterior lesion is more irregular at its base, while the other is smoother in nature (Fig. 8.10a-b). All bony changes for both lesions are isolated to the outer table (Fig. 8.10c). The more anterior lesion extends three-quarters through the outer table, but does not enter the diploic space. Critically, the diploic space architecture is observed to be normal in character and organization and is not involved in any pathological process. Differential diagnoses for these lesions should include scalp infection, potentially caused by organisms related to contaminated wounds, such as *Staphylococcus aureus* and *Streptococcus pyogenes* (Group A *Streptococcus*). These are the most important and common bacterial causes of skin and soft tissue infections (SSTIs) worldwide. *S. pyogenes* causes well-known infections in the superficial keratin layer (impetigo), the superficial epidermis (erysipelas), the subcutaneous tissue (cellulitis), the fascia (necrotizing fasciitis), or muscle (myositis and myonecrosis; Stevens & Bryant 2016; Bessen 2009). *S. pyogenes* infections have been reported for the scalp (Mastro *et al.* 1990). This type of bacterial infection has particularly high rates of infection in summer months (Ferrieri *et al.* 1972) and is often clinically observed in individuals

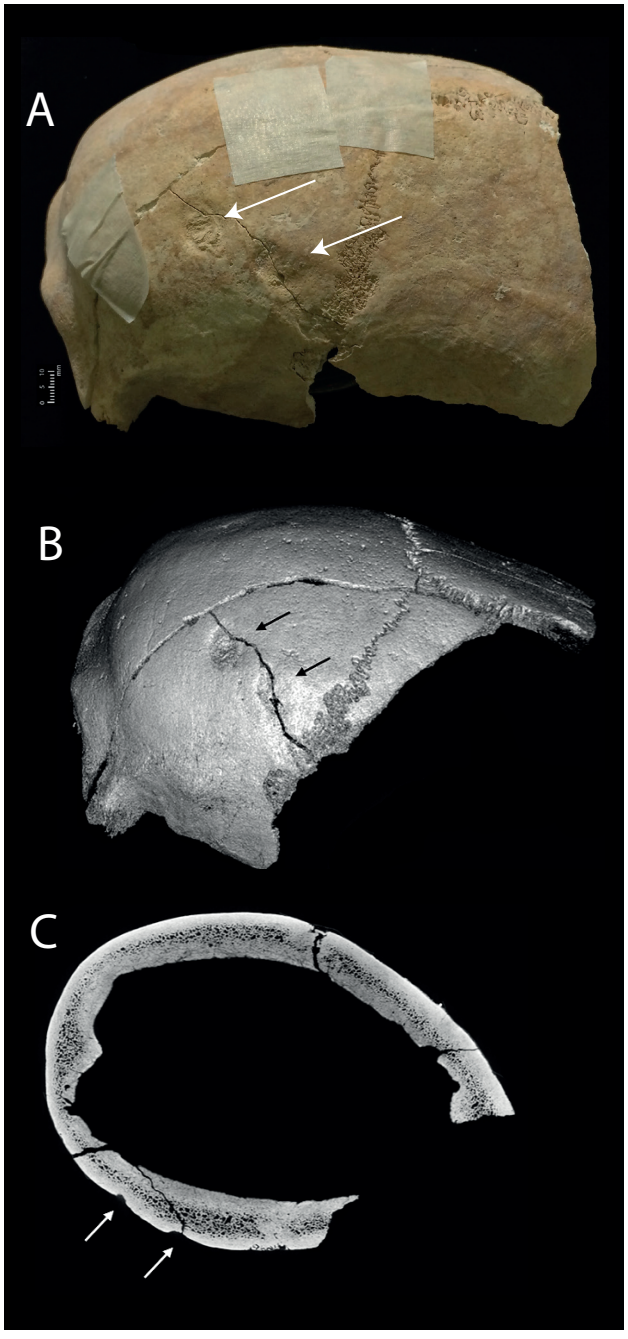

Figure 8.10. *a) Fragmentary remains of adult possible male cranium (FB0006) from Context (1238) of the Circle, featuring two focal depressions on the ectocranial surface of the left supero-lateral aspect of the frontal squama; b) 3D render of fragmentary remains; c) cross-section from CT data of fragmentary remains, showing that both focal depressions do not extend deeper than the outer table. Scale bar: 1 cm (photograph only). (Photos Ronika. K. Power; radiological images captured by L. Buck, Cambridge Biotomography Centre; processed by J. Magnussen & M. Pardey, Macquarie Medical Imaging).*

whose occupation or recreational activities result in cutaneous cuts or abrasions (Adams 2002; Fehrs *et al.* 1987; Wasserzug *et al.* 2009).

Similarly, *S. aureus* causes significant global health burdens owing to its virulence, highly contagious nature, ease of transmission and tendency to recur (Creech *et al.* 2016). This is particularly as a result of its capacity to persist in the environment for long intervals (Knox *et al.* 2012; Miller *et al.* 2015), placing those who live, work and socialize in close quarters, such as households, at high risk (Knox *et al.* 2012; Miller *et al.* 2015). In clinical studies, up to 70% of patients diagnosed with *S. aureus* infections will experience recurrent infections within one year (Kaplan *et al.* 2014; Miller *et al.* 2015) however, the role of antimicrobial resistance must be kept in mind when referring to modern contexts. It is considered the most prevalent pathogen associated with skin and soft tissue infections (Creech *et al.* 2016) *S. aureus* has a predilection for the scalp, face and shoulders, but any bodily region may be affected (Creech *et al.* 2016). Although these infections are usually superficial, they have significant morbidity implications for sufferers and communities, including pain, scarring and the various social, economic and psychological implications of chronic ill health (Creech *et al.* 2016).

Further differential diagnoses should include neoplastic disease, such as scalp tumours including squamous cell carcinoma (SCC) or basal cell carcinoma (BCC). These are the most common non-melanoma skin cancers that affect the head and neck (Dundar *et al.* 2017; Mendenhall *et al.* 2007). The prevailing aetiologies for SCC and BCCs are genetic factors and sun exposure (Sewell *et al.* 2003; Buzzell 1996), the latter of which is plentiful in Malta at any time of human occupation. Consideration should be weighted towards the bacterial infections described above, as non-melanoma skin cancers are likely to compromise the outer table and involve diploë (Dundar *et al.* 2017), which is not observed in this case.

Lesion type and healing status: Erosive; Healed.
Lesion preservation: Excellent.
Differential diagnosis: Infection, Neoplasm.

8.5.2.3. FB0016: Parietal, occipital and other cranial fragments

Context:	(951)
Grid Ref:	96E/114N
Year of Excavation:	BR94
Other Details:	Area X, Spit 1, Skull 9

Element identification and preservation:
A group of assorted cranial fragments, including a fragmented right parietal, occipital and other non-diagnostic cranial fragments. The elements all appear to be derived from an adult individual/s, according to their size, architectural character and cranial suture development (Buikstra & Ubelaker 1994, 32ff.; White & Folkens 2005, 369ff.; White *et al.* 2012, 389ff.). Unfortunately, these elements are too fragmentary to retain key anatomical landmarks for sex assessment according to diagnostic criteria (Buikstra & Ubelaker 1994, 15ff.;

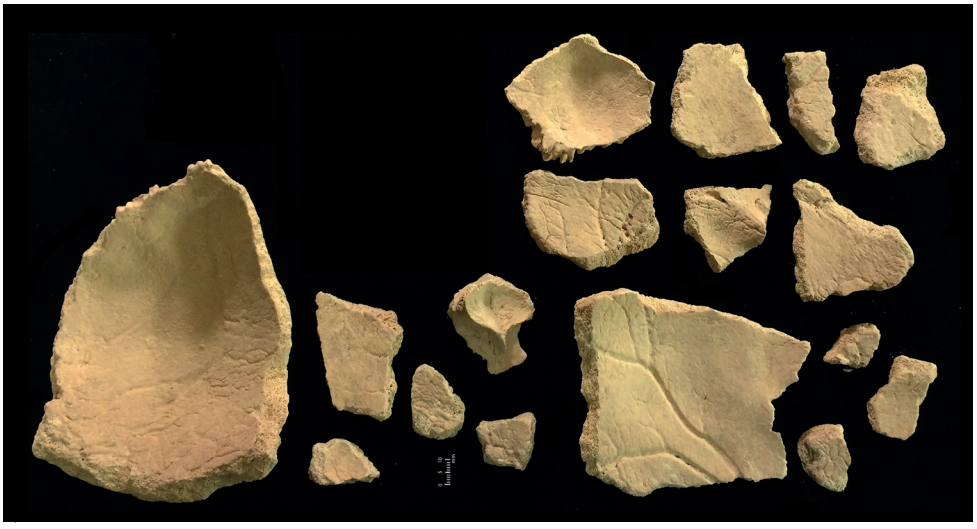

Figure 8.11. *Assorted adult cranial fragments (FB0016) from Context (951) of the Circle, including right parietal, occipital and non-diagnostic pieces. The fragments all exhibit abnormal endocranial focal impressions, classified as hypervascularity. Scale bar: 1 cm. (Photos Ronika. K. Power).*

White & Folkens 2005, 385ff.; White *et al.* 2012, 408ff.). Although these fragments present a similar colour, character, expression of pathology, taphonomic change and there is no duplication of the fragments, it is not possible to state with absolute certainty that they may all be attributed to the same individual. The extant elements are in fair condition. All damage is assessed to be *postmortem*.

Macroscopic observations:
These assorted cranial fragments are observed to have abnormal endocranial impressions (Fig. 8.11). These endocranial impressions can be classified as hypervascularity; the impressions consist of diffuse vascular networks of shallow tunnel-like etching emitting from the meningeal grooves. In section, it is noted that the character of the cortical ectocranial and endocranial portions of the cranial fragments are hardly distinguishable and not easily differentiated from the diploë.

Porotic hyperostosis is observed across the ectocranial surface of at least one cranial fragment. Extant portions of the lesion are observed on a possibly left anterior parietal fragment, extending superiorly and medially from the superior temporal line to encompass all the extant area of the parietal squama.

The porosity consists of a range of holes ranging from very small (<1.0 mm Ø) to large in size (>1.0 mm Ø) that are tightly spaced and, in some cases, do coalesce. The cortical bone appears thickened in some areas of the lesion. The lesion exhibits mixed activity phases, presenting both healed and active states, suggesting it was chronic at the time of death.

Lesion types: Mixed (Lytic; Proliferative); Chronic (Active; Healing).
Lesion preservation: Good; Incomplete because of *postmortem* damage.
Differential diagnosis: Infectious; Metabolic; Endocrine.

8.5.2.4. FB0017: Parietal, occipital, temporal and other cranial fragments

Context:	(951)
Grid Ref:	n/d
Year of Excavation:	BR1994
Other Details:	n/d

Element identification and preservation:
A group of assorted cranial fragments, including a fragmented parietal, occipital, right temporal and other non-diagnostic cranial fragments. The elements all appear to be derived from an adult individual/s, according to their size, architectural character and cranial suture development (Buikstra & Ubelaker 1994, 32ff.; White & Folkens 2005, 369ff.; White *et al.* 2012, 389ff.). Although reliable sexually dimorphic criteria exist for sex assessment of human crania (Buikstra & Ubelaker 1994, 15ff.; White & Folkens 2005, 385ff.; White *et al.* 2012, 408ff.), these elements are too fragmentary to retain key anatomical landmarks for analyses. One fragment of right temporal presents an extant mastoid process, but it is of indeterminate character and should be approached with caution for sex assessment in isolation. Although these fragments present a similar colour, character, expression of pathology, taphonomic change, and there is no duplication of the fragments, it is not possible to state with absolute certainty that they may all be attributed to the same individual. The extant elements are in fair condition. All damage is assessed to be *postmortem*.

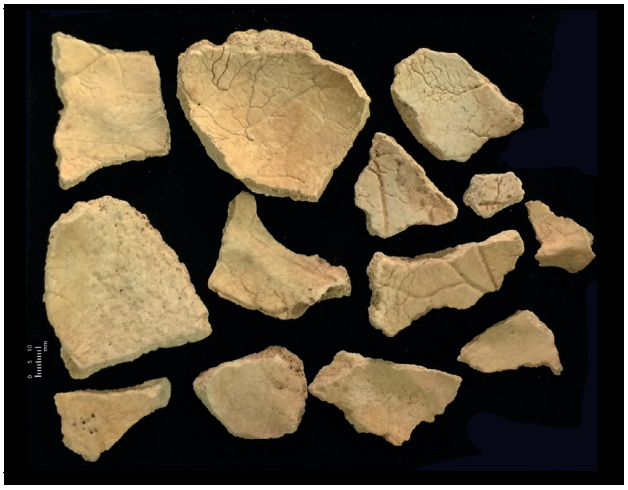

Figure 8.12. *Assorted adult cranial fragments (FB0017) from Context (951) of the Circle, including parietal, occipital, right temporal and non-diagnostic pieces. The fragments all exhibit abnormal endocranial focal impressions, classified as hypervascularity. Scale bar: 1 cm. (Photos Ronika. K. Power).*

Macroscopic observations:
The fragmented parietal and the other non-diagnostic cranial fragments are observed to have abnormal endocranial impressions (Fig. 8.12). These endocranial impressions can be classified as hypervascularity; the impressions are observed to consist of diffuse vascular networks of shallow tunnel-like etching emitting from the meningeal grooves.

Lesion type: Lytic.
Lesion preservation: Good; Incomplete because of *postmortem* damage.
Differential diagnosis: Infectious; Metabolic; Endocrine.

8.5.2.5. FB0018: Parietal fragment
Context: (951)
Grid Ref: 98E/116N
Year of Excavation: BR94
Other Details: n/d

Element identification and preservation:
An isolated right parietal fragment, likely from an adult individual, according to its size and architectural character (Buikstra & Ubelaker 1994, 32ff.; White & Folkens 2005, 369ff.; White *et al.* 2012, 389ff.). Although reliable sexually dimorphic criteria exist for sex assessment of human crania (Buikstra & Ubelaker 1994, 15ff.; White & Folkens 2005, 385ff.; White *et al.* 2012, 408ff.), this element is too fragmentary to retain key anatomical landmarks for analyses. The extant element is in fair condition. All damage is assessed to be *postmortem*.

Macroscopic observations:
The right parietal fragment is observed to have abnormal endocranial impressions located on the cortical bone of the central area of the fragment; the impressions emit from the terminal aspects of the meningeal grooves (Fig. 8.13). These impressions can be classified as hypervascularity consisting of localized vascular networks of shallow channel-like etching and including diffuse micro- and macroporosity amongst the impressions. The margins are smooth, rounded and well-demarcated. The remaining surrounding endocranial surface is uneven and flaky because of taphonomic change.

Figure 8.13. *Adult right parietal fragment (FB0018) from Context (951) of the Circle. The fragment exhibits abnormal endocranial focal impressions, classified as hypervascularity. Scale bar: 1 cm. (Photos Ronika. K. Power).*

Lesion type: Lytic
Lesion preservation: Good; Incomplete because of *postmortem* damage.
Differential diagnosis: Infectious; Metabolic; Endocrine.

8.5.2.6. FB0019: Parietal fragments
Context: (951)
Grid Ref: 98E/116.5-117N
Year of Excavation: BR94
Other Details: Area X

Element identification and preservation:
Two left parietal fragments. The element/s appears to be derived from an adult individual/s, according to their size and architectural character (Buikstra & Ubelaker 1994, 32ff.; White & Folkens 2005, 369ff.; White *et al.* 2012, 389ff.). Although reliable sexually dimorphic criteria exist for sex assessment of human crania (Buikstra & Ubelaker 1994, 15ff.; White & Folkens 2005, 385ff.; White *et al.* 2012, 408ff.), these fragments are too fragmentary to retain key anatomical landmarks for analyses. The extant fragments are in fair condition. All damage is assessed to be *postmortem*.

Macroscopic observations:
The fragments are observed to have abnormal endocranial impressions (Fig. 8.14a). These endocranial impressions can be classified as mild hypervascularity; the impressions are observed to consist of localized vascular networks of shallow channel-like etching emitting from the meningeal grooves.

Lesion type: Lytic.
Lesion preservation: Good; Incomplete because of *postmortem* damage.
Differential diagnosis: Infectious; Metabolic; Endocrine.

8.5.2.7. FB0020: Parietal fragments
Context: (951)
Grid Ref: 96E/114N
Year of Excavation: BR94
Other Details: Area X, Spit 1, Mixed Bone

Element identification and preservation:
Two right parietal fragments. The element/s appears to be derived from an adult individual/s, according to their size and architectural character (Buikstra &

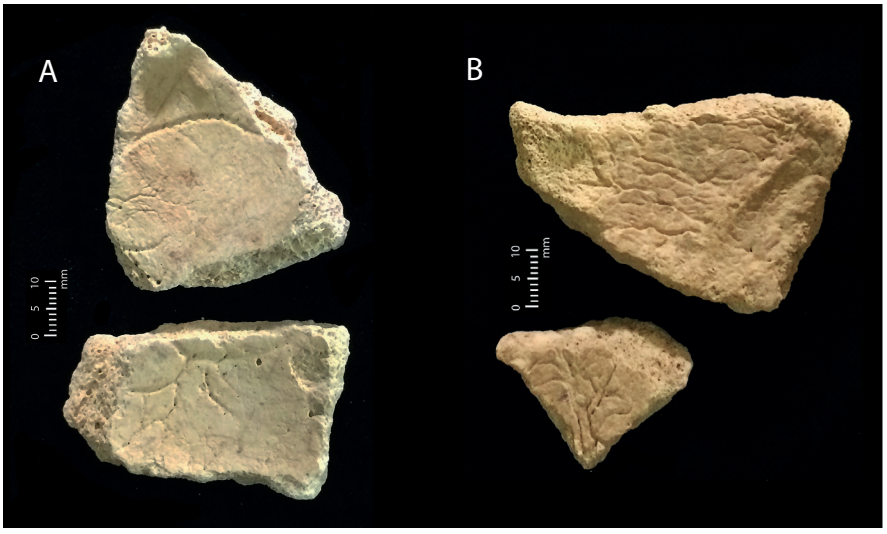

Figure 8.14. *a) Adult left parietal fragments (FB0019) from Context (951) of the Circle. The fragments exhibit abnormal endocranial focal impressions, classified as hypervascularity; b) Adult right parietal fragments (FB0020) from Context (951) of the Circle. The fragments exhibit abnormal endocranial focal impressions, classified as hypervascularity. Scale bar: 1 cm. (Photos Ronika. K. Power).*

Ubelaker 1994: 32ff.; White & Folkens 2005, 369ff.; White *et al.* 2012, 389ff.). Although reliable sexually dimorphic criteria exist for sex assessment of human crania (Buikstra & Ubelaker 1994, 15ff.; White & Folkens 2005, 385ff.; White *et al.* 2012, 408ff.), these fragments are too fragmentary to retain key anatomical landmarks for analyses. The extant fragments are in fair condition. All damage is assessed to be *postmortem*.

Macroscopic observations:
These fragments are observed to have abnormal endocranial impressions (Fig. 8.14b). The endocranial impressions can be classified as hypervascularity consisting of diffuse vascular networks of shallow channel-like etching. The margins are characterized to be smooth, rounded and well-demarcated. The remaining surrounding endocranial surface is uneven and flaky because of taphonomic change.

Lesion type: Lytic.
Lesion preservation: Good. Incomplete because of *postmortem* damage.
Differential diagnosis: Infectious; Metabolic; Endocrine.

8.5.2.8. FB0021: Frontal and parietal fragments

Context:	(518)
Grid Ref:	97E/113N
Year of Excavation:	BR94
Other Details:	Bone 2

Element identification and preservation:
A group of assorted cranial fragments, including a fragmented left parietal and frontal bones which refit. The elements all appear to be derived from an adult individual, according to their size, architectural character and cranial suture development (Buikstra & Ubelaker 1994, 32ff.; White & Folkens 2005, 369ff.; White *et al.* 2012, 389ff.). Although reliable sexually dimorphic criteria exist for sex assessment of human crania (Buikstra & Ubelaker 1994, 15ff.; White & Folkens 2005, 385ff.; White *et al.* 2012, 408ff.), these elements are too fragmentary to retain key anatomical landmarks for analyses. The extant elements are in fair condition. All damage is assessed to be *postmortem*.

Macroscopic observations:
The refitted left parietal fragments and frontal fragments are observed to have abnormal endocranial impressions and lesions (Fig. 8.15). The parietal fragment is observed to have an abnormal endocranial long and deep lesion running inferior and adjacent to the left endocranial aspect of the coronal suture. The extant portion of the lesion, measuring 1.78 mm deep, maximum 34.32 mm length and 4.11 mm width, is observed to cut through the endocranial cortical bone and part of the diploë. A part of the margin of the inferior aspect of the lesion is sharp; the exposed diploë at the base of the lesion is billowed. Although fragmented, the lesion seems to continue on the supero-lateral aspect of the parietal. Additional lesions, although narrower, are observed posterior to the long and deep lesion mentioned earlier. The characteristics are similar in nature to the long lesion.

Macroporosity (≥1.0 mm Ø) extends across a maximum area of 3.3 mm Ø, and is observed on the parietal to the posterior aspect of the long lesion described earlier. The margins of these circular lesions are smooth and rounded.

Focal macroporosity (≥1.0 mm Ø) and irregular channel-like lesions are observed on the frontal bone adjacent to the left coronal suture just anterior and

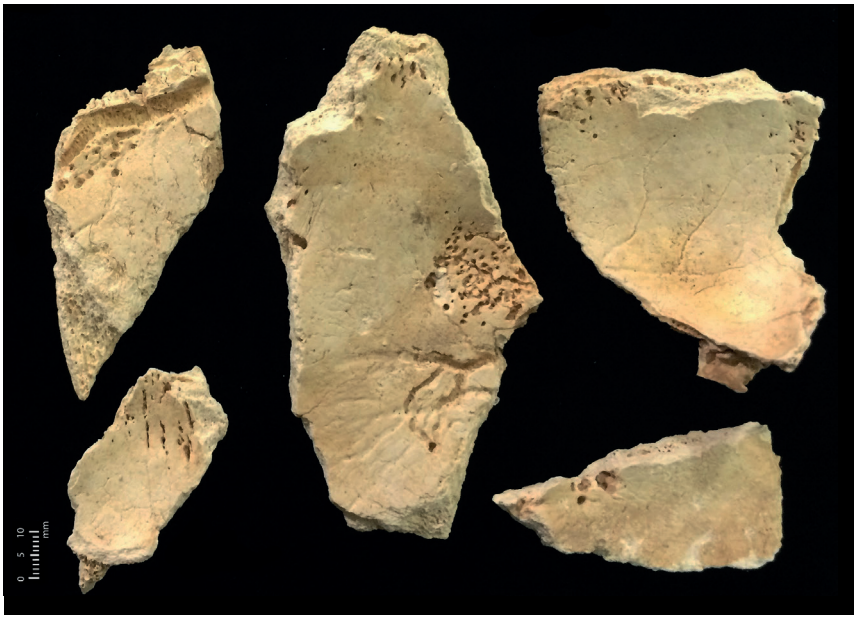

Figure 8.15. *Assorted adult cranial fragments (FB0021) from Context (518) of the Circle, including left parietal and frontal bones which refit. The fragments all exhibit abnormal endocranial focal impressions, classified as hypervascularity. Scale bar: 1 cm. (Photos Ronika. K. Power).*

superior to the long lesion observed on the parietal fragment and described earlier. The lesion occupies an area approximately 22.4 mm x 35.1 mm. The margins of these lesions are smooth and rounded; however, *postmortem* damage is also observed in this area. The macroporosity ranges in size with a maximum of 4.0 mm and minimum of 1.0 mm Ø.

Lesion type: Lytic.
Lesion preservation: Good; Incomplete because of *postmortem* damage.
Differential diagnosis: Infectious; Metabolic; Endocrine.

8.5.2.9. FB0022: Parietal and other cranial fragments

Context:	(838)
Grid Ref:	95.6E/119N
Year of Excavation:	BR93
Other Details:	Skull 7

Element identification and preservation:
A group of assorted cranial fragments, including a fragmented parietal bone/s and other non-diagnostic cranial fragments. The elements all appear to be derived from an adult individual/s, according to their size, architectural character and cranial suture development (Buikstra & Ubelaker 1994, 32ff.; White & Folkens 2005, 369ff.; White *et al.* 2012, 389ff.). Although reliable sexually dimorphic criteria exist for sex assessment of human crania (Buikstra & Ubelaker 1994, 15ff.; White & Folkens 2005, 385ff.; White *et al.* 2012, 408ff.), these elements are too fragmentary to retain key anatomical landmarks for analyses. Although these fragments present a similar colour, character, expression of pathology, taphonomic change and there is no duplication of the fragments, it is not possible to state with certainty that they may all be attributed to the same individual. The extant elements are in fair condition. All damage is assessed to be *postmortem*.

Macroscopic observations:
The cranial fragments are observed to have abnormal endocranial impressions located on the cortical bone (Fig. 8.16). These endocranial impressions can be classified as hypervascularity consisting of diffuse vascular networks of shallow channel-like etching emitting from the meningeal grooves; one parietal fragment presents these impressions within the sagittal sinus. The margins are characterized to be smooth, rounded and well-demarcated. The remaining surrounding endocranial surface is uneven and flaky because of taphonomic change.

Lesion type: Lytic.
Lesion preservation: Good; Incomplete because of *postmortem* damage.
Differential diagnosis: Infectious; Metabolic; Endocrine.

Figure 8.16. *Assorted adult cranial fragments (FB0022) from Context (838) of the Circle, including parietal and non-diagnostic pieces. The fragments all exhibit abnormal endocranial focal impressions, classified as hypervascularity. Scale bar: 1 cm. (Photos Ronika. K. Power).*

8.5.2.10. FB0023: Frontal fragment

Context:	(1268)
Grid Ref:	98/110
Year of Excavation:	BR94
Other Details:	Unit 3 Spit 2

Element identification and preservation:
Fragment of adult frontal bone, consisting of the frontonasal suture, glabella, left supraorbital margin and a portion of the left frontal squama. *Postmortem* damage has fragmented and exposed the frontal sinus. The element appears to be derived from an adult individual, according to its size, architectural character and the pathology described below (Buikstra & Ubelaker 1994, 32ff.; White & Folkens 2005, 369ff.; White *et al.* 2012, 389ff.). Sex assessment is possible female, based on evaluation of the cranial sexually dimorphic traits presented in Buikstra and Ubelaker (1994, 20), including supraorbital margin (2/5), and supraorbital ridge/glabella (2/5). The extant element is in fair condition and represents ~10% of a complete cranium. All damage is assessed to be *postmortem*.

Macroscopic observations:
Proliferation of bone is observed on the endocranial surface of a fragment of frontal bone (Fig. 8.17). The lesion presents as a billowing mass of dense cortical bone either side of the frontal crest. The element is fragmentary, so the full extent of the lesion is not preserved. The extant portion of the lesion occupies the entire endocranial surface area extending approximately 73.5 mm superiorly from the endocranial aspect of nasion; approximately 24.8 mm to the right of the frontal crest (maximum extant portion); approximately 54.3 mm to the left of the frontal crest (intact); and is approximately 3.5 mm in height compared to the surrounding cortical surface. The greatest concentration of osseous deposition is observed immediately bilateral to the frontal crest. Small islands of bone deposition are observed at the lesion periphery on the left side, with maximum dimensions of 7.8 mm length by 4.4 mm width by 1.0 mm height. In some areas, the margins of the lesions are observed to sit proud of the endocranial cortex, but in other areas, and particularly in fragmented section, the proliferation merges with the underlying bone. No cranial sutures are retained on this fragment, so it is not possible to comment on the level of sutural fusion.

Cribra orbitalia is observed on the left orbital roof, occupying the complete anterior aspect. The maximum dimensions of the extant lesion are 23.4 mm length by 11.6 mm width. The lesion presents as capillary-like impressions, aligning with Stuart-Macadam's Type 1 lesion category (1991, 109, Figures 9.3a & b). The right orbital roof is fragmented and absent.

Radiological observations:
The lesion is observed as a proliferation of the diploic space within the frontal fossa, with extension into the

endocranial cavity and very little overlying cortical bone. The lesion presents a lobulated appearance. In places, the hypertrophic activity is observed to fold over itself in a wave-like organization – as illustrated by cross-section images (Fig. 8.17d). Multiple areas are observed where trabeculae extend up to the cortical surface. In this case, the proliferation is restricted to the trabecular component of the bone rather than the cortex – this is an exostosis similar to palatine and mandibular tori. The lesion does not present characteristic features of cortical osteoma or other hypertrophic expansions of diploic space into the cranial cavity, so these are excluded from differential diagnoses. The lesion does, however, exhibit characteristic features of *hyperostosis calvaria interna*, more specifically *hyperostosis frontalis interna* (Cvetković *et al.* 2018; Hershkovitz *et al.* 1999).

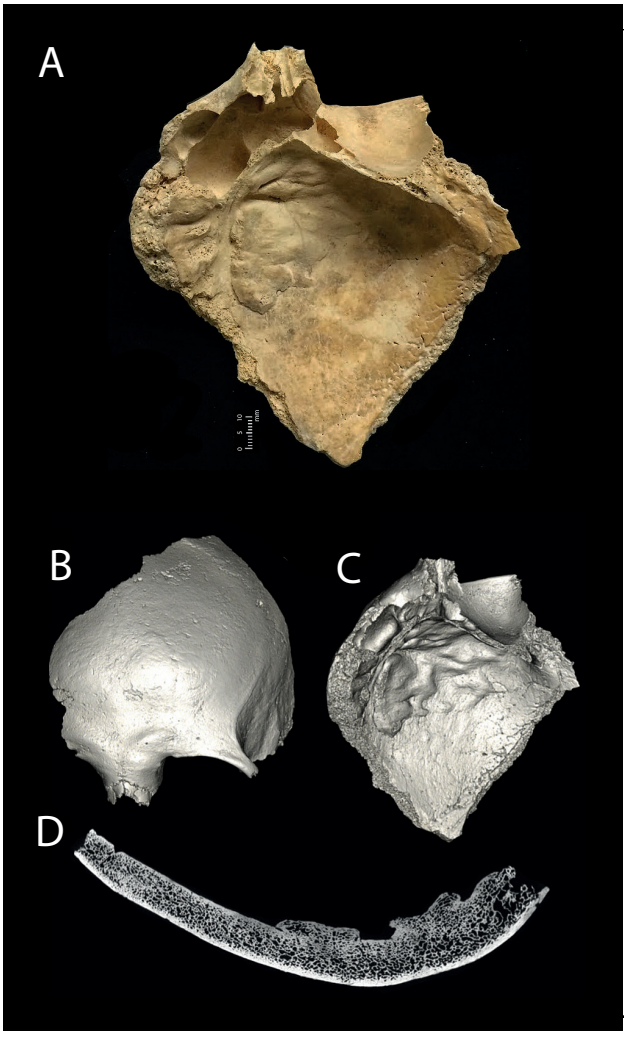

Figure 8.17. *A selection of photographic and radiological images pertaining to a fragment of adult possible female frontal bone (FB0023) from Context (1268) of the Circle sample, detailing a proliferative endocranial lesion within the frontal fossa, including: a) endocranial view; b) 3D render anterior view; c) 3D render endocranial view; d) cross-section from CT data. Scale bar: 1 cm (photograph only). (Photo Ronika. K. Power; radiological images captured by L. Buck, Cambridge Biotomography Centre; processed by J. Magnussen & M. Pardey, Macquarie Medical Imaging).*

Lesion type: Proliferative.
Lesion preservation: Excellent; Incomplete because of *postmortem* damage.
Differential diagnosis: Metabolic; Endocrine.

8.5.2.11. FB0024: Frontal fragment

Context:	(1268)
Grid Ref:	99/110
Year of Excavation:	BR94
Other Details:	Spit 3, Unit 3

Element identification and preservation:
Fragment of adult frontal bone, partial left and right nasal bones, partial frontal processes of left and right maxillae, partial right zygoma, and partial right greater wing of sphenoid. The extant frontal retains the frontonasal suture, glabella, left and right supraorbital margins and the majority of the frontal squama. *Postmortem* damage has fragmented and exposed the inferior aspect of the frontal sinus. The element appears to be derived from an adult individual, according to its size, architectural character and the pathology described below (Buikstra & Ubelaker 1994, 32ff.; White & Folkens 2005, 369ff.; White *et al.* 2012, 389ff.). Sex assessment is possible female, based on evaluation of the cranial sexually dimorphic traits presented in Buikstra and Ubelaker (1994, 20), including supraorbital margin (2/5), and supraorbital ridge/glabella (2/5). The extant element is in fair condition and represents ~15% of a complete cranium. All damage is assessed to be *postmortem*.

Macroscopic observations:
A small, discrete area of bone proliferation is observed on the endocranial aspect of a fragment of frontal bone (Fig. 8.18a-c). The lesion presents as a clearly demarcated, billowing concentration of dense cortical bone on the right side of the frontal crest, lateral to its approximate apex. Although the element is fragmentary, the lesion is observed to be intact. The maximum dimensions of the lesion are 12.4 mm length by 9.1 mm width by 1.9 mm height. The lesion appears to be continuous with the underlying endocranial cortex, with the exception of the most infero-lateral aspect on

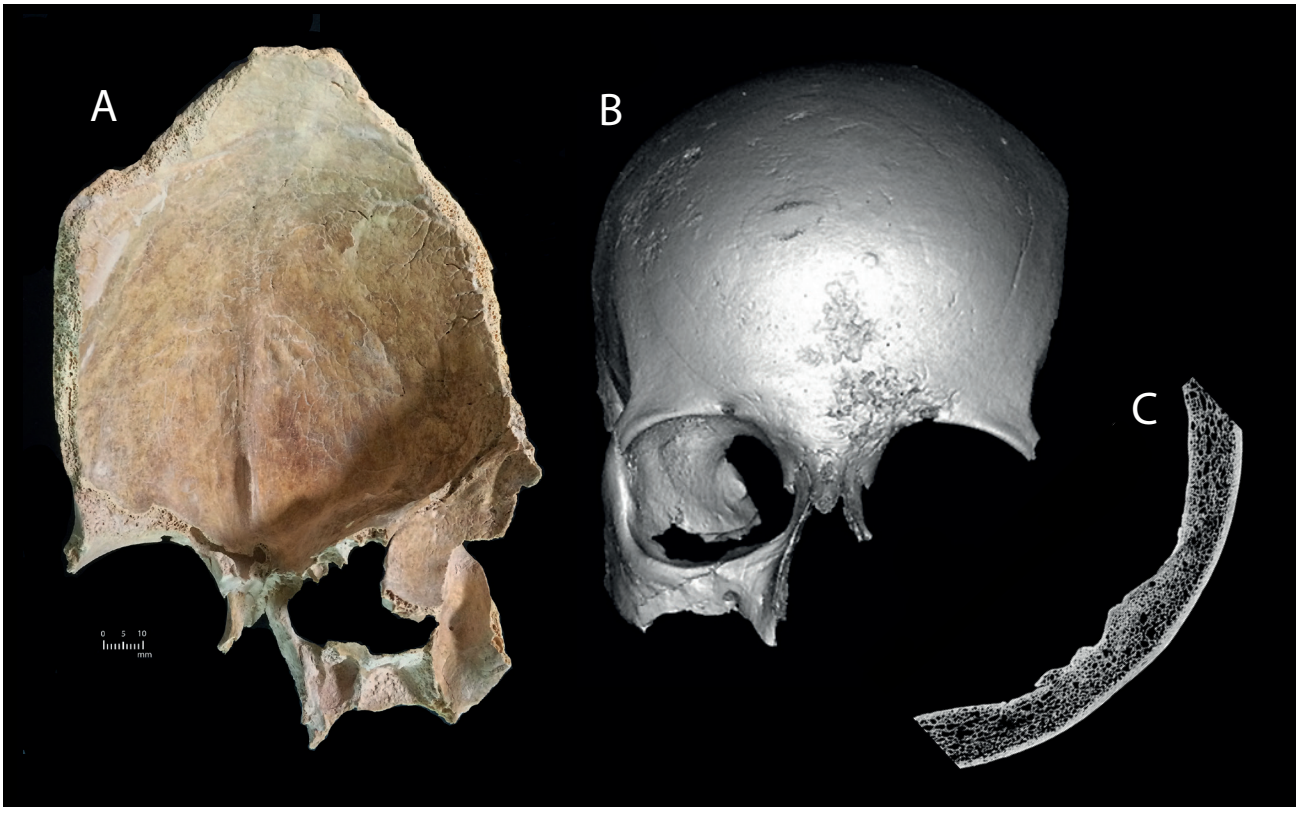

Figure 8.18. *A selection of photographic and radiological images pertaining to a fragmentary adult possible female cranium (FB0024), with extant portions of adult frontal bone, partial left and right nasal bones, partial frontal processes of left and right maxillae, partial right zygoma, and partial right greater wing of sphenoid from Context (1268) of the Circle sample, detailing a proliferative endocranial lesion within the frontal fossa, including: a) endocranial view; b) 3D rendered anterior view; c) cross-section from CT data. Scale bar: 1 cm (photograph only). (Photo Ronika. K. Power; radiological images captured by L. Buck, Cambridge Biotomography Centre; processed by J. Magnussen & M. Pardey, Macquarie Medical Imaging).*

the right side, which is observed to sit proud of the cortex. Note that a button osteoma is also observed on the ectocranial surface of the frontal bone, located approximately 43.3 mm supero-lateral to nasion on the left side (immediately lateral to the nasion-bregma subtense [FRF]; Howells 1973, 181). The lesion presents as a slightly domed, circular focal deposition of dense bone, approximately 3.5 mm Ø, 0.3 mm in height. The margins of the lesion are clearly demarcated and discontinuous with the cortical surface.

Cribra orbitalia is also observed in both orbital roofs. The left orbital roof is fragmented and only partially preserved, but the right orbital roof is intact. The *cribra orbitalia* observed in the right orbital roof, occupies the antero-lateral quadrant. The maximum dimensions of the lesion are 19.4 mm length by approximately 10.1 mm width. The lesions present as larger foramina with a tendency to cluster together and link into a trabecular structure, interspersed with capillary-like impressions, aligning with Stuart-Macadam's Type 4 lesion category (1991, 109, Figs. 9.3a & b). The lesion appears to have been active at the time of death.

Radiological observations:
The lesion is observed as a proliferation of the diploic space within the frontal fossa, with trabeculae extending into the cranial cavity and featuring very little overlying cortical bone. Here again, we see folding hypertrophic activity in places, as previously observed for FB0023 (§8.5.2.10, above), although less advanced in this case (Fig. 8.18c). The lesion is situated at the superior aspect of the frontal crest, calling for consideration as possible calcification associated with the superior sagittal sinus. It is, however, distinctly separate from the anterior aspect of the superior sagittal sinus, thus excluding this option. Further considerations should include falcine or parafalcine calcification, and calcified

meningioma of the frontal bone. Meningiomas are primary central nervous system tumours that arise from arachnoidal cap cells of the leptomeninges (arachnoid and pia mater; Oya *et al.* 2011; Sanson & Cornu 2000; Wiemels *et al.* 2010). They may be discounted on this occasion, however, as the extension of trabeculae does not resemble characteristic neoplastic involvement of the diploë. Rather, this appears to be another – albeit minor – case of *hyperostosis calvaria interna*, more specifically *hyperostosis frontalis interna* (Cvetković *et al.* 2018; Hershkovitz *et al.* 1999).

Lesion type: Proliferative.
Lesion preservation: Excellent; Incomplete because of *postmortem* damage.
Differential diagnosis: Metabolic; Endocrine.

8.5.2.12. FB0025: Frontal and parietal fragments

Context:	(960)
Grid Ref:	99/112
Year of Excavation:	BR94
Other Details:	Spit 4, Unit 10

Element identification and preservation:
Fragmentary adult frontal bone, consisting of the frontonasal suture, glabella, left and right supraorbital margins and a portion of the frontal squama. These fragments refit with additional fragments of the supero-medial aspects of the left and right parietal squamae. The elements appear to be derived from an adult individual, according to their size, architectural character, sutural development and the pathology described below (Buikstra & Ubelaker 1994, 32ff.; White & Folkens 2005, 369ff.; White *et al.* 2012, 389ff.). Sex assessment is possible male, based on evaluation of the cranial sexually dimorphic traits presented in Buikstra and Ubelaker (1994, 20), including supraorbital margin (4/5), and supraorbital ridge/glabella (4/5). The extant element is in fair condition and represents ~15% of a complete cranium. All damage is assessed to be *postmortem*.

Macroscopic observations:
Six refitting fragments of frontal and left and right parietal bones were examined. The largest two fragments of frontal and parietal and one small fragment of frontal exhibit pronounced, generalized, diffuse bone proliferation on the endocranial aspects (Fig. 8.19a-c). The two fragments of parietal bone exhibit general thickening of the diploë in the areas immediately bilateral to the sagittal suture (and sulcus), and across the left sagittal squama. These two fragments are continuous in character with the previously mentioned fragments, but do not refit directly. The lesion observed on the two fragments

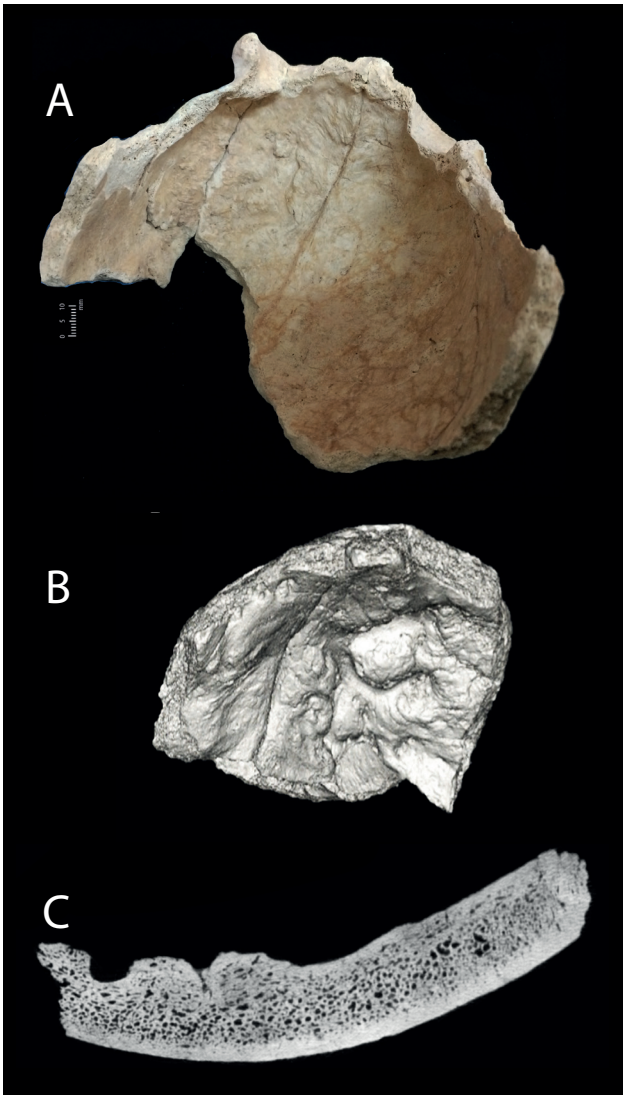

Figure 8.19. *A selection of photographic and radiological images pertaining to a fragmentary adult possible male cranium (FB0025), with extant portions of adult frontal bone from Context (960) of the Circle sample, detailing a proliferative endocranial lesion within the frontal fossa, including: a) endocranial view; b) 3D render endocranial view; c) cross-section from CT data. Scale bar: 1 cm (photograph only). (Photo Ronika. K. Power; radiological images captured by L. Buck, Cambridge Biotomography Centre; processed by J. Magnussen & M. Pardey, Macquarie Medical Imaging).*

of frontal and parietal and one small fragment of frontal present as extensive, billowing, massive bone proliferation, occupying the entire frontal fossa, bilateral to the frontal crest, extending superiorly past the sagittal sulcus towards the endocranial aspects of bregma and the sagittal suture, traversing onto the frontal angle of the

left parietal bone on the extant portion of the fragment. As a result of osseous proliferation, the frontal crest has been enveloped and now appears as a cleavage. As a result of fragmentation, the full extent of the lesion is not known. Arachnoid fovea are observed around the extant peripheral aspects of the lesion. When observed macroscopically, in both intact and fragmented portions of the lesion, the lesion appears to be continuous with the underlying endocranial cortex.

The two fragments of parietal bone are observed to be generally thickened in character. In section, the diploë is well-organized and the endo- and ectocranial cortices are clearly demarcated. A lesion is observed to traverse the entire extant supraorbital ridge-glabella complex on both left and right aspects of the frontal bone. The lesion presents as capillary-like impressions, interspersed with microporosity (<1.0 mm Ø). The lesion is most severe at the highest point of the supraorbital ridges, which are extremely robust on this individual. On the left side, the lesion is observed to extend inferiorly into the antero-medial aspect of the orbital roof. The lesion appears to have been healing at the time of death.

Radiological observations:
Once again, the endocranial lesion is observed as a proliferation of the diploic space within the frontal fossa, with trabeculae extending into the cranial cavity in an undulating organization and featuring very little overlying cortical bone. As reported for FB0023 and FB0024 (§8.5.2.10 & §8.5.2.11, above), we see folding hypertrophic osseous activity in places (Fig. 8.19c). The lesion presents sharply demarcated margins with no associated demineralization. This appears to be another case of *hyperostosis calvaria interna*, more specifically *hyperostosis frontalis interna* (Cvetković *et al.* 2018; Hershkovitz *et al.* 1999).

Lesion types: Proliferative; Lytic.
Lesion preservation: Good; Incomplete because of *postmortem* damage.
Differential diagnosis: Metabolic; Endocrine; Infectious.

8.5.2.13. FB0026: Frontal and parietal fragments

Context:	(979)
Grid Ref:	101/109
Year of Excavation:	BR93
Other Details:	Quad XA/H

Element identification and preservation:
Fragment of adult frontal and right parietal bones, consisting of glabella, left and supraorbital margins and orbital roofs and portions of the left and right frontal squama; however, there is significant *postmortem* damage to the right aspect of the frontal squama. A small portion of the supero-medial aspect of the right parietal squama is retained and continuous with the frontal fragment. Additional refitting parietal fragments are also retained. *Postmortem* damage has fragmented and exposed the frontal sinus. The element all appears to be derived from an adult individual, according to their size, architectural character, sutural development and the pathology described below (Buikstra & Ubelaker 1994, 32ff.; White & Folkens 2005, 369ff.; White *et al.* 2012, 389ff.). Sex assessment is possible male, based on evaluation of the cranial sexually dimorphic traits presented in Buikstra and Ubelaker (1994, 20), including supraorbital margin (4/5), and supraorbital ridge/glabella (4/5). The extant element is in fair condition and represents ~10% of a complete cranium. All damage is assessed to be *postmortem*.

Macroscopic observations:
Fragment of frontal and right parietal bones. Small, discrete areas of bone proliferation are observed on the endocranial aspect of a fragment of frontal and parietal bones. The lesion presents as four clearly demarcated, billowing concentrations of dense cortical bone islands bilateral to the apex of the frontal crest, plus plate-like lamellar osseous deposits bilateral to and overlying the frontal crest (Fig. 8.20a-d). There is also a lamellar osseous deposit on the right aspect of the frontal squama, approximately 22.5 mm supero-lateral to the apex of the frontal crest. Although the element is fragmentary, the extant lesion is observed to be intact, although its full extent is not known. The billowing cortical bone islands range in size from 4.5 mm length by 2.3 mm width by 0.7 mm height to 7.1 mm length by 6.6 mm width by 3.7 mm height. These aspects of the lesion are observed to be both continuous and discontinuous with the underlying endocranial cortex; the singular billowing deposit on the right aspect of the frontal fossa is continuous with the endocranial surface, while the three billowing deposits on the left aspect of the frontal fossa are continuous with the endocranial surface on the medial side, yet sit proud of the endocranial surface on the lateral side. The plate-like lamellar osseous deposits merge with the endocranial surface in their lateral and inferior aspects, yet sit proud of the cortex on their superior and medial aspects.

Capillary-like vascular impressions surround the billowing bone island deposits and traverse the plate-like lamellar deposits. These vascular impressions extend the entire extant length of the sagittal sulcus on this fragment, as well as the sagittal sulcus and its immediately bilateral area on refitted fragments. Note that all cranial sutures on all fragments of this

cranium are observed to be obliterated on both endo- and ectocranial surfaces.

Cribra orbitalia is observed on the left and right orbital roofs, occupying the antero-lateral quadrants. The maximum dimensions of the lesion are 20.8 mm length by 13.4 mm width on the left orbital roof and 17.4 mm length by 9.8 mm width on the right orbital roof. In both orbits, the lesion presents as capillary-like impressions, aligning with Stuart-Macadam's Type 1 lesion category (1991, 109, Figs. 9.3a & b).

A button osteoma is observed on the posterior aspect of the right parietal bone, approximately 37.0 mm lateral to lambda. The lesion presents as a slightly domed, irregularly shaped focal deposition of dense bone, approx. 10.0 mm in maximum Ø, 0.9 mm in height. The margins of the lesion are diffuse and continuous with the cortical surface.

Radiological observations:
Here again, we observe an endocranial lesion characterized by proliferation of the diploic space within the frontal fossa. Trabeculae extend into the cranial cavity as large lobulated ridges with very little overlying cortical bone. Vascular channels traverse through the trabeculae. As reported for FB0023, FB0024 and FB0025 (§8.5.2.10–12, above), we see folding hypertrophic osseous activity in places (Fig. 8.20c-d). The lesion presents sharply demarcated margins and there is no associated demineralization observed. This appears to be another case of *hyperostosis calvaria interna*, more

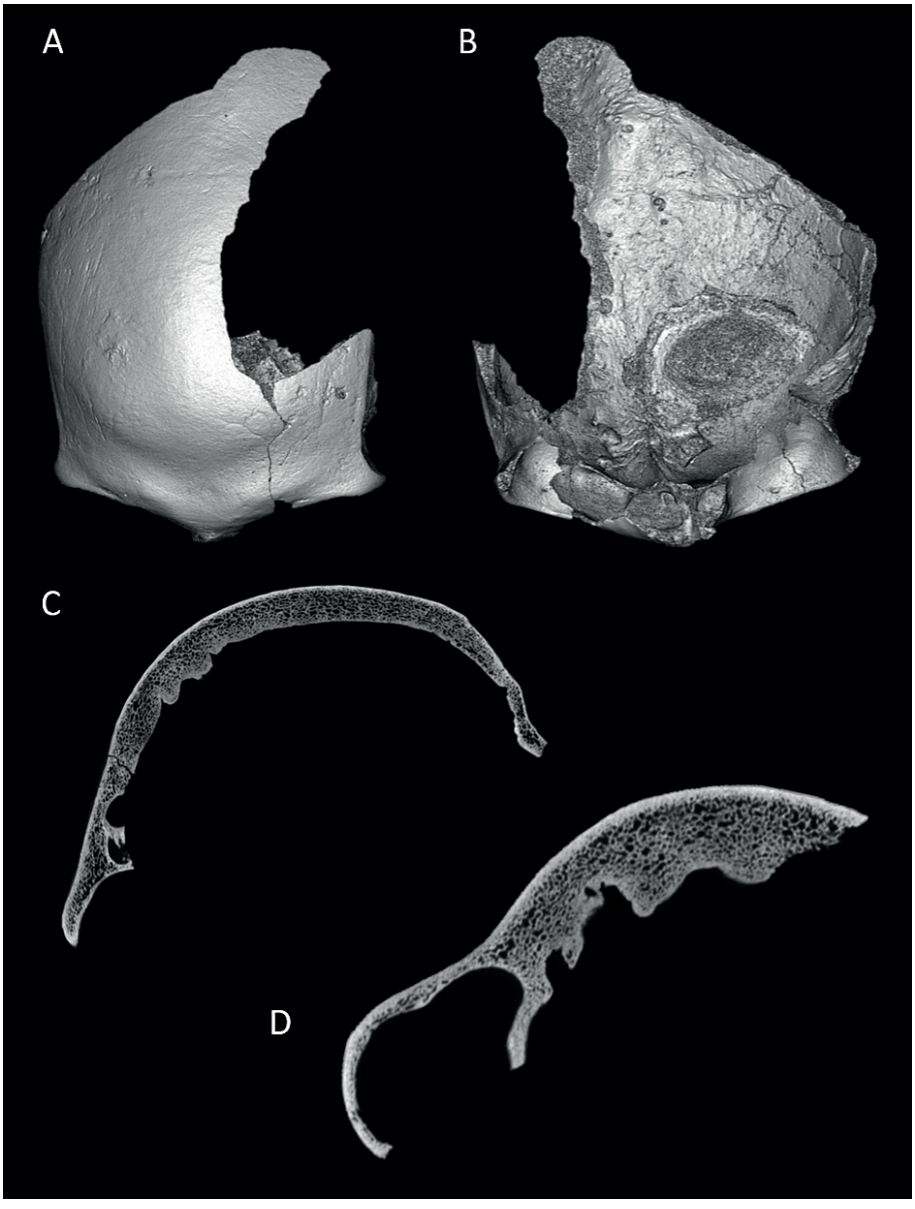

Figure 8.20. *A selection of radiological images pertaining to a fragmentary adult possible male cranium (FB0026), with extant portions of frontal and right parietal bones from Context (979) of the Circle sample, detailing a proliferative endocranial lesion within the frontal fossa, including: a) 3D render anterior view; b) 3D render endocranial view; c–d) cross-sections. Radiological images captured by L. Buck, Cambridge Biotomography Centre; processed by J. Magnussen & M. Pardey, Macquarie Medical Imaging.*

specifically *hyperostosis frontalis interna* (Cvetković *et al.* 2018; Hershkovitz *et al.* 1999).

Lesion types: Proliferative; Lytic.
Lesion preservation: Excellent; Incomplete because of *postmortem* damage.
Differential diagnoses: 1) Metabolic; Endocrine; 2) Neoplastic.

8.5.3. Post-cranial pathology
A selection of case studies featuring post-cranial pathology are presented below, including observations of vertebrae, humeri, ulnae, and a femur, tibia and fibula. Where available, radiological observations supplement macroscopic descriptions.

8.5.3.1. FB0031: Second cervical vertebra

Context:	(951)
Grid Ref:	n/d
Year of Excavation:	BR93
Other Details:	E3, No.37

Element identification and preservation:
Fragment of an adult second cervical vertebra (axis), consisting of the body, dens/odontoid process and a small portion of the left and right superior articular facets. Age estimation is based on the degree of fusion (Scheuer & Black 2000, 180ff.) and the extreme pathology described below. At present, there are no methods of sex assessment for isolated and fragmented vertebrae. The fragment represents ~30% of a complete second cervical vertebra. The extant element is in very good condition. All damage is assessed as *postmortem*.

Macroscopic observations:
When viewed both anteriorly and posteriorly, the dens is observed to be postero-laterally shifted on its axis towards the right side by approximately 10° (Fig. 8.21). When viewed anteriorly, the articular facet for the first cervical vertebra (atlas) is also observed to be postero-laterally displaced to the right side, again by approximately 10°. No fracture lines are observed with the naked eye.

Substantial osseous change is observed on the extant portion of the right superior articular facet (Fig. 8.21b); here, macroporosity of <2.0 mm Ø indicates the presence of subchondral cysts. In addition, ≥7 deep channels of striations traverse the extant facet face are observed, occupying a space of less than 2 cm^2. Eburnation is observed on the most lateral and superior aspects of the striations. Joint contour change is

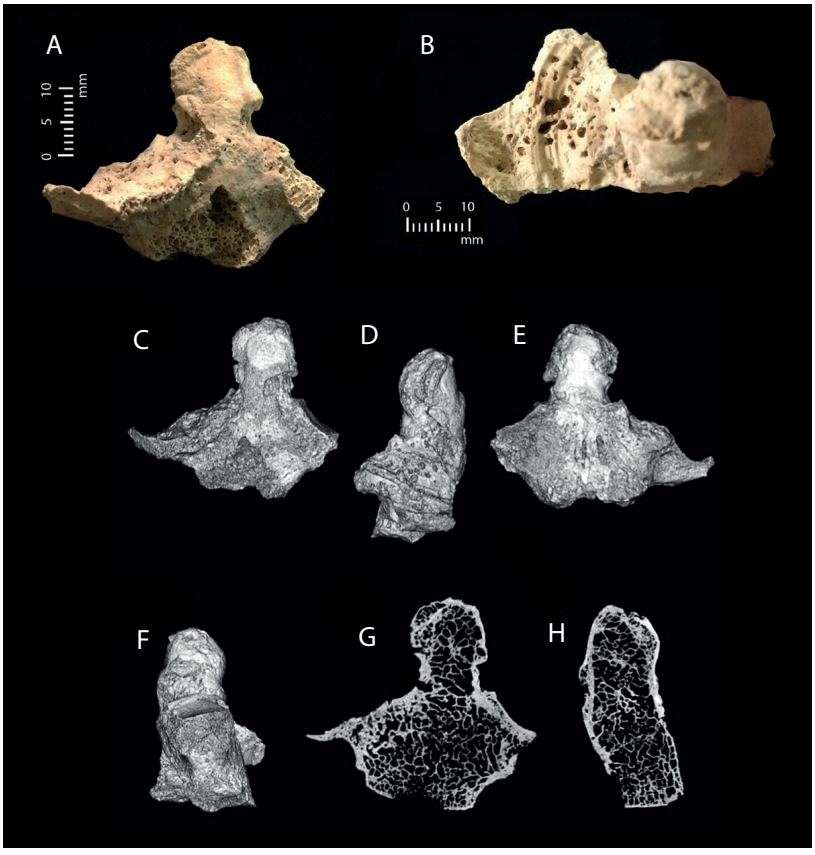

Figure 8.21. *A selection of photographic and radiological images pertaining to a fragmentary adult second cervical vertebra (axis) (FB0031) from Context (951) of the Circle sample, exhibiting severe degenerative joint disease and dysplasia: a) anterior view; b) superior view, displaying joint contour change and eburnation on right superior articular facet; c) 3D render anterior view; d) 3D render right lateral view; e) 3D render posterior view; f) 3D render left lateral view; g) coronal cross-section from CT data; h) sagittal cross-section. Scale bar: 1 cm (photographs only). (Photos Ronika K. Power; radiological images captured by L. Buck, Cambridge Biotomography Centre; processed by J. Magnussen & M. Pardey, Macquarie Medical Imaging).*

also apparent, with the extant medial and lateral borders of the facet appearing spread and diffused, and the postero-medial border of the facet extended in a medial direction, intruding into the vertebral foramen. No eburnation is observed on the dens articular facet for the first cervical vertebra and no osseous change is observed on the extant portion of the left superior articular facet. The osseous changes observed on the right superior articular facet are consistent with degenerative joint disease.

Radiological observations:
Observed subchondral cysts and morphological and joint contour changes to the right superior articular facet are consistent with advanced cervical osteoarthritis (Fig. 8.21g-h). Despite the described displacement of the dens, there is no radiological indication that a fracture was sustained by this element. In clinical cases, it is rare to see individuals aged 50+ without atlantoaxial joint contour change (Zapletal *et al.* 1995). The bony irregularity described for the odontoid process is most likely related to age and activity-related degenerative change.

Lesion type and healing status: Mixed; Dysplastic; Active.
Lesion preservation: Excellent.
Differential diagnosis: Degenerative Joint Disease; Activity-related change.

8.5.3.2. FB0029: Twelfth thoracic vertebra

Context:	(1024)
Grid Ref:	98/113
Year of Excavation:	BR93
Other Details:	n/d

Element identification and preservation:
Fragment of an adult twelfth thoracic vertebra, consisting of the vertebral body, neural arch and superior and inferior articular facets. The element has been evaluated to numerical order according to the position and orientation of the superior and inferior articular

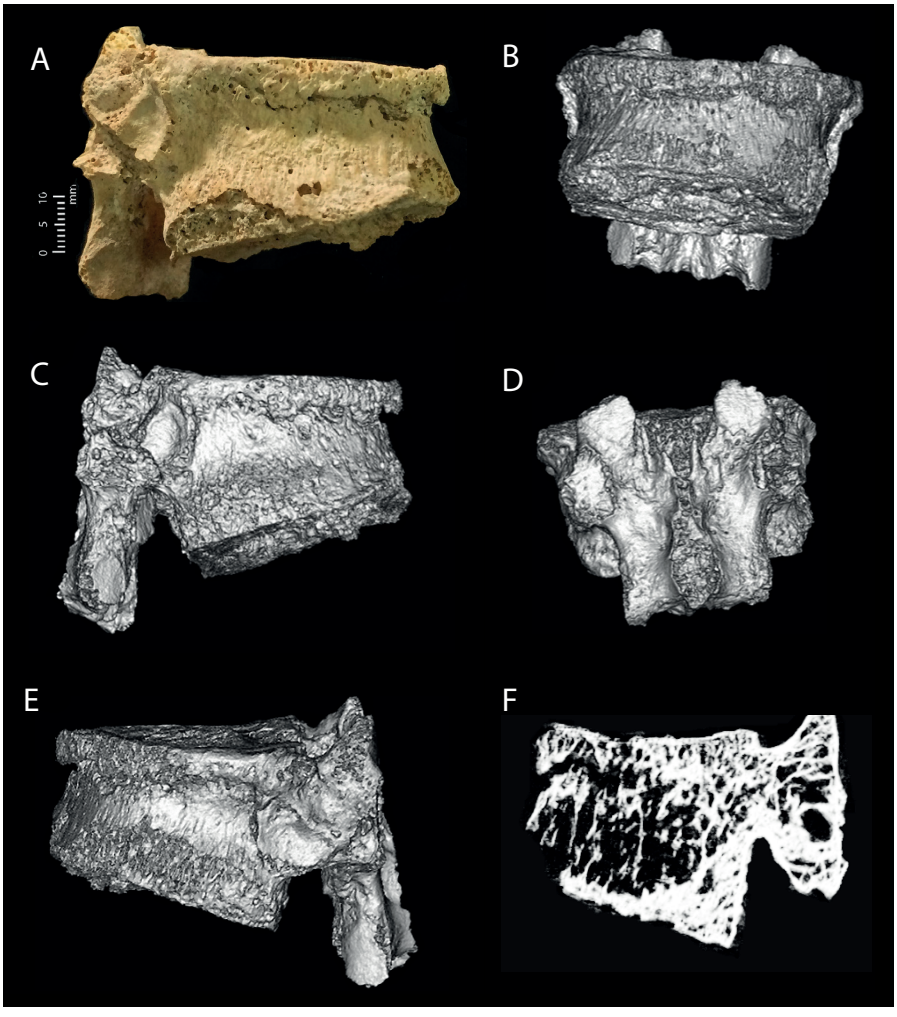

Figure 8.22. *A selection of photographic and radiological images pertaining to a fragmentary adult twelfth thoracic vertebra (FB0029) from Context (1024) of the Circle sample, exhibiting a compression fracture, intervertebral osteochondrosis and a Schmorl's Node: a) right lateral view; b) 3D render anterior view; c) 3D render right lateral view; d) 3D render posterior view; e) 3D render left lateral view; f) sagittal cross-section from CT data detailing fracture extending from anterior vertebral body through to the pedicle and pars interarticularis. Scale bar: 1 cm (photograph only). (Photo Ronika K. Power; radiological images captured by L. Buck, Cambridge Biotomography Centre; processed by J. Magnussen & M. Pardey, Macquarie Medical Imaging).*

facets and the costal articular facet. Age estimation is based on the degree of fusion of the overall element as well as the appearance and fusion of the superior and inferior annular rings (Scheuer & Black 2000: 183ff; esp. 211.). At present, there are no methods of sex assessment for isolated and fragmented vertebrae. The fragment represents ~30% of a complete second cervical vertebra. The extant element is in very good condition. All damage is assessed as *postmortem*.

Macroscopic observations:
The vertebral body exhibits a compression fracture on the anterior superior aspect (Fig. 8.22). The fracture is observed to be a clearly demarcated, approximately horizontal line that extends across the anterior and left and right lateral aspects of the vertebral body, approximately 6.5 mm immediately inferior to the superior border, terminating approximately 10.0 mm anterior to the costal articular facets on both left and right sides. The compression has resulted in the anterior aspect of the vertebral body assuming a wedge-shaped presentation: the height at the posterior aspect of the body is approximately 29.0 mm; while at the anterior aspect the body height is approximately 20.0 mm. Vertebral body fractures are commonly attributed to a vertical force-induced hyperflexion injury (Crawford-Adams 1983; Roberts & Manchester 2005, 105), which may include falling or jumping from a height and landing on the feet. This category of trauma is referred to as a compression fracture. Although compression fractures may occur as a result of vertical force injuries to healthy bone, differential diagnoses should also consider the possibility of underlying osteoporosis making the bone weak and susceptible to trauma (Brickley 2002; Brickley & Ives 2008; Roberts & Manchester 2005, 105).

There is a small amount of osseous change on the anterior superior aspect of the vertebral body, within the perimeter of the annular ring. This change presents as macroporosity (>1.0 mm Ø), cortical erosion and disorganization, which is slightly compromised by *postmortem* damage and diagenesis. It is likely that the changes described here are associated with degeneration of the cartilaginous joint surface of the intervertebral space (Roberts & Manchester 2005, 140). This type of degenerative disc disease is variably known as spondylosis and/or intervertebral osteochondrosis, presenting as porosity, pitting and disorganization of the vertebral body superior and/or inferior surfaces, sometimes accompanied by the formation of new bone (Rodgers 2000).

The inferior aspect of the vertebral body also presents osseous change, presenting as rough, irregular hypertrophy across the anterior third of the body, and also surrounding a convex feature on the posterior third of the body, which resembles a Schmorl's node. This change appears to be *antemortem* in nature and is thus not associated with the *perimortem* compression fracture described for this element, above. Schmorl's nodes are also associated with degenerative disc disease, whereby the herniating disc contents induce pressure erosion on the vertebral body surfaces (Roberts & Manchester 2005, 140; Rodgers 2000, 168). The specific aetiology of Schmorl's nodes is idiopathic (Park *et al.* 2015; Saluja *et al.* 1986), with associations ranging from trauma, infection, osteoporosis and neoplastic disease (Park *et al.* 2015; Resnick & Niwayama 1988). It should be noted that this element was identified within the same context as FB0030 (§8.5.3.3, below).

Radiological observations:
Anterior wedge compression fracture of the vertebral body, with 39% anterior height loss. The fracture line is visible through the vertebral body into the pedicle and *pars interarticularis*. There is significant disruption of the anterior body cortex, which is observed to have folded down upon itself as a result of the insult. Some trabeculae are observed to overlap posteriorly because of impaction, and a band of sclerosis above and below the fracture line in the posterior vertebral body indicates that the insult occurred moderately if not significantly *premortem*. This fracture has occurred alongside pre-existing severe osteoporosis; generalized demineralization and cortical bone loss is observed across the entire vertebral body, demonstrating osteopenia. An inferior endplate disc intrusion (Schmorl's node) is also observed.

Lesion types and healing status: Trauma; Mixed; Active.
Lesion preservation: Excellent; Incomplete because of fragmentation.
Differential diagnosis: Trauma; Metabolic; Degenerative Joint Disease.

8.5.3.3. FB0030: Lumbar vertebra

Context:	(1024)
Grid Ref:	98/113
Year of Excavation:	BR93
Other Details:	n/d

Element identification and preservation:
Fragment of an adult lumbar vertebral body of unknown order (possibly fourth or fifth – assessed according to the position and orientation of the extant superior articular facet); only the body, left pedicle and a portion of the left superior articular facet are extant. Age estimation is based on the degree of fusion of the overall element as well as the appearance and fusion

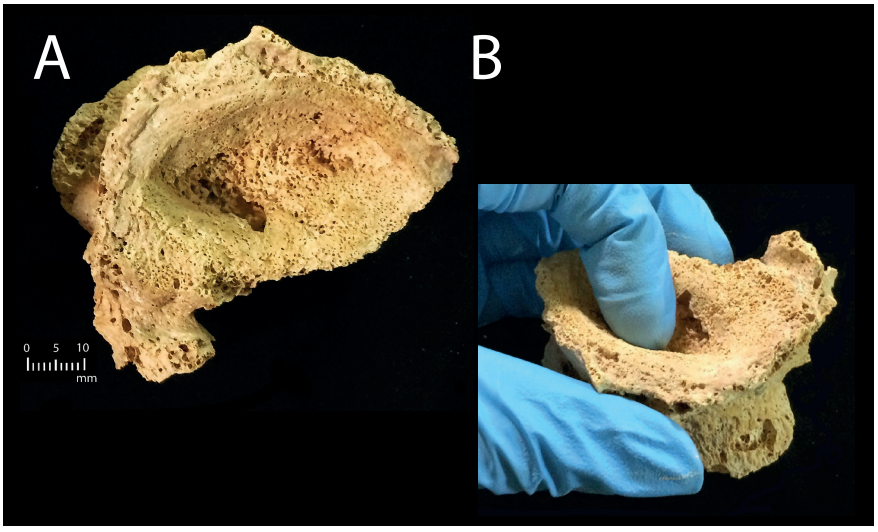

Figure 8.23. *Fragment of adult lumbar vertebral body of unknown order (FB0030) from Context (1024) of the Circle sample, exhibiting a central compression fracture: a) superior view; b) left supero-lateral view, detailing depth of central depression. Scale bar: 1 cm. (Photos Ronika K. Power).*

of the superior and inferior annular rings (Scheuer & Black 2000, 183ff; esp. 211.). At present, there are no methods of sex assessment for isolated and fragmented vertebrae. The fragment represents ~50% of a complete lumbar vertebra. The extant element is in very good condition. All damage is assessed as *postmortem*.

Macroscopic observations:
The extant portion of the vertebral body exhibits a compression fracture towards its central portion on the superior aspect on the coronal plane, creating a concave depression (Fig. 8.23a-b). On the anterior aspect of the body, the extant portion of this depression commences immediately posterior to the annular ring, and then steeply declines at an angle >45°; the depth of the compression fracture is approximately 13.6 mm. The fracture margin is discernible on the anterior aspect of the lesion, with the stark discontinuity of cortical bone presenting as an approximately straight line, adjacent to the exposed underlying trabeculae. At the antero-lateral aspects of the lesion, the fracture margin presents as V-shaped tears in the cortical bone, overlying the exposed trabeculae. *Postmortem* damage on the posterior and inferior aspects obfuscates the full extent of the lesion, so further observations are not possible.

As discussed above, vertebral body compression fractures are commonly attributed to a vertical force-induced hyperflexion injury (Roberts & Manchester 2005, 105). Although compression fractures may occur as a result of vertical force injuries to healthy bone, differential diagnoses should consider the possibility of underlying osteoporosis making the bone weak and susceptible to trauma (Brickley 2002; Brickley & Ives 2008; Roberts & Manchester 2005, 105). Marginal osteophytes are also observed on the left supero-antero-lateral aspects of the vertebral body.

It should be noted that this element was identified within the same context as FB0029 (§8.5.3.2, above). Considering these elements present similar forms of insult, it is possible that they may originate from the same individual. For further discussions of how pathology may assist in attempts to posthumously reunite individuals in highly fragmented and commingled assemblages, see §8.6, below.

Lesion type and healing status: Trauma; Healed.
Lesion preservation: Excellent; Incomplete because of *postmortem* damage.
Differential diagnosis: Trauma; Metabolic; Activity-related change.

8.5.3.4. FB0027: First lumbar vertebra

Context:	(1206)
Grid Ref:	99/111
Year of Excavation:	BR94
Other Details:	Unit 18

Element identification and preservation:
Fragmentary adult possible first lumbar vertebra. The position is estimated from the narrowness of the superior and inferior articular facets, and length and orientation of the spinous process in relation to the lamina. Approximately one-third of the vertebral body is extant on the left side, with the fragmentation margin observed to transect the body on the sagittal plane, exposing the trabecular bone. The remaining two-thirds of the vertebral body on the right side are not extant. The pedicle and right transverse process are also absent, and only the base of the right superior articular facet is extant. The apex of the left superior articular facet is also damaged, and the left transverse

process is broken and absent. Age estimation is based on the degree of fusion of the overall element as well as the appearance and fusions of the superior and inferior annular rings (Scheuer & Black 2000, 183ff; esp 211.). At present, there are no methods of sex assessment for isolated and fragmented vertebrae. The fragment represents ~65% of a complete lumbar vertebra. The extant element is in very good condition. All observed damage is attributed to *postmortem* processes.

Macroscopic observations:
The extant portion of the vertebral body exhibits a healed compression fracture towards its central portion on the superior aspect, creating a concave depression (Fig. 8.24a-e). The innermost extant portion of this depression is located approximately 17.1 mm posterior to the most anterior aspect of the vertebral body, and approximately 15.0 mm medial to the most lateral extant aspect of the vertebral body, and approximately 8.2 mm deep to the most lateral-superior extant aspect of the vertebral body. On the extant portion of the superior aspect of the vertebral body, a ridge of irregular, rough, disorganized bone of approximately 5.1 mm width and approximately 2.6 mm height is observed directly superior to the fracture margin, extending from the fragmentation margin in a curvilinear, postero-lateral direction across the surface to terminate at the supero-lateral margin of the vertebral body.

As discussed above, vertebral body compression fractures are commonly attributed to a vertical force-induced hyperflexion injury (Roberts & Manchester 2005, 105). Although compression fractures may occur as a result of vertical force injuries to healthy bone, differential diagnoses should consider the possibility of underlying osteoporosis making the bone weak and susceptible to trauma (Brickley 2002; Brickley & Ives 2008; Roberts & Manchester 2005, 105).

Many of the underlying trabeculae are damaged because of *postmortem* processes, so further observations are not possible. Eburnation is observed on the extant portion of the left superior and left and right inferior articular facets. On the left superior articular facet, a thin strip of eburnation is observed on the most antero-superior aspect of the extant facet border. As

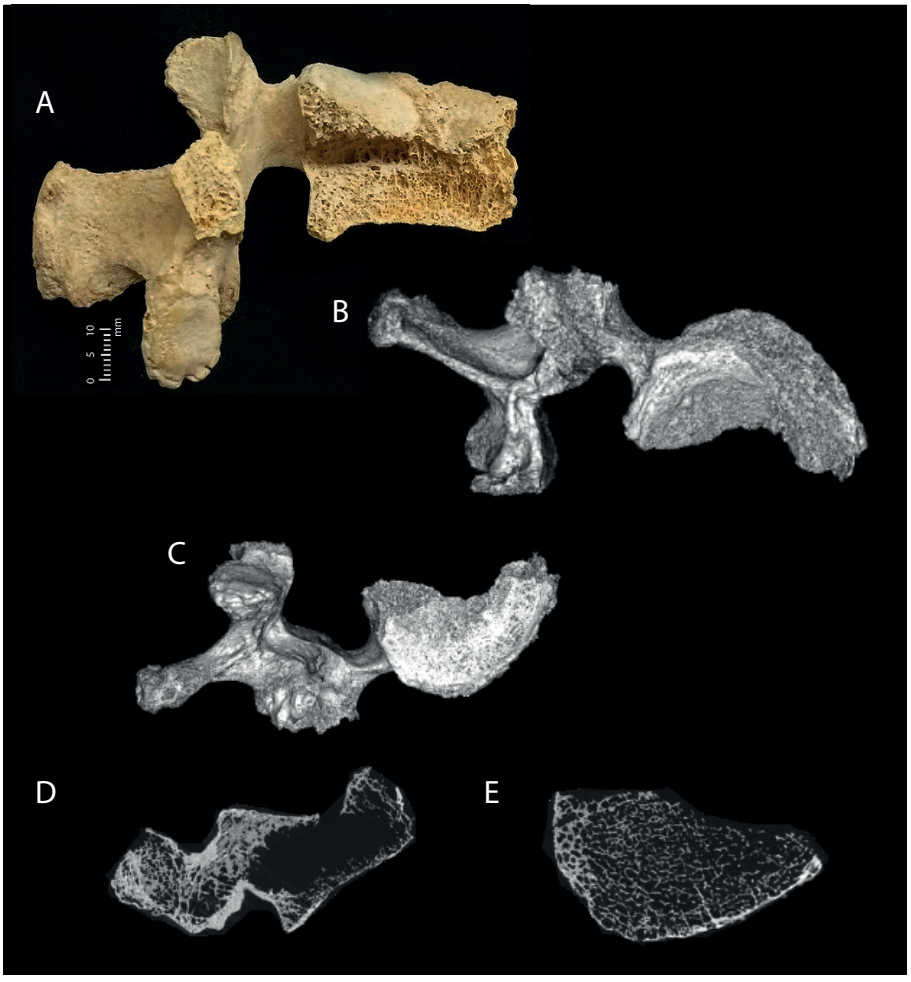

Figure 8.24. *A selection of photographic and radiological images of a fragment of adult possible first lumbar vertebra (FB0027) from Context (1026) of the Circle sample, exhibiting a central compression fracture: a) right lateral view; b) 3D render superior view; c) 3D render inferior view; d) sagittal cross-section from CT data detailing depth of central depression; e) transverse cross-section detailing osteopenia indicative of osteoporosis. Scale bar: 1 cm (photograph only). (Photos Ronika K. Power; radiological images captured by L. Buck, Cambridge Biotomography Centre; processed by J. Magnussen & M. Pardey, Macquarie Medical Imaging).*

a result of fragmentation, the full extent of the lesion is not known. The dimensions of the extant portion of the lesion are 5.2 mm length by 1.1 mm width. The lesion comprises a focal, narrow strip of dense, highly reflective bone. On the left inferior articular facet, tiny eburnation points are observed along the most postero-superior aspects of the facet border, extending across a length of approximately 11.3 mm. On the right inferior articular facet, eburnation is observed on the most postero-superior aspect of the facet in an approximate crescent-shaped lesion with maximum dimensions of approximately 11.5 mm length by 4.5 mm width; and tiny eburnation points are observed along the anterior aspect of the facet border, extending across a length of approximately 14.0 mm. In all aspects, the lesion is characterized as a discrete area of dense, highly reflective bone.

Radiological observations:
Significant vertebral endplate crush fracture. There has been an estimated 35% anterior height loss, and 56% central height loss (Fig. 8.24d). This is typical expression of central endplate collapse as opposed to a vertebral body compression fracture associated with purely traumatic origins. Here again, we observe characteristic signs of severe osteopenia indicative of osteoporosis – general demineralization and diminution of trabeculae (Fig. 8.24e). The vertebral body lost structural integrity and with axial loading the intervertebral disc has intruded into the end plate. Of the extant facet joints, there is evidence of moderate hypertrophic change in this individual, indicative of degenerative joint disease.

Lesion types and healing status: Trauma; Healed; Mixed; Active.
Lesion preservation: Excellent; Incomplete because of *postmortem* damage.
Differential diagnosis: Trauma; Degenerative Joint Disease; Metabolic.

8.5.3.5. FB0028: Lumbar vertebra

Context:	(951)
Grid Ref:	n/d
Year of Excavation:	BR94
Other Details:	Misc. A4

Element identification and preservation:
The element consists of a fragmented lumbar vertebral body of unknown order; only the body is extant. The body itself is incomplete, being fragmented anterior to the bilateral pedical bases and the anterior wall of the vertebral foramen. Age estimation is based on the degree of fusion of the overall element as well as the appearance and fusion of the superior and inferior annular rings (Scheuer & Black 2000, 183ff; esp 211). At present, there are no methods of sex assessment for isolated and fragmented vertebrae. The fragment represents ~45% of a complete lumbar vertebra. The extant element is in very good condition. All damage is assessed as *postmortem*.

Macroscopic observations:
The extant portion of the vertebral body exhibits a compression fracture towards its central portion on the superior aspect on the sagittal plane, creating a

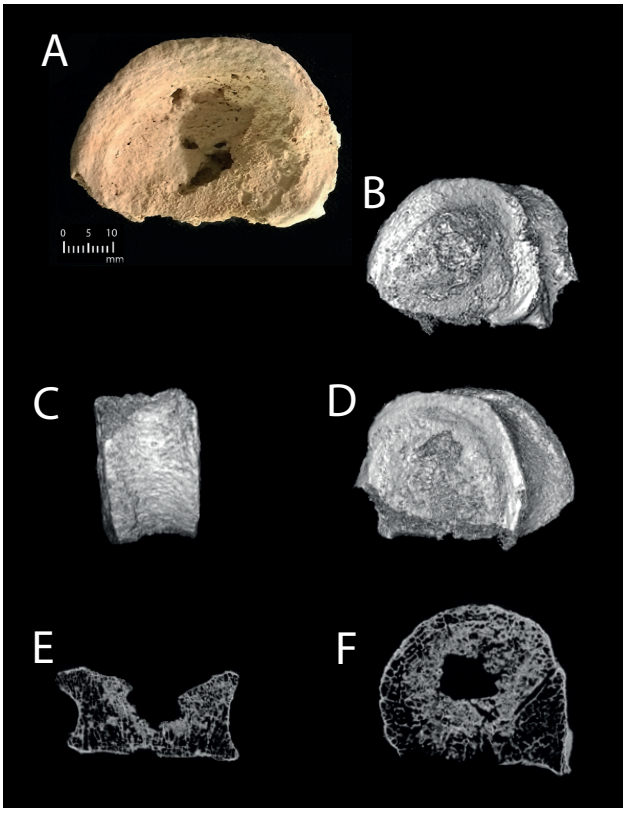

Figure 8.25. *A selection of photographic and radiological images of a fragment of adult lumbar vertebral body of unknown order (FB0028) from Context (951) of the Circle sample, exhibiting a central compression fracture: a) superior view; b) 3D render right supero-lateral view; c) 3D render anterior view; d) 3D render left infero-lateral view; e) coronal cross-section from CT data detailing depth of central depression; f) transverse cross-section detailing osteopenia indicative of osteoporosis. Scale bar: 1 cm (photograph only). (Photos Ronika K. Power; radiological images captured by L. Buck, Cambridge Biotomography Centre; processed by J. Magnussen & M. Pardey, Macquarie Medical Imaging).*

concave depression (Fig. 8.25a-f). On the anterior aspect of the body, the extant portion of this depression commences immediately posterior to the annular ring, and then steeply declines at an angle >45°; the true depth of the compression fracture is unable to be determined because of *postmortem* damage. One aspect of the fracture margin is extant on the right anterior superior aspect of the vertebral body, with a sharp discontinuity between the cortical surfaces on either side of the margin, while the cortical surfaces are still intact. *Postmortem* damage on the posterior and central aspects obfuscates the full extent of the lesion, so further observations are not possible.

As discussed above, vertebral body compression fractures are commonly attributed to a vertical force-induced hyperflexion injury (Roberts & Manchester 2005, 105). Although compression fractures may occur as a result of vertical force injuries to healthy bone, differential diagnoses should consider the possibility of underlying osteoporosis making the bone weak and susceptible to trauma (Brickley 2002; Brickley & Ives 2008; Roberts & Manchester 2005, 105).

Radiological observations:
Another vertebral endplate crush fracture. There has been significant disc intrusion through the endplate; the element has lost approximately 30% height overall with bowing of the endplate, and 72% height centrally at the site of disc intrusion (Fig. 8.25e-f). The margins are observed to be quite sclerotic; implying this insult occurred a long time before death. The insult has once again occurred because of pre-existing moderate trabecular loss, demonstrating osteopenia, characteristic of osteoporosis. Although the insult appears to be more extreme than those described for FB0027 and FB0029 (§8.5.3.4 & §8.5.3.2, above), the underlying osteopenic condition appears to be slightly less severe (Fig. 8.25f).

Lesion type and healing status: Trauma; Healed.
Lesion preservation: Excellent; Incomplete because of *postmortem* damage.
Differential diagnosis: Trauma; Metabolic.

8.5.3.6. FB0032: Lumbar vertebra

Context:	(662)
Grid Ref:	98-99/107
Year of Excavation:	BR91
Other Details:	Quad X

Element identification and preservation:
Fragment of an adult lumbar vertebra of unknown order (possibly fourth or fifth – assessed from the position and orientation of the extant superior articular facet); only the body, right pedicle and a portion of the left superior articular facet and lamina are extant. Age estimation is based on the degree of fusion of the overall element as well as the appearance and fusions of the superior and inferior annular rings (Scheuer & Black 2000, 183ff; esp. 211). At present, there are no methods of sex assessment for isolated and fragmented vertebrae. The fragment represents ~30% of a complete second cervical vertebra. The extant element is in very good condition. All damage is assessed as *postmortem*.

Macroscopic observations:
The extant portion of the vertebral body exhibits a compression fracture on the left supero-lateral aspect on the sagittal plane, creating a concave depressio*n* (Fig. 8.26). On the anterior aspect of the body, the extant portion of this depression commences immediately posterior to the annular ring, and then steeply declines at an angle of >45°; the maximum extant depth of the compression fracture is approximately 3.6 mm, however the full extent of the lesion is obfuscated as a result of *postmortem* damage. The fracture margin is discernible on the anterior aspect of the lesion, with the compression of the superior border of the body creating a ridge approximately 5.0 mm thick, which traverses the entire anterior aspect of the body. The compression has resulted in the anterior aspect of the vertebral body assuming a wedge-shaped presentation: the height at the posterior aspect of the body is approximately 26.5 mm; while at the anterior aspect the body height is approximately 19.5 mm. All bone surrounding the fracture site is intact and continuous, there is no evidence of new bone deposition, so the insult is determined to have occurred *antemortem* and is

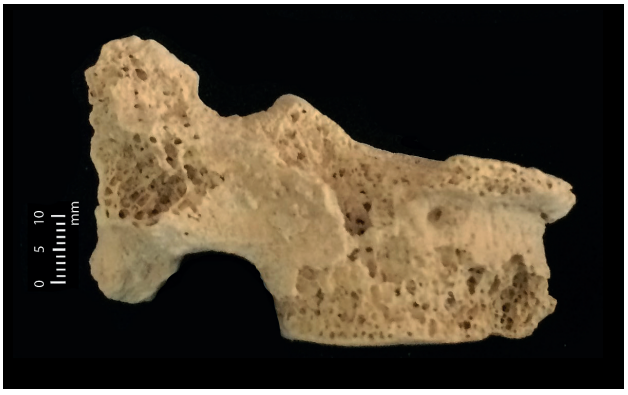

Figure 8.26. *Fragment of adult lumbar vertebral body of unknown order (FB0032) from Context (662) of the Circle sample, exhibiting an anterior compression fracture; right lateral view. Scale bar: 1 cm. (Photo Ronika K. Power).*

fully healed. *Postmortem* damage on the posterior and inferior aspects obfuscates the full extent of the lesion, so further observations are not possible.

As discussed above, vertebral body compression fractures are commonly attributed to a vertical force-induced hyperflexion injury (Roberts & Manchester 2005, 105). Although compression fractures may occur as a result of vertical force injuries to healthy bone, differential diagnoses should consider the possibility of underlying osteoporosis making the bone weak and susceptible to trauma (Brickley 2002; Brickley & Ives 2008; Roberts & Manchester 2005, 105). Marginal osteophytes are observed on the right infero-lateral aspects of the vertebral body – the full extent of osteophyte development is obfuscated as a result of *postmortem* damage.

Lesion types and healing status: Trauma; Healed; Proliferative.
Lesion preservation: Excellent, Incomplete because of *postmortem* damage.
Differential diagnosis: Trauma; Metabolic; Activity-related change.

8.5.3.7. FB0007: Humerus

Context:	(951)
Grid Ref:	n/d
Year of Excavation:	BR94
Other Details:	B1–13

Element identification and preservation:
Fragment of a right adult humerus. At the distal aspect, the element is fragmented inferior to the deltoid tuberosity so that approximately half of the diaphysis is retained. At the proximal aspect, the element is fragmented at the approximate surgical neck so that the supero-medial features are absent, including the humeral head. Proximally and anteriorly the fragmentation line is medial to the lesser tubercle running inferiorly to the approximate surgical neck. Posteriorly, only part of the trabecular bone is retained in the region of the head and surgical neck. The fragmentation described here pertains to *postmortem* damage, however it is important to note that the extant element was severely dysplastic *in vivo*, as discussed further, below. It is thus difficult to attribute the extant features to typical anatomical landmarks. As a result of the *postmortem* fragmentation, it is likely that some observations of pathology are obfuscated. Adult age estimation is based on the extant size of the element as well as the relative thickness of the diaphyseal cortex. At present, there are no reliable methods of sex assessment for isolated humeri. Although Bass (1995, 156) reports on several methods based on metric analyses including the head vertical and transverse diameters (Dittrick 1979; Dittrick & Suchey 1986; Dwight 1905; Krogman 1962; Stewart 1979); length and epicondylar width (Thieme 1957; Rodgers 1999); and a single variable complex (France 1983), there is still little confidence in these methods as reliable stand-alone indicators of sexual dimorphism without further studies. A further non-metric approach to sex assessment of the adult humerus is that proposed by Trotter (1934) whereby the septal aperture (or supratrochlear foramen) occurs slightly more frequently in females than males. In any case, the element under study is too fragmentary and dysplastic to submit to any of these modes of analysis. The fragment represents ~55% of a complete humerus. The extant element is in good condition. All damage is assessed as *postmortem*.

Macroscopic observations:
A complex non-reduced healed fracture is observed on the proximal metaphysis and proximal half of the diaphysis of the right humerus (Fig. 8.27a-h). The lesion is located at the approximate surgical neck. The element is severely dysplastic as a result of the fracture complex which includes at least one complete oblique displaced fracture and one metaphyseal compression/crush fracture. When viewed anteriorly, the extant proximal third of the humeral metaphysis has been infero-laterally displaced (Fig. 8.27a), possibly associated with a complete oblique displaced fracture. When viewed medially, the humeral head is posteriorly and inferiorly displaced (Fig. 8.27b), possibly associated with a metaphyseal compression/crush fracture.

From posterior and lateral views, bony callus is observed to envelop the lateral aspect of the diaphysis (Fig. 8.27c-d), with the extant portion emanating from a point 12.3 mm superior to the most superior aspect of the deltoid tuberosity and extending 39.9 mm in a supero-lateral direction. When viewed anteriorly (Fig. 8.27a), bony callus is also observed to extend from the diaphysis to meet the displaced complete fracture fragment approximately 38.9 mm inferior to the superior aspect of the greater tubercle. The anterior portion of bony callus emanates approximately 8.8 mm directly anterior to the most superior aspect of the deltoid tuberosity. Posteriorly the bony callus is 39.0 mm in length and has a maximum width of 30.1 mm. The maximum antero-posterior width of the callus is 25.7 mm.

The surface of the bony callus is observed to be smooth and even in some areas, while undulating, billowing and/or porous in others. The undulating areas are characterized by peaks and troughs of new bone deposition with diffuse circular and oval pitting.

Figure 8.27. *A selection of photographic and radiological images pertaining to a fragmentary adult right humerus (FB0007) from Context (951) of the Circle sample, detailing a complex non-reduced healed fracture of the proximal metaphysis and diaphysis in the region of the surgical neck, including: a) anterior view; b) medial view; c) posterior view; d) lateral view; e) coronal cross-section from CT data; f–h) transverse cross-sections of varying heights moving superiorly to inferiorly through the bony callus. Scale bar: 1 cm (photographs only). (Photos Ronika K. Power; radiological images captured by L. Buck, Cambridge Biotomography Centre; processed by J. Magnussen & M. Pardey, Macquarie Medical Imaging).*

The pits range from 0.6–4.6 mm Ø, meaning that both macroporosity and microporosity are observed; the pits are generally well-defined with smooth margins. The extent and character of the extant callus and the associated porosity suggests that the element may have been subject to infectious processes such as osteomyelitis which were no longer active at the time of death of the individual. As a result of the *post-mortem* fragmentation, it is impossible to assess reliably the overall healing status of the complex fracture of this element.

Postmortem fragmentation enables components of the fracture complex to be observed in cross-section. As a result, a possible third complete transverse fracture is observed for the diaphysis approximately 56.4 mm supero-medial to the most superior point of the deltoid tuberosity. New bone deposition is observed on the margin of this transverse fracture, indicating that it had not unified with any associated superior bone fragments within the fracture complex.

Roberts and Manchester report that humerus fractures are not common in archaeological populations (2005, 105), so the evidence presented here is particularly valuable to the palaeopathological discourse. Clinical reports provide indications that proximal humerus fractures are most often observed in elderly women with osteoporosis who have suffered a falling accident (Crawford-Adams 1983; cf Buhr & Cooke 1959; Roberts & Manchester 2005, 95). In the absence of any other diagnostic elements or biomolecular analyses, however, the demographic profile of this individual remains unknown.

Radiological observations:
A great deal of osseous remodelling is observed radiologically for the proximal aspect of the humerus (Fig. 8.27e-h). The diaphyseal cortex appears demineralized and denuded, indicative of disuse atrophy. The new bone deposition is not of a high density or quality, but rather it is comprised of several thin layers with

a porotic appearance. There is a discernible margin between the original cortex and the new bone. The features observed here nonetheless indicate that the cortex was being re-established with some ongoing biomechanical stress and weightbearing at the time of death – although the poor quality and density of the remodelled bone and underlying cortex are suggestive of prolonged disuse atrophy. It is apparent that this individual has survived for a long time after the initial insult, indicative of a level of care administered to them within their community while recuperating from this very serious injury.

The fractures described above are most likely because of a combination of impaction, rotation and comminution – potentially associated with a falling accident, direct trauma, and/or rotational injuries (especially forced external rotation), in isolation or combination. Areas of irregular dysplastic bone could be *myositis ossificans traumatica*, or partially resorptive change associated with comminuted fragments being resorbed into surrounding tissue; it is not possible to distinguish between them radiologically.

Lesion type and healing status: Trauma; Healing.
Lesion preservation: Good; Incomplete because of *postmortem* damage.
Differential diagnosis: Trauma.

8.5.3.8. FB0015: Humerus

Context:	(951)
Grid Ref:	n/d
Year of Excavation:	BR93
Other Details:	G1, No.42

Element identification and preservation:
Right adult humerus, fragmented proximally and distally *postmortem*. The proximal fragmentation margin is located at the approximate mid-shaft of the diaphysis, inferior to the deltoid tuberosity. The proximal fragments of this element are not retained. At the distal aspect, the element is fragmented in an approximately diagonal manner across the metaphysis. The fragmentation margins are sharp and linear, indicative of excavation trauma. From an anterior perspective, the fragmentation line transects the lateral epicondyle, radial fossa, coronoid fossa and medial epicondyle. The distal fragment is retained. Adult age estimation is based on the size of the extant element, the relative thickness of the diaphyseal cortex and the complete fusion of the distal epiphysis (Scheuer & Black 2000, 274). As discussed above, there are currently no reliable methods of sex assessment for isolated humeri. The fragment represents ~55% of a complete humerus and is in excellent condition. All damage is assessed as *postmortem*.

Figure 8.28. *Fragment of adult right humerus (FB0015) from Context (951) of the Circle sample, exhibiting dysplasia of the of the mid-diaphysis; anterior view. Scale bar: 1 cm. (Photo Ronika K. Power).*

Macroscopic observations:
The mid-shaft of the diaphysis is dysplastic (Fig. 8.28). When viewed anteriorly, the extant supero-lateral aspect of the fragmented diaphysis is observed to be misshapen, bowing laterally relative to the infero-lateral aspect of the element. The most infero-lateral point of this misshapen area may be placed at approximately 36.4 mm from the most superior extant point of the lateral aspect of the diaphysis. The character of the cortical surface of this area is even and smooth and generally continuous with the surrounding bone surface, except for the most inferior aspect which is more rugose.

When viewed anteriorly, the medial aspect of the diaphysis communicates with the previously mentioned dysplasia by reflecting slight misalignment through bowing parallel to the lateral aspect of the element at this level. Inferior to this described dysplasia,

the diaphysis descends inferiorly in a normal manner. When viewed laterally it is possible that the distal aspect of the element may curve anteriorly.

The dysplasia is attributed to a healed fracture with associated displacement of muscle attachments subsequent to healing; the continuous and even character of the cortical surface in the region of the feature is suggestive of this being a historic insult. As discussed above, humerus fractures are infrequently observed in archaeological populations and as such this example is of particular interest for understanding lived experiences of trauma and care within Neolithic Maltese populations.

Lesion type and healing status: Trauma; Healed.
Lesion preservation: Excellent; Incomplete because of *postmortem* damage.
Differential diagnosis: Trauma; Congenital variation; Activity-related change.

8.5.3.9. FB0008: Ulna

Context:	(354)
Grid Ref:	n/d
Year of Excavation:	BR89
Other Details:	Area 3, Unit 75

Element identification and preservation:
Right adult ulna, fragmented distally *postmortem*. The fragmentation margin is located in the distal quarter of the diaphysis, transecting the superior aspect of the pronator ridge. The distal fragment is not retained. There is a slight amount of *postmortem* damage observed on the infero-medial aspect of the olecranon, on the medial margin of the trochlear notch, extending onto the coronoid process. Adult age estimation is based on the size of the extant element, the relative thickness of the diaphyseal cortex and the complete fusion of the proximal epiphysis (Scheuer & Black 2000, 298ff.). Although Purkait (2001) devised

Figure 8.29. *A selection of photographic and radiological images pertaining to a fragmentary adult right ulna (FB0008) from Context (354) of the Circle sample, detailing a healed fracture of the distal diaphysis, including: a) antero-medial view; b) 3D render posterior view; c) 3D render postero-lateral view; d) 3D render anterior view; e) coronal cross-section from CT data; f–g) transverse cross-sections moving superiorly to inferiorly through the bony callus, detailing fracture dynamics. Scale bar: 1 cm (photograph only). (Photos Ronika K. Power; radiological images captured by L. Buck, Cambridge Biotomography Centre; processed by J. Magnussen & M. Pardey, Macquarie Medical Imaging).*

a discriminant function for metric sex assessment of ulnae, it is not widely applied as it is yet to be comprehensively tested beyond the population on which it was based. As such, there are currently no reliable methods of sex assessment for isolated ulnae (Bass 1995, 175; White & Folkens 2005). The fragment represents ~90% of a complete ulna and is in very good condition. All damage is assessed as *postmortem*.

Macroscopic observations:
A healed fracture is observed on the distal third of the diaphysis of the right ulna (Fig. 8.29a-g). The element is slightly dysplastic as a result of the fracture which has healed completely. When viewed anteriorly, the healed fracture margin runs from a point along the interosseous crest 147.5 mm inferior to the most inferior point of the radial notch; the fracture margin then diverts infero-medially 14.9 mm superior to the most superior point of the pronator ridge.

Bony callus is observed to envelop the entire circumference of the diaphysis in the location of the fracture; when viewed anteriorly the maximum callus length is 31.8 mm and maximum width is 19.1 mm. The extant surface of the bony callus across this feature is continuous in character with the surrounding bone. When viewed medially an oval-shaped area of *postmortem* damage is observed in the bony callus 25.9 mm supero-posterior to the pronator ridge.

Forearm and wrist (radius and ulna) fractures have been observed in both archaeological and modern populations across cultures (Buhr & Cooke 1959; Judd 2000; Roberts & Manchester 2005). It is likely that this fracture was caused by an acute and direct insult to the forearm *in vivo* (Roberts & Manchester 2005, 90), either as a result of intentional interpersonal violence (such as defending a blow to the head) or accidental injury, such as a falling accident or misadventure involving animals (Judd 2004; Jurmain 1999).

Radiological observations:
A completely healed transverse fracture is observed in the distal third of the ulna diaphysis with minor residual angulation and discontinuity of the underlying native cortex (Fig. 8.29e-g). Periosteal new bone has bridged the defect and has been exuberant in activity. The fracture is completely healed but malaligned. Malalignment is approximately 15°; and the offset at the fracture site is approximately 34% (Fig. 8.29*e*). There is no evidence of sequestrum or involucrum, and no evidence of infection. The periosteal new bone is trabeculated, indicating that this is a very old fracture, which occurred many years before death (Fig. 8.29f-*g*). Transverse fractures of the distal ulnar diaphysis are commonly associated with self-defence – so-called 'parry' or 'nightstick' fractures, named from injuries sustained by modern individuals' holding up the forearm in front of the face to defend themselves when struck with a police baton, or any direct trauma to the forearm (Ali *et al.* 2019; Cai *et al.* 2013; Court-Brown & Caesar 2006; Cybulski 2014; Du Toit & Gräbe 1979; Glencross & Boz 2014; Hooper 1974; Klaus 2014; Knüsel & Smith 2014, 10; Ortner 2003; Redfern 2015; Roberts & Manchester 2005; however, cf Judd 2008). Falls and twisting injuries more commonly result in spiral fractures (Mackay *et al.* 2000), which lead to a greater extent of periosteal and cortical remodelling than observed for this individual.

Lesion type and healing status: Trauma; Healed
Lesion preservation: Excellent.
Differential diagnosis: Trauma; Congenital variation; Activity-related change.

8.5.3.10. FB0009: Ulna

Context:	(951)
Grid Ref:	n/d
Year of Excavation:	BR93
Other Details:	H1, No.6

Element identification and preservation:
Left adult ulna, fragmented and complete. The element is fragmented distal to the midpoint of the diaphysis. The fragmentation margins are clean and sharp, and both retained proximal and distal fragments perfectly refit. Adult age estimation is based on the size of the extant element, the relative thickness of the diaphyseal cortex and the complete fusion of the proximal epiphysis (Scheuer & Black 2000, 298ff.). As previously mentioned, there are currently no reliable methods of sex assessment for isolated ulnae (Bass 1995, 175). The extant element is in excellent condition. All damage is assessed as *postmortem*.

Macroscopic observations:
A healed fracture is observed on the distal quarter of the diaphysis of the left ulna (Fig. 8.30a-f). The element is slightly dysplastic; it is observed that the distal quarter of the diaphysis is misaligned in a lateral direction by 10°. This dysplasia is also clearly observed from a posterior aspect. The extant surface area surrounding the fracture is continuous in character with the surrounding bone and the fracture margin is not visible. When viewed anteriorly the most infero-lateral aspect of the healed fracture is located 21.4 mm superior to the most infero-lateral aspect of the radial articulation.

It is likely that this fracture was caused by an acute and direct insult to the forearm *in vivo* (Roberts

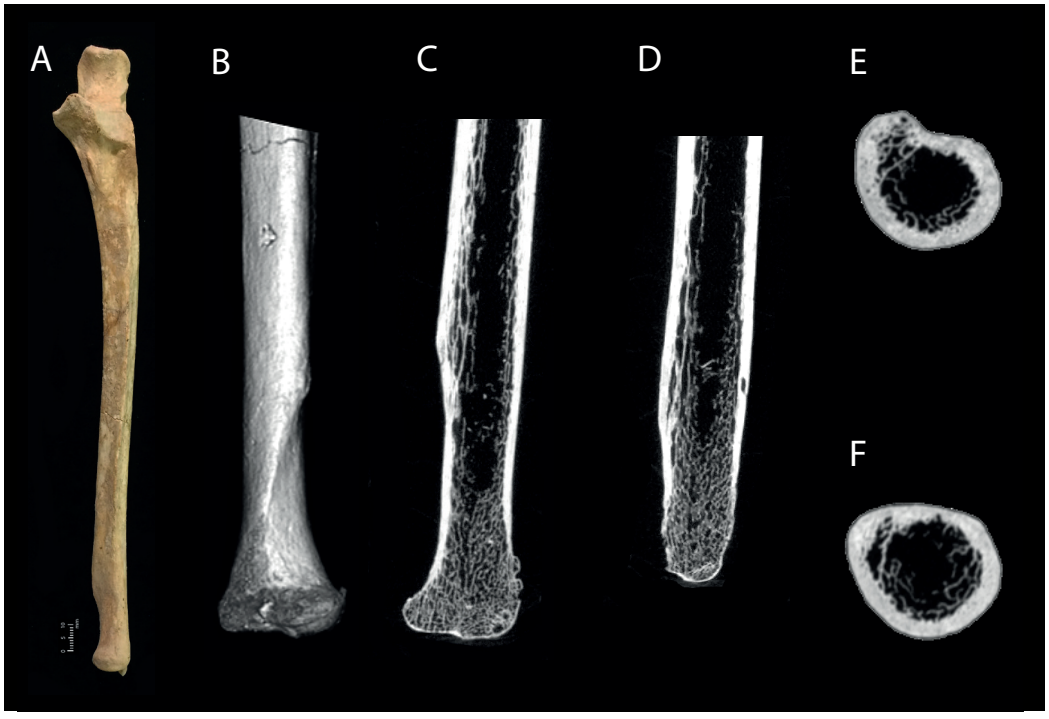

Figure 8.30. *A selection of photographic and radiological images pertaining to an adult left ulna (FB0009) from Context (951) of the Circle sample, detailing a healed fracture of the distal diaphysis, including: a) anterior view; b) 3D render, lateral view; c–d) coronal cross-sections from CT data, detailing cortical dysplasia and deeper internal margin of medullary wall; e–f) transverse cross-sections moving superiorly to inferiorly through the diaphysis, internal margin of medullary wall. Scale bar: 1 cm (photograph only). (Photo Ronika K. Power; radiological images captured by L. Buck, Cambridge Biotomography Centre; processed by J. Magnussen & M. Pardey, Macquarie Medical Imaging).*

& Manchester 2005, 90), either as a result of intentional interpersonal violence or accidental injury (Judd 2004; Jurmain 1999). It is suggested that this fracture occurred many years *antemortem*, as there are no observable fracture or callus margins. The cortex surrounding the dysplastic area is smooth and continuous.

Radiological observations:
Slight dysplasia is observed in the distal ulnar diaphysis. Although the element appears relatively underwhelming in cross section, we nonetheless note a bulge in the cortex at the site of dysplasia with focal cortical thinning (Fig. 8.30c-d). Small vascular channels are observed to pierce the cortex, although this is normal. In cross-section, a thin internal margin is observed to delineate a narrower internal wall of the medullary cavity, possibly indicating an original margin displaced by a fracture (Fig. 8.30c-f). In the absence of periosteal reaction, the extensive cortical remodelling suggests this is a long-standing abnormality. See comments above regarding possible causes of this abnormality (FB0008; §8.5.3.9). This represents a long-term healed and slightly remodelled fracture.

Lesion type and healing status: Trauma; Healed.
Lesion preservation: Excellent.
Differential diagnosis: Trauma; Congenital variation; Activity-related change.

8.5.3.11. FB0010: Ulna

Context:	(960)
Grid Ref:	99E/113N
Year of Excavation:	BR94
Other Details:	Spit 3, No.7–8

Element identification and preservation:
Left adult ulna, fragmented distally *postmortem*. The fragmentation margin is located in the distal quarter of the diaphysis, immediately superior to the ulnar head. The distal fragment is not retained. There is a slight amount of *postmortem* damage observed on the proximal aspect of the olecranon. Adult age estimation is based on the size of the extant element, the relative thickness of the diaphyseal cortex and the complete fusion of the proximal epiphysis (Scheuer & Black 2000, 298ff.). As mentioned above, there are currently

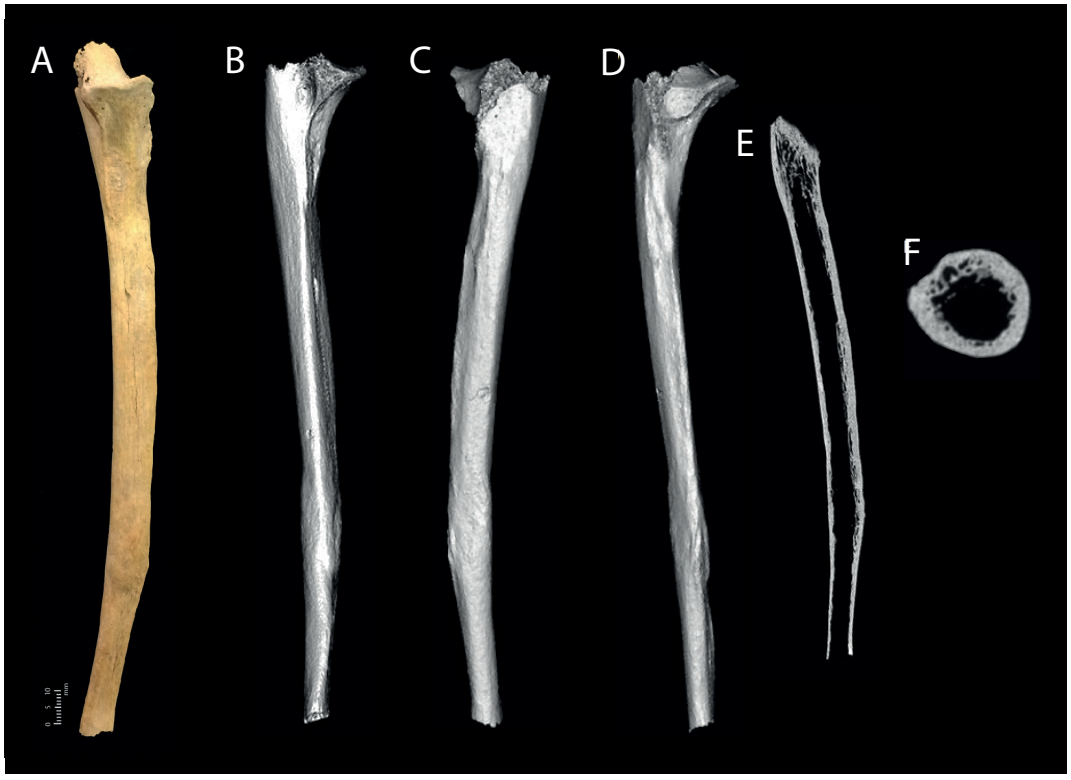

Figure 8.31. *A selection of photographic and radiological images pertaining to a fragmented adult left ulna (FB00010) from Context (960) of the Circle sample, detailing a healed fracture of the distal diaphysis, including: a) anterior view; b) 3D render medial view; c) 3D render posterior view; d) 3D render lateral view; e) coronal cross-section from CT data detailing dysplasia; f) transverse cross-section detailing cortical thinning and altered trabeculation. Scale bar: 1 cm (photograph only). (Photo Ronika K. Power; radiological images captured by L. Buck, Cambridge Biotomography Centre; processed by J. Magnussen & M. Pardey, Macquarie Medical Imaging).*

no reliable methods of sex assessment for isolated ulnae (Bass 1995, 175). The fragment represents ~95% of a complete ulna. The extant element is in excellent condition. All damage is assessed as *postmortem*.

Macroscopic observations:
A healed fracture is observed on the distal quarter of the diaphysis of the left ulna (Fig. 8.31a-f). The element is slightly dysplastic; it is observed that the distal quarter of the diaphysis is misaligned in a lateral direction at the approximate most superior point of the pronator ridge. This dysplasia is also clearly observed from a posterior aspect.

From an anterior view, bony callus is observed with the extant portion emanating from a point 10.4 mm superior to the most superior aspect of the pronator ridge and extending superiorly 21.2 mm with a maximum width of 7.8 mm. The surface of the bony callus is observed to be smooth and even in most areas, while slightly billowing in others. The extant surface area surrounding the fracture is continuous in character where the surrounding bone and the fracture margin are not visible.

Here again, it is likely that this fracture was caused by an acute and direct insult to the forearm *in vivo* (Roberts & Manchester 2005, 90), either as a result of intentional interpersonal violence or accidental injury (Judd 2004; Jurmain 1999). It is also suggested that this fracture occurred many years *antemortem*, as there are no observable fracture or callus margins. The cortex surrounding the dysplastic area is smooth and continuous.

Radiological observations:
A completely healed transverse fracture is observed on the distal ulna diaphysis. The element is dysplastic distal to the fracture site; the diaphysis is diverted 22° from the proximal aspect (Fig. 8.31e). At the fracture site, cortical irregularity and loss of cortical thickness is noted, as well as altered trabeculation (Fig. 8.31f). On the convex side of the curvature there is overall cortical thinning and remodelling at the site of prior

injury. See comments above regarding possible causes of this fracture (FB0008; §8.5.3.9).

Lesion type and healing status: Trauma; Healed.
Lesion preservation: Excellent.
Differential diagnosis: Trauma; Congenital variation; Activity-related change.

8.5.3.12. FB0011: Ulna

Context:	(951)
Grid Ref:	98E/116.5–117N
Year of Excavation:	BR94
Other Details:	Area X

Element identification and preservation:
Right adult ulna, fragmented *postmortem*. The fragmentation margin is located in the distal quarter of the diaphysis, in the region of the pronator ridge. The styloid process is fragmented and absent. The proximal aspect of the element is not retained. Adult age estimation is based on the size of the extant element, the relative thickness of the diaphyseal cortex and the complete fusion of the distal epiphysis (Scheuer & Black 2000, 298ff.). As mentioned before, there are currently no reliable methods of sex assessment for isolated ulnae (Bass 1995, 175). The fragment represents ~15% of a complete ulna. The extant element is in excellent condition. All damage is assessed as *postmortem*.

Macroscopic observations:
A complete healed fracture is observed on the distal quarter of the diaphysis of the right ulna (Fig. 8.32a-g). When viewed from a lateral aspect, the distal portion of the element is displaced posteriorly and superiorly to the proximal portion. The element is slightly dysplastic; it is observed that the distal third of the diaphysis is misaligned in a lateral direction by approximately 5°.

Bony callus is observed to envelop the circumference of the diaphysis. When viewed anteriorly, the extant portion of callus emanates from a point 36.5 mm superior to the most inferior aspect of the radial articulation, extending superiorly 14.6 mm with a maximum width of 13.4 mm. When viewed laterally the maximum callus length is 18.0 mm with a maximum width of 16.5 mm. The surface of the bony callus is smooth and even in most areas, while slightly billowing in others. The extant surface area of the bony callus is continuous in character with the surrounding bone, and the fracture margin is not visible.

Figure 8.32. *A selection of photographic and radiological images pertaining to a fragmented adult right ulna (FB00011) from Context (951) of the Circle sample, detailing a healed fracture of the distal diaphysis, including: a) antero-lateral view; b) 3D render lateral view; c) 3D render posterior view; d) 3D render medial view; e) sagittal cross-section from CT data, detailing impaction and overlap of cortices and bony callus; f) coronal cross-section, detailing fracture site and bony callus; g) transverse cross-section, detailing bony callus and trabecular reorganization. Scale bar: 1 cm (photograph only). (Photo Ronika K. Power; radiological images captured by L. Buck, Cambridge Biotomography Centre; processed by J. Magnussen & M. Pardey, Macquarie Medical Imaging).*

Once again, it is likely that this fracture was caused by an acute and direct insult to the forearm *in vivo* (Roberts & Manchester 2005, 90), either as a result of intentional interpersonal violence or accidental injury (Judd 2004; Jurmain 1999).

Radiological observations:
Observed radiologically, the fracture plane appears to be simple and transverse (Fig. 8.32e-g). The extant element presents relatively minor angulation because of the fracture, with only small amounts of impaction and overlap between cortices (Fig. 8.32e-f). Extensive, healthy bony remodelling is observed, indicating that the injury is completely healed. The extant cortex looks dense and consistent at both proximal and distal aspects, with no evidence of complicating factors including disuse or infection (Fig. 8.32g). The insult is located in the classical position for so-called 'nightstick' fractures, presenting the possibility that this fracture may have been sustained in an act of self-defence. See comments above for further description (FB0008; §8.5.3.9).

Lesion type and healing status: Trauma; Healed.
Lesion preservation: Excellent.
Differential diagnosis: Trauma.

8.5.3.13. FB0012: Ulna

Context:	(799)
Grid Ref:	107E/114N
Year of Excavation:	BR93
Other Details:	Layer 37, Complete Skeleton

Element identification and preservation:
Complete left adult ulna. Adult age estimation is based on the size of the extant element and the complete fusion of both proximal and distal epiphyses (Scheuer & Black 2000, 298ff.). As mentioned before, there are currently no reliable methods of sex assessment for isolated ulnae (Bass 1995, 175). The element is in excellent condition.

Macroscopic observations:
A complete healed fracture is observed at the root of the styloid process (Fig. 8.33). The fractured styloid process fragment is absent. When viewed inferiorly the fracture margin is observed to be irregular with disorganized pitting. The pits are approximately ≤0.5 mm Ø. New bone deposition is observed at the disto-lateral aspect of the ulna, extending superiorly from the fracture margin with the most superior point approximately 13.6 mm superior to the fracture margin. The surface of the new bone deposition is characterized as even. Here again, it is likely that this fracture was caused by an acute and direct insult to the wrist *in vivo* (Roberts & Manchester 2005, 90), either as a result of intentional interpersonal violence or accidental injury, such as a fall onto an open hand (Judd 2004; Jurmain 1999).

Entheseal change is observed on the superior point of the pronator ridge. This entheseal change is characterized by marked bone deposition of approximately 6.9 mm in length and 3.7 mm in width. When viewed from a medial aspect the superior point of this deposition is 49.0 mm superior to the radial articulation. The surface of this deposition is in general smooth

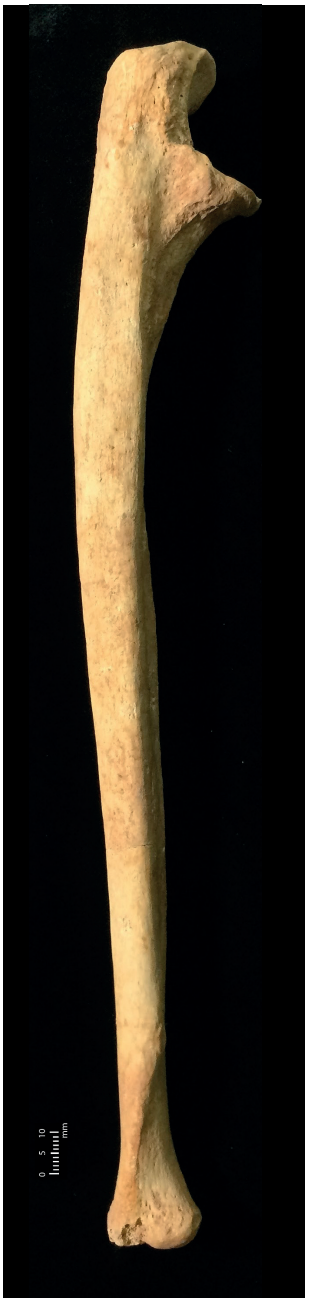

Figure 8.33. *Complete adult left ulna (FB0012) from Context (799) of the Circle sample, exhibiting healed fracture of the styloid process; medial view. Scale bar: 1 cm. (Photo Ronika K. Power).*

with rounded margins. The cortical bone within and across this feature is continuous with the surrounding elements. It is possible that the activity related change is associated with the trauma described above.

Lesion type and healing status: Trauma; Healed; Proliferative.
Lesion preservation: Excellent.
Differential diagnosis: Trauma; Activity-related change; Congenital variation.

8.5.3.14. FB0013: Ulna

Context:	(997)
Grid Ref:	94-94.4E/112–114N
Year of Excavation:	BR93
Other Details:	Area X

Element identification and preservation:
Right adult ulna, fragmented *postmortem*. The fragmentation margin is located in the distal quarter of the diaphysis, in the region of the pronator ridge. The proximal aspect of the element is not retained. Adult age estimation is based on the size of the extant element, the relative thickness of the diaphyseal cortex and the complete fusion of the distal epiphysis (Scheuer & Black 2000, 298ff.). As mentioned before, there are currently no reliable methods of sex assessment for isolated ulnae (Bass 1995, 175). The fragment represents ~20% of a complete ulna and is in excellent condition. All damage is assessed as *postmortem*.

Figure 8.34. *Fragmentary adult right ulna (FB0013) from Context (997) of the Circle sample, exhibiting healed fracture of the styloid process; antero-lateral view. Scale bar 1 cm. (Photo Ronika K. Power).*

Macroscopic observations:
A complete healed fracture is observed at the root of the styloid process of the right ulna (Fig. 8.34). The ulna is fragmented, only the distal third is extant. The fractured styloid process fragment is absent. When viewed inferiorly the fracture margin is observed to be quite even, smooth and continuous with the surrounding bone. New bone deposition is observed at the disto-medial aspect of the ulna, extending superiorly from the fracture margin with the most superior point being approximately 10.2 mm superior to the fracture margin. The surface of the new bone deposition is characterized as even.

As with the other example, it is likely that this fracture was caused by an acute and direct insult to the wrist *in vivo* (Roberts & Manchester 2005: 90), either as a result of intentional interpersonal violence or accidental injury, such as a fall onto an open hand (Judd 2004; Jurmain 1999).

Lesion type and healing status: Trauma; Healed.
Lesion preservation: Excellent.
Differential diagnosis: Trauma; Activity-related change; Congenital variation.

8.5.3.15. FB0001: Femur

Context:	(1241)
Grid Ref:	106E/104N
Year of Excavation:	BR94
Other Details:	Area H [E], Spit 5, Bone No.11

Element identification and preservation:
Intact left adult femur. Slight *postmortem* damage is observed around the inferior and posterior aspects of the femoral head, and the antero-medial aspects of the cortical surface of the medial epicondyle. Adult age estimation is based on the size of the extant element and the complete fusion of both proximal and distal epiphyses (Scheuer & Black 2000, 375ff.). Although metric sex estimation methods for femora have been employed by biological anthropologists for more than a century, they should be used with caution considering they were developed on temporally and geographically distinct populations exclusive of the central Mediterranean (Black 1978; Di Bennardo & Taylor 1979; Dittrick 1979; Işçan & Miller-Shaivitz 1986; Krogman 1962; Pearson 1917; Reichs 1986; Spruiell 1984; Stewart 1979; Thieme 1957; White & Folkens 2005). In any case, it is not possible to apply metric analysis to this element as it is both fragmentary (femoral head) and dysplastic in all the required regions, because of the pathology described below. The femur is approximately 95% complete and the element is in excellent condition. All damage is assessed as *postmortem*.

Macroscopic observations:
A complete transverse fracture is observed on the approximate proximal third of the femoral diaphysis (Fig. 8.35a-f). The fracture is not reduced and the element is severely dysplastic; the proximal third of the femoral diaphysis has been anteriorly displaced to overlie the posterior aspect of the fracture margin. The most inferior point of the healed lesion (callus) on the anterior aspect of the element is situated at approximately 160.6 mm inferior to the most superior point of the greater trochanter; the most superior point of the callus on the posterior aspect of the element is situated at approximately 117.3 mm inferior to the most superior point of the greater trochanter. The extent to which the anterior and posterior components of the fractured diaphysis overlie each other is approximately 42.5 mm.

The fracture has completely healed. The misalignment is characterized by slight medial rotation of the distal two-thirds of the diaphysis, and lateral and posterior displacement of the proximal third of the diaphysis. The healed fracture is enveloped by a bony callus on both posterior and anterior aspects.

On the anterior aspect a gap is observed between the most inferior point of the callus and the anterior diaphyseal surface (Fig. 8.35a). There is evidence of displaced muscle attachment on the posterior aspect of the element (Fig. 8.35c); the *linea aspera* is observed to be significantly laterally displaced, commencing lateral to the lesser trochanter on the most postero-lateral aspect of the diaphysis, it then descends distally for approximately 73.5 mm before traversing medially and then inferiorly to assume a sigmoid presentation across both medial and lateral aspects of the callus. The *linea aspera* assumes its normal presentation immediately inferior to the terminal point of the callus at approximately the distal third of the diaphysis.

Figure 8.35. *Photographic and radiological images pertaining to an adult left femur (FB0001) from Context (1241) of the Circle sample, detailing a complete non-reduced healed transverse fracture with severe dysplasia and diaphyseal discontinuity, including: a) anterior view; b) medial view; c) posterior view; d) lateral view; e) sagittal cross-sections detailing diaphyseal discontinuity, medullary cavity malalignment and bony callus; f) transverse cross-section from CT data detailing diaphyseal discontinuity, medullary cavity malalignment and bony callus. Scale bar: 1 cm (photographs only). (Photos Ronika K. Power; radiological images captured by L. Buck, Cambridge Biotomography Centre; processed by J. Magnussen & M. Pardey, Macquarie Medical Imaging).*

Eburnation is observed on the postero-medial aspect of the medial femoral condyle articular surface. The maximum dimensions of the lesion are: 15.5 mm length by 8.3 mm width. Microporosity (<1.0 mm Ø) is noted within the lesion. The lesion most likely developed because of the dysplasia of the element associated with the trauma described above and corresponding misalignment of the knee joint surfaces. This lesion suggests that the element was used for weight-bearing after the fracture was healed.

A bony ridge is observed on the antero-lateral aspect of the left proximal femur (8.35b & d). On the anterior aspect the ridge starts at 25.0 mm distal to the top of greater trochanter and extends diagonally 18.9 mm to the lateral aspect of the femur. It then turns at approximately 110° to extend horizontally, turning around the lateral aspect of the femur for approximately 29.5 mm (using a tape measure because of the curvature of the feature). The lateral-most aspect of the feature is located 40.5 mm distal to the top of the greater trochanter; the terminal point of the feature is located 43.7 mm diagonal and supero-lateral to the lesser trochanter. The feature is most likely developed as a result of the dysplasia of the element associated with the trauma described above and corresponding misalignment of the proximal joint surface and other muscle attachment areas. This lesion further indicates that the element was used for weight-bearing following healing of the fracture.

Radiological observations:
A complete fracture is observed at the approximate proximal one-third point of the left femoral diaphysis. The fracture margin is observed to be relatively straight (Fig. 8.35e), presenting as a transverse line suggestive of a direct lateral impact injury of great force. Injuries of this kind are often clinically associated with significant falls or direct impact injuries (Bucholz & Jones 1991). At the fracture site, the new bone is thick and regular. There are no signs of irregularity or lamellation suggestive of infection.

There is significant overlap, angulation and impaction at the fracture margins. The central points of the medullary cavities of the proximal and distal femoral components are 32.0 mm displaced (Fig. 8.35e-f). Considering the diameter of the diaphysis at the fracture point is only 27.0 mm, this is a significant displacement. The distance between the closest adjacent cortices is 7.0 mm; this gap has been successfully bridged by new bone deposition and restored in healing. The medullary cavities are observed to be patent in both proximal and distal components of the fractured element. The distal aspect of the diaphysis is angulated at the fracture margin by 40° (Fig. 8.35e).

The femoral head presents some *postmortem* damage on its antero-inferior and posterior aspects. The extant trabeculae are all well-preserved and organized. There is no evidence for subchondral cysts, and no osteophytes are observed at the supero-lateral margins. The extant portion of the femoral head maintains a regular joint contour. The absence of all indicators of degenerative joint disease, morphological change or disuse atrophy suggest that this joint functioned effectively and bore weight in the time subsequent to the fracture incident and prior to the time of death.

There is mild bony irregularity or osteophytosis in the region of the greater trochanter, leading to further bony crests and significant entheseal changes along the superior half of the *linea aspera*. The *linea aspera* is distorted proximally as it approaches the fracture site; distally it appears very wide (Fig. 8.35c). These changes are consistent with periosteal new bone deposition within the adjacent musculature alongside remodelling – *myositis ossificans traumatica.* At the distal aspect of the element, marginal osteophytes are observed on the medial and lateral aspects of medial condyle; on the condylar notch; and on the lateral condyle. The medial condyle presents a slightly irregular contour. Widespread subchondral sclerosis is observed at the lateral margin of the lateral condyle, however there are no subchondral cysts.

The severity of this injury prompts consideration of trauma management in this prehistoric context. Significant blood loss is associated with profound proximal femoral fractures such as this – an individual can lose a quarter to one-third of their total blood volume from this category of injury (Buchloz & Jones 1991; American College of Surgeons 2012). At the very least, the individual who sustained this injury would have been in shock, experiencing tachycardia and hypotension (Buchloz & Jones 1991; American College of Surgeons 2012), yet they survived without any modern clinical intervention. Moreover, they completely recovered from the injury without localized complication or infection and went on to effectively use the affected limb for a long time after healing was complete and before their ultimate demise. This individual's case represents a significant finding in the (pre)history of therapeutic practices, including the dimensions of acute care, convalescence and rehabilitation.

Lesion types and healing status: Trauma; Healed; Proliferative; Active.
Lesion preservation: Excellent.
Differential diagnoses: Trauma; Degenerative Joint Disease; Activity-related change.

8.5.3.16. FB0003: Tibia, fibula
Context: (783)
Grid Ref: 95E/110N
Year of Excavation: BR91
Other Details: n/d

Element identification and preservation:
The distal aspects of a right adult tibia and fibula are observed to be fused and fragmented. For the tibia, only the medial malleolus, distal articular surface and antero-lateral aspect of the metaphysis are extant; the fragmentation margin diagonally transects the metaphysis exposing the trabecular and cortical bone in section. For the fibula, only the distal quarter of the diaphysis is extant; the proximal fragmentation margin is at the approximate peak of the triangular subcutaneous area, while the distal margin is at the approximate metaphyseal line. The proximal fragments of both elements are not retained. Adult age estimation is based on the size of the extant elements, the relative thicknesses of the diaphyseal cortices and the complete fusion of the distal tibial epiphyses (Scheuer & Black 2000, 399ff.). Although metric sex estimation methods for tibiae are often employed by biological anthropologists, they should also be used with caution considering they were developed on temporally and geographically distinct populations (Bass 1995; Holland 1991; Işçan & Miller-Shaivitz 1984a, 1984b; Işçan *et al.* 1994; Kieser *et al.* 1992; Singh *et al.* 1975). Regardless, it is not possible to apply metric analysis to this element because of its highly fragmentary and incomplete state. Both elements are approximately 10% complete. The extant elements are in good condition. All damage is assessed to be *postmortem*.

Macroscopic observations:
The right tibial metaphysis and fibula diaphysis are fused distally at their respective interosseous borders (Fig. 8.36a-d) by a bony bridge between the elements which is consistent in appearance with the surrounding cortical bone. For the tibia, the most distal fusion point starts at approximately 4.10 mm superior to the inferior articular surface, at approximately the fibular notch. It is not possible to describe the precise anatomical location of the fusion for the fibula, as the distal aspect is fragmented as a result of *postmortem* damage. The length of the fused position of these elements is 64.0 mm, measure from the most distal to most proximal points. The distal aspect of the fibula diaphysis is observed to be dysplastic; the extant proximal aspect

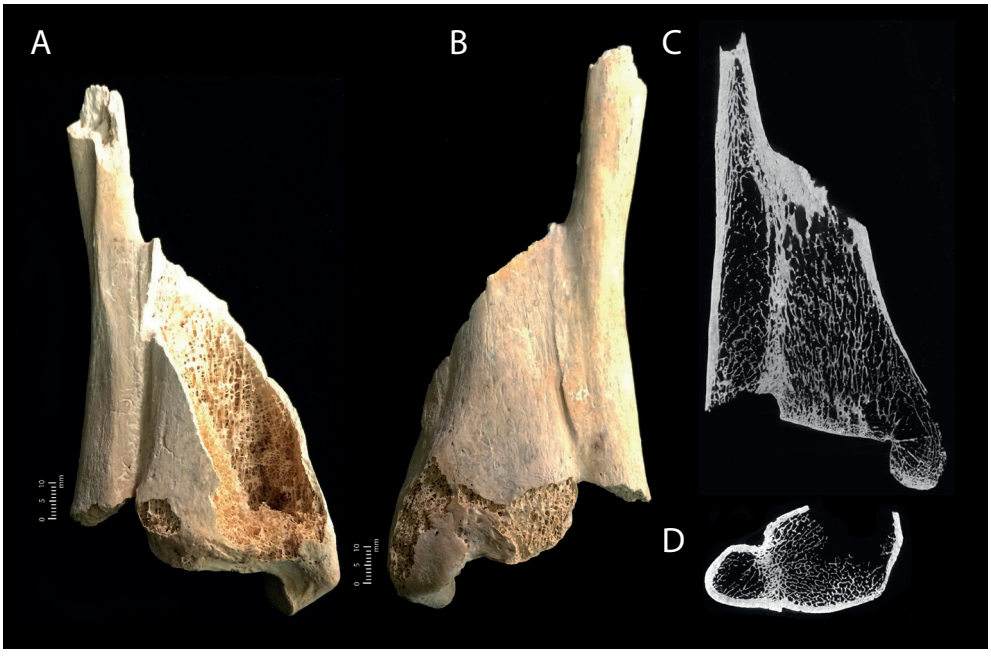

Figure 8.36. *Photographic and radiological images pertaining to fragmentary adult right tibia and fibula (FB0003) from Context (783) of the Circle sample, detailing complete fusion of the distal diaphysis and metaphyses at the interosseous border, including: a) anterior view; b) posterior view; c) coronal cross-section from CT data detailing the complete extent of fusion; d) transverse cross-section at the fusion site detailing the commonality of trabeculae. Scale bar: 1 cm (photographs only). (Photos Ronika K. Power; radiological images captured by L. Buck, Cambridge Biotomography Centre; processed by J. Magnussen & M. Pardey, Macquarie Medical Imaging).*

of the fibula diaphysis is diverted from the anatomical midline and fused portion by approximately 10°.

Radiological observations:
The fragmentary distal aspects of the right adult tibia and fibula are completely fused across the distal tibiofibular syndesmosis. The medial malleolus appears to have been healthy at the time of death, and the tibial plafond is preserved. The most distal aspect of the fibula is absent. A thick corticated margin is observed between the two elements, which extends for a substantial segment. Furthermore, there is a commonality of trabeculae between the elements with only a slight remnant of cortex in the intermediate space. This is classified as tibiofibula coalition, or tibiofibular synostosis, a condition only rarely described in orthopaedic literature (Sureka *et al.* 2012). This can be either a congenital or acquired condition; in the case of the latter, trauma such as ankle fracture or eversion ankle sprain is the most common aetiology, particularly in the case of distal joint involvement (Fu *et al.* 2003; Munjal *et al.* 2004; O'Dwyer 1991; Vitale & Fallat 1990). Sureka *et al.* (2012) report that tibiofibular synostosis may also be secondary to iatrogenic causes or pre-existing conditions including so-called 'kissing' osteochondroma, *fibrodysplasia ossificans progressiva*, subperiosteal haemorrhage (a sequela of scurvy or haemophilia) and fluorosis (Bostman 1993; Fu *et al.* 2003; Lee *et al.* 2010). Although iatrogenic causes may be ruled out for this prehistoric individual, it is likely that the structural changes described here may be attributed to a traumatic incident many years prior to the time of death, considering the almost-common medullary cavity, smooth remodelled cortices with no periosteal thickening or irregularity. In considering how this may have affected the lived experience of the afflicted individual, clinical cases of distal tibiofibular syndesmosis report relatively rigid, stable joints with minimal loss of mobility and no pain directly associated with the coalition *per se* (Sureka *et al.* 2012).

Lesion type and healing status: Proliferative; Healed.
Lesion preservation: Excellent.
Differential diagnosis: Trauma; Congenital; Activity-related change; Metabolic.

8.6. Methodology case study: periosteal lesions in Context (960)

Periosteal lesions were rarely observed across the full assemblage of excavated remains; however, a concentration of elements within Context (960) demonstrated this pathology. Context (960) is dated to *c*. 2530–2475 cal. BC, late within the site's use, although some remains were residual and dated to as early as 2850 cal. BC (Malone *et al*. 2019). The previous summary of pathological observations within the assemblage noted, but did not quantify, observations of 'extra cortical new bone' (Stoddart *et al.* 2009a, 325). Within Context (960), two adjacent 1x1 m grid squares contained 12 elements presenting periosteal lesions of varied expression and severity. These elements are represented by 44 fragments deriving from non-adult and adult individuals. The assemblage excavated from Context (960) contained nearly 12,000 fragments of human bone and only one articulated skeleton (Stoddart *et al.* 2009a, 149); this discrete deposit of pathological elements is therefore exceptional. These elements are described below, according to grid square. Interestingly, element distribution corresponds with biological age, with only adult elements presenting periosteal lesions in one 1 × 1 m grid square, and only non-adult elements presenting periosteal lesions in the adjacent grid square. Below, radiological observations supplement macroscopic descriptions of the lesions on these elements in all cases. This integrated approach enhances differential diagnosis and represents a greater level of attention than is typically paid to fragmented remains, providing the opportunity to assess the potential of this methodology to re-unite remains from discrete individuals in fragmentary and commingled contexts. Differential diagnosis of periosteal lesions on singular elements is not recommended (Weston 2008, 57). We therefore discuss varied possible pathogeneses in the case of each element, before assessing the potential relationship between the adult and non-adult elements, respectively.

8.6.1. Context (960) adult remains

8.6.1.1. FB0033: Radius

Context:	(960)
Grid Ref:	99/112
Year of Excavation:	BR94
Other Details:	Unit 2, Spit 4

Element identification and preservation:
Left adult radius refitted from two fragments presenting a diagonal and stepped *postmortem* fracture at the distal point of the proximal third of the diaphysis. These fragments are observed to conjoin well. The proximal and distal metaphyses and the radial tubercle are fragmented *postmortem* and these portions are not retained. Several small patches of red ochre are observed on the extant portion of the diaphysis. Adult age estimation is based on the size of the extant element and the relative thickness of the diaphyseal cortex (Scheuer & Black 2000, 289ff.). Bass (1995, 168) reports that several attempts have been made to establish metric sex determination

for the radius, however they have not been successful in characterizing dimorphism from a single isolated bone, much less for a fragmentary element (cf White 2012, 415). Additional studies show that ossification timing of particular epiphyses of the distal humerus and proximal radius can successfully determine biological sex in 70% of cases (Garn *et al.* 1996, 106). However, considering the fragmentary and disarticulated nature of this element and individual, we are unable to access either of these criteria. The extant portion of the element represents ~90% of a complete radius and the fragments are in good condition. All damage is assessed as *postmortem*.

Macroscopic observations:
Periosteal new bone deposition is observed in four focal areas: the radial tubercle, the proximal aspect of the interosseous crest, the lateral aspect of the middle third of the diaphysis and on the extant portion of the distal metaphysis (Fig. 8.37a-d). In all cases where the lesion can be viewed in cross-section from fragmentation margins, no changes to the underlying cortex are observed. There are no indications of fracture, cloaca, or sequestra on the extant portion of the element.

The extant portion of the radial tubercle is enveloped by periosteal new bone, although the medial and most elevated aspect of the radial tubercle has been eroded because of *postmortem* damage which obfuscates further observations of pathology. On the anterior aspect, the lesion commences approximately 16.9 mm from the proximal fragmentation margin, continuing for 22.6 mm. The lesion commences approximately 13.9 mm from the proximal fragmentation margin on the medial aspect and extends for 25.4 mm. On the posterior aspect, the lesion commences approximately 11.7 mm from the proximal fragmentation margin and continues for 18.8 mm. Using a flexible paper tape measure, the maximum width of the lesion is 29.0 mm medio-laterally across the centre of the radial tubercle. The maximum length of the lesion along the medial aspect of the radial tubercle is 25.4 mm. The lesion exhibits mixed activity phases, presenting lamellar bone interspersed with microporosity (<1.0 mm Ø) on the anterior and posterior aspects and woven bone with capillary impressions and microporosity alongside the fragmentation margins on the radial tubercle. The centre of the extant lesion can be viewed in cross-section at the fragmentation margin and the periosteal woven bone is observed to sit proud of the underlying cortex. In relation to the surrounding cortex, the lesion differs in colour and presents increased porosity. The margins of the lesion are diffuse, less dense and more porous.

On the proximal aspect of the interosseous crest, periosteal woven bone extends across the fragmentation margin of the two diaphyseal fragments which are observed to re-fit. On the medial aspect, the lesion commences approximately 50.3 mm from the proximal fragmentation margin and extends for 48.6 mm. The maximum width of the lesion is 6.8 mm, taken 5.0 mm proximal to the fragmentation margin of the diaphyseal fragments using a flexible paper tape. On the peripheral margins of the lesion, bony plaque deposits and microporosity are observed. In some areas, the plaque-like deposits assume a striated position because of their location overlying the interosseous crest. In the central portion of the lesion, rugose plaque deposits are interspersed with microporosity. Some *postmortem* damage to the centre of the lesion may obfuscate further observations of pathology. The lesion differs in colour to the surrounding cortex; the plaque-like deposits are denser and more rugose. At the centre of the lesion, the periosteal new bone is observed to sit proud of the underlying cortex.

On the lateral aspect of the middle third of the diaphysis, the lesion commences approximately 6.4 mm from the proximal fragmentation margin and continues for 19.7 mm. The maximum width, taken antero-posteriorly across the centre of the lesion measures 6.0 mm. The lesion exhibits mixed activity phases. In the distal two thirds of the lesion, well-healed and diffuse plaque-like bone is interspersed with microporosity. In the proximal third, the lesion appears to be slightly more active; it is more rugose, and there is more separation and definition between the periosteal new bone and the cortex. A small amount of *postmortem* damage is observed on the proximal aspect of the lesion. The lesion is a slightly different colour to the surrounding cortex, although the margins are diffuse.

On the extant portion of the distal metaphysis, periosteal new bone is observed on the anterior surface, the distal aspect of the interosseous crest and medial aspect of the posterior surface. On the anterior surface, the extant portion of the lesion occupies an approximately triangular shape, extending from the most lateral inferior border to the interosseous crest. The midpoint of the lesion on the anterior surface is located approximately 29.3 mm superior to the distal fragmentation margin on the sagittal plane. On the medial aspect, the extant portion of the lesion extends 34.0 mm proximal to the distal fragmentation margin. On the postero-medial aspect, the extant portion of the lesion is also observed to occupy an approximately triangular shape; the midpoint of the lesion is located 17.4 mm proximal to the distal fragmentation margin on the sagittal plane. The maximum length of the lesion is 34.3 mm on the medial aspect. The maximum width of the lesion is approximately 33.0 mm, taken 4.0 mm proximal to the distal fragmentation margin using a flexible paper tape. The lesion presents mixed activity phases. The peripheral

Figure 8.37. *Photographic images pertaining to fragmented adult left radius (FB0033) from Context (960) of the Circle sample, depicting refitted fragments and periosteal lesions in the regions of the radial tubercle, proximal aspect of the interosseous crest and distal metaphysis, including: a) anterior view; b) medial view; c) 3D rendered lateral view; d) posterior view. Scale bar: 1 cm. (Photos Jess E. Thompson; radiological images captured by L. Buck, Cambridge Biotomography Centre; processed by J. Magnussen & M. Pardey, Macquarie Medical Imaging).*

margins on the anterior and posterior surfaces present smooth plaque-like deposits interspersed with diffuse microporosity. Within the central portion of the lesion, both micro- and macroporosity (≥1.0 mm Ø) are observed. Clusters of microporosity are observed on the antero-lateral aspect with pores occasionally coalescing and partial capillary impressions truncated by the fragmentation margin. On the antero-medial aspect, single and coalescing macropores are present. On the medial aspect, the distal three-quarters of the lesion presents a more rugose topography of woven bone interspersed with microporosity. The proximal quarter of the lesion presents a smooth plaque-like deposit of bone. On the posterior aspect, the central portion of the lesion presents woven bone and microporosity. The margins of the extant portion of the lesion on the anterior and posterior aspect are diffuse and not well-demarcated; they do not differ in colour to the surrounding cortex although they are denser. On the medial and posterior aspect, the lesion is observed to differ in colour.

Radiological observations:
A minor area of periosteal new bone deposition is observed on the extant portion of the radial tubercle. Mid-diaphysis, in the area of the refitted fragmentation margins, cortical bone loss is observed, although this may be attributed to *postmortem* taphonomic damage. The distal diaphysis and distal metaphysis present a thick layer of periosteal new bone deposition which is radiolucent and very well-remodelled. This lesion is well-organized and exhibits dense bone with regular and smooth margins, indicating a long and chronic process which may have been halted in the process of remodelling.

There is no evidence of fracture or typical sequelae (i.e. cloaca, sequestra) on the extant radius, suggesting the lesions are unlikely to be the result of traumatic fracture or infectious processes such as osteomyelitis. The lesions on the interosseous surface and on the distal metaphysis present diffuse margins and are therefore not characteristic of subperiosteal haematomata (Ortner 2003, 84). Periosteal new bone forms in response to damage to the periosteum, including even relatively minor tearing and stretching (Richardson 2001). The lesions on the extant element are observed on attachment sites for the *Mm. biceps brachii*, *flexor pollicis longus,* and *pronator quadratus*. These muscles are involved in flexion and pronation of the forearm, thumb flexion,

and gripping with the hand (Parkin & Logan 2007, 138). Repetitive activity-related microtrauma may have resulted in chronic periosteal inflammation. This phenomenon is commonly reported amongst athletes as a result of overuse and overloading of the forearm, and may co-occur with stress fractures (Meese & Sebastianelli 1996; Meijer *et al.* 2017).

Lesion type and healing status: Mixed; Mixed.
Lesion preservation: Excellent.
Differential diagnosis: Activity-related change.

8.6.1.2. FB0034: Ulna

Context:	(960)
Grid Ref:	99/112
Year of Excavation:	BR94
Other Details:	Unit 21, Spit 4

Element identification and preservation:
Left adult ulna refitted from two fragments presenting a transverse *postmortem* fracture across the pronator ridge. These fragments are observed to conjoin well. The distal metaphysis and epiphysis are absent as a result of further fragmentation immediately superior to the distal metaphysis. Slight areas of *postmortem* damage are observed on the anterior-most aspects of the olecranon and the coronoid process, the radial notch, infero-medial to the margin of the trochlear notch, and on the postero-medial aspect of the olecranon. Diffuse flecks and patches of red ochre are observed across the extant portion of the diaphysis. Adult age estimation is based on the size of the extant element, the relative thickness of the diaphyseal cortex and the complete fusion of the proximal epiphysis (Scheuer & Black 2000, 298ff.). As mentioned before, although Purkait (2001) devised a discriminant function for metric sex assessment of ulnae, this method is not widely applied (Bass 1995, 175; White & Folkens 2005). Furthermore, it is not possible to apply metric analysis to this element because of its fragmentary and incomplete state. The fragment represents ~95% of a complete ulna and is in good condition. All damage is assessed as *postmortem*.

Macroscopic observations:
The periosteal new bone extends across the extant anterior and lateral aspects of the proximal metaphysis, although *postmortem* damage may obfuscate further observations of pathology (Fig. 8.38a-d). On the anterior surface, the lesion commences on the inferior aspect of

Figure 8.38. *Photographic images pertaining to fragmented adult left ulna (FB0034) from Context (960) of the Circle sample, depicting refitted fragments and periosteal lesions in the regions of the proximal metaphysis and the distal third of the diaphysis, traversing the fragmentation margin, including: a) anterior view; b) medial view; c) lateral view; d) posterior view. Scale bar: 1 cm. (Photos Jess E. Thompson).*

the coronoid process and extends for approximately 51.0 mm, measured with a flexible paper tape. On the lateral aspect, the lesion commences approximately 18.9 mm from the proximal epiphysis and continues for approximately 59.5 mm. The maximum length of the lesion is 59.5 mm on the lateral aspect. The maximum width of the lesion is 34.0 mm taken medio-laterally from the centre of the ulnar tuberosity with a flexible paper tape. The lesion exhibits mixed activity phases. A plaque-like deposit of woven bone is observed on the ulnar tuberosity, interspersed with microporosity and small bony nodules. Well-healed smooth deposits of bone are observed inferior to the coronoid process. On the antero-lateral aspect, the lesion exhibits woven bone incorporating both micro- and macroporosity. Infero-medial to the trochlear notch, a depression is observed, measuring 12.1 mm proximal to distal and 3.6 mm superior to inferior. Woven bone continuous with the surrounding lesion is observed within this depression and, alongside microporosity, four macropores are present. The lesion is denser, more porous and lighter in colour than the surrounding cortex.

On the distal third of the diaphysis, periosteal woven bone is observed on the interosseous crest extending across the fragmentation margin of the two diaphyseal fragments which are observed to re-fit (Fig. 8.38a & c). On the distal fragment, the lesion continues across the anterior surface to the pronator ridge. The distal fragmentation margin truncates the lesion and some *postmortem* damage to the woven bone is observed, obfuscating full observation of pathology. The lesion commences on the lateral aspect of the proximal fragment, 9.5 mm superior to the re-fit fragmentation margin and extends for 39.2 mm. On the anterior aspect, the lesion commences on the distal fragment, 8.1 mm distal to the conjoined fragmentation margin and extends over the extant portion of the diaphysis for 39.3 mm. The maximum length of the lesion is 39.3 mm on the anterior aspect. The maximum width of the lesion, using a flexible paper tape, is 10.0 mm taken medio-laterally along the distal aspect of the pronator ridge. The plaque-like deposits of bone assume a striated organization along the interosseous crest and pronator ridge, interspersed with microporosity. In relation to the surrounding cortex, the lesion is more porous and differs in colour. In cross-section, when viewed from the fragmentation margins, the periosteal woven bone sits proud of the underlying cortex. There are no indications of fracture, cloaca, or sequestra on the extant portion of the element.

Radiological observations:
On the lateral margin of the proximal diaphysis, the periosteal lesions are in the process of healing and appear long-standing. The lesion presents mixed activity phases: components of the lesion exhibit spiculated and active presentation, while other components appear to be in a more advanced stage of remodelling. The underlying cortex is observed to be in poor condition, presenting a diffuse, poorly demarcated lesion characterized by small radiolucent holes, which worsens in areas where the overlying lesion is irregular in expression. This appearance is referred to as 'moth-eaten' in radiological descriptions, describing a true permeative process of bone (Brant & Helms 2012). In the region of the mid-diaphysis, the bone is observed to present healthy tissue with thick and well-preserved cortices. Toward the distal diaphysis, there is further periosteal new bone deposition and the underlying cortex is thin, pockmarked and trabeculated.

There is no evidence of fracture or typical sequelae (i.e. cloaca, sequestra) on the extant ulna, suggesting the lesions are unlikely to be a result of traumatic fracture or infectious processes such as osteomyelitis. The lesions present diffuse margins and are not characteristic of subperiosteal haematomata (Ortner 2003, 84). As mentioned before, periosteal new bone forms in response to damage to the periosteum, including even relatively minor tearing and stretching (Richardson 2001). Notably, lesions are present on articular and interosseous surfaces, in this case on attachment sites for the *Mm. supinator*, *brachialis*, *pronator quadratus*, *extensor carpi ulnaris* and *flexor digitorum profundus*. These muscles are involved in elbow flexion, forearm pronation and supination, wrist flexion and extension, and finger flexion (Parkin & Logan 2007, 138, 140). Thus, chronic periosteal inflammation in this case may be a result of repetitive activity-related microtrauma. Activity-related ulnar periostitis is reported amongst athletes as a result of overuse and overloading of the forearm muscles (e.g. Grossfeld *et al.* 1998; Meese & Sebastianelli 1996).

Lesion type and healing status: Mixed; Mixed.
Lesion preservation: Excellent.
Differential diagnosis: Activity-related change.

8.6.1.3. FB0035: Femur

Context:	(960)
Grid Ref:	99/112
Year of Excavation:	BR94
Other Details:	Unit 16, Spit 4

Element identification and preservation:
Fragmentary and incomplete left adult femur. Many fragments are very small and most represent the distal epiphysis. The two largest fragments comprise the majority of the diaphysis and are observed to refit

along a transverse *postmortem* fracture which transects the *linea aspera* at the approximate mid-point. The proximal diaphysis is fragmented diagonally superior to the spiral line, and the distal diaphysis is fragmented irregularly across the popliteal surface. Small areas of *postmortem* damage are present on the postero-lateral margin of the *linea aspera*, and on the antero-medial aspect of the proximal third of the diaphysis. Longitudinal cortical cracks and root etching are observed on the proximal third of the diaphysis, eroding areas of the cortical surface and the periosteal lesions. Diffuse flecks and patches of red ochre are observed across the extant portion of the diaphysis. Adult age estimation is based on the size of the extant element (Scheuer & Black 2000, 375ff.). Although metric sex estimation methods for femora have been employed by biological anthropologists for more than a century (references in §8.5.3.15, above) it is not possible to apply metric analysis to this element as it is both fragmentary and incomplete. The femur is ~75% complete and the extant portions of the element are in fair condition. All damage is assessed as *postmortem*.

Macroscopic observations:
Periosteal new bone is observed on the anterior aspect of the proximal diaphysis and on the anterior and lateral aspects of the distal diaphysis (Fig. 8.39a-c). All lesions are affected by *postmortem* taphonomic damage and the fragmentation of the proximal and distal diaphysis truncates the lesions, obfuscating full observation of pathology. There are no indications of fracture, cloaca, or sequestra on the extant portions of the element.

On all aspects, the lesion is observed adjacent to the proximal fragmentation margin. From the proximal fragmentation margin on the anterior aspect of the extant proximal diaphysis, the lesion extends for approximately 162.6 mm. On the posterior aspect, the lesion extends for approximately 210.0 mm, traversing the two re-fitted diaphyseal fragments. On the lateral aspect, the lesion extends for 170.8 mm, again traversing the re-fitted fragments. On the medial aspect, the lesion extends for approximately 144.6 mm. The maximum length of the extant portion of the lesion is 210.0 mm on the posterior aspect along the *linea aspera*. The maximum width of the lesion is 75.0 mm, taken antero-posteriorly along the pectineal line using a flexible paper tape. The lesion exhibits mixed activity phases. On the antero-medial aspect, the peripheral margins of the extant portion of the lesion present well-healed lamellar bone interspersed with diffuse microporosity. On the antero-lateral aspect, islands of periosteal woven bone have been

Figure 8.39. *Photographic and radiological images pertaining to fragmented adult left femur (FB0035) from Context (960) of the Circle sample, depicting refitted fragments and periosteal lesions on the proximal and distal thirds of the diaphysis, including: a) anterior view; b) lateral view; c) posterior view; d) transverse cross-section from CT data at the proximal diaphysis demonstrating cortical demineralization and separation between the cortex and periosteal lesion on the lateral aspect of the linea aspera; e) transverse cross-section at mid-diaphysis demonstrating cortical irregularity and radiolucent holes (so-called 'moth-eaten' appearance); f) transverse cross-section at the proximal aspect of the distal third of the diaphysis demonstrating cortical demineralization and radiolucent holes (so-called 'moth-eaten' appearance). Scale bar: 1 cm (photographs only). (Photos Jess E. Thompson; radiological images captured by L. Buck, Cambridge Biotomography Centre; processed by J. Magnussen & M. Pardey, Macquarie Medical Imaging).*

eroded by *postmortem* damage. On the extant portion of the lesion, plaque-like deposits of woven bone are interspersed with microporosity. On the posterior aspect, periosteal woven bone envelops the pectineal line, spiral line, gluteal tuberosity and *linea aspera*, exhibiting extensive microporosity. Extending distally, the medial lip of the *linea aspera* presents woven bone with extensive microporosity, while the lateral lip presents well-healed bone with diffuse microporosity. The margins of the lesion are diffuse and not well-demarcated on the antero-medial aspect, although the posterior margins of the lesion are marked by rugosity. The lesion differs in colour to the surrounding cortex and exhibits less dense and more porous bone. When viewed from the fragmentation margins, the periosteal woven bone sits proud of the underlying cortex and no cortical change is observed.

On the anterior aspect of the distal diaphysis, the lesion commences approximately 45.8 mm superior to the distal fragmentation margin. On the lateral aspect, the lesion commences approximately 109.5 mm superior to the distal fragmentation margin. The maximum length of the extant portion of the lesion is 109.5 mm on the lateral aspect. The maximum width of the lesion is 58.0 mm, taken 5.0 mm proximal to the distal fragmentation margin using a flexible paper tape. The extant portion of the lesion exhibits well-healed lamellar bone and microporosity. The margins are diffuse and not well demarcated, differing in colour to the surrounding cortex and demonstrating increased porosity. When viewed from the fragmentation margin, the periosteal new bone is observed to sit proud of the underlying cortex and cortical thickness has decreased, measuring 0.8 mm on the anterior aspect and 1.1 mm on the lateral aspect. The area usually occupied by dense cortical bone now presents focal micro- to macroporosity and cancellous proliferation, an apparent extension of trabecular bone within the medullary cavity. When held in the hand, the extant element feels very light as compared to the weight of 'normal' bone.

Radiological observations:
The proximal fragment presents slightly more extant cortex than the refitted fragment of the middle and distal diaphysis. However, the cortex is observed to be in poor condition, presenting an eroded and poorly demarcated lesion characterized by small radiolucent holes (Fig. 8.39d-f). Such cortical change is unlikely to be the result of diagenetic processes; the outermost portion of the cortex is better preserved than the endosteal aspect, most likely a result of demineralization because of pathological processes. Focal periosteal new bone is present around the *linea aspera*, tracking its full length on the extant portion of the element. A partial boundary is observed between the cortex and the lesion, and the underlying cortex exhibits increased porosity and is relatively irregular in appearance. The cortex is markedly thin and demineralized across the extant portion of the element, compared with the expected cortical thickness of an adult femoral mid-diaphysis. Bone density loss across the element demonstrates osteopenia and may signal osteoporosis.

Both the proximal and distal lesions are truncated by *postmortem* fragmentation, indicating that periosteal new bone deposition extended onto the metaphyseal surfaces and was more widespread across the element than is observable. Given that the proximal and distal metaphyses and epiphyses are absent because of fragmentation and cannot be assessed, fracture must be considered in the differential diagnosis. While it is not possible to ascertain whether this element was fractured *in vivo*, the evidence for extensive minor periosteal reaction and cortical resorption may be related and important factors to consider in the differential diagnosis. Sequelae and long-term effects of femoral fractures which may stimulate periosteal reaction and/or cortical bone loss include osteomyelitis, localized disuse osteoporosis or osteopenia, and reflex sympathetic dystrophy. Typical infectious indicators are not observed on the extant element and the cortex has been compromised as a result of demineralization rather than erosive processes associated with infection. The diffuse nature of the lesions and the extensive cortical change may instead support a systemic pathogenesis (Ortner 2003). Osteoporosis and traumatic fracture, especially of the hip, have a complex relationship. Reduced mobility secondary to fracture may lead to localized osteoporosis (Bartl *et al.* 2007, 111–3; Kiratli 2003), while generalized osteoporosis or osteopenia increases the likelihood of bone fracture following trauma as a result of significant reduction in bone density (Ortner 2003, 410ff.; Warriner *et al.* 2011). Reflex sympathetic dystrophy (or complex regional pain syndrome) is occasionally experienced following fracture, sprain, venous or nerve damage, and may also result in osteoporosis, amongst other complications (Borchers and Gershwin 2014, 246). Additionally, the involvement of the *linea aspera* may indicate the co-occurrence of activity-related microtrauma and/or altered biomechanics.

Lesion type and healing status: Mixed; Mixed.
Lesion preservation: Moderate.
Differential diagnosis: Activity-Related Change; Metabolic; Trauma.

8.6.1.4. FB0036: Tibia

Context:	(960)
Grid Ref:	99/112
Year of Excavation:	BR94
Other Details:	Units 2 & 33, Spit 4

Element identification and preservation:
Fragmentary and incomplete right adult tibia represented by five fragments, four of which are observed to refit. The refitted portion of the element represents the approximate mid-point of the diaphysis and extends to the distal diaphysis, which is fragmented superiorly to the distal metaphysis. The fragments present diffuse root etching and focal areas of erosion on the lesions and adjacent to the fragmentation margins. Small flecks and patches of red ochre are observed on many fragments. Adult age estimation is based on the size of the extant element and the relative thicknesses of the diaphyseal cortex (Scheuer & Black 2000, 399ff.). Although metric sex estimation methods for tibiae are often employed by biological anthropologists (Bass 1995; Holland 1991; Işçan & Miller-Shaivitz 1984a, 1984b; Işçan *et al.* 1994; Kieser *et al.* 1992; Singh *et al.* 1975), it is not possible to apply metric analysis to this element because of its highly fragmentary and incomplete state. The element is ~35% complete and the extant portions of the element are in fair condition. All damage is assessed to be *postmortem*.

Macroscopic observations:
Periosteal new bone is observed on all extant fragments; fragmentation truncates the lesions and thus obfuscates a full observation of pathology. When viewed from the fragmentation margins, the periosteal lesions sit proud of the underlying cortex and no cortical change is observed. On the extant portions of the element, there are no indications of fracture, cloacae or sequestra.

On the anterior aspect, the extant portion of the lesion extends across four fragments which are observed to re-fit (Fig. 8.40a – only three fragments are visible in this view). The lesion extends across the full length of the fragments for 243.3 mm. The maximum width of the extant portion of the lesion is approximately 29.0 mm, using a flexible paper tape. The lesion demonstrates mixed activity phases. The proximal three-quarters present well-healed smooth deposits of bone with diffuse microporosity. The distal quarter exhibits rugose plaque-like deposits of bone with microporosity, although *postmortem* taphonomic damage obfuscates a full observation of the lesion. With respect to the surrounding cortex, the lesion demonstrates increased porosity and the distal quarter differs in colour.

On the lateral aspect of the distal third of the diaphysis, periosteal new bone deposition traverses the length of the extant fragment (Fig. 8.40b). The lesion is truncated both proximally and distally and has been partially eroded by *postmortem* root damage, obfuscating a full observation of pathology. The maximum length of the extant portion of the lesion is 126.6 mm along the interosseous surface. The maximum width of the lesion is 26.0 mm, using a flexible paper tape. The lesion exhibits mixed activity phases. The peripheral

Figure 8.40. *Photographic and radiological images pertaining to fragmented adult right tibia (FB0036) from Context (960) of the Circle sample, depicting periosteal lesions on the refitted fragments of the proximal diaphysis and on the distal third of the diaphysis, including: a) anterior view of refitted fragments of proximal diaphysis; b) lateral view of distal third of diaphysis; c) transverse cross-section from CT data toward distal fragmentation margin of distal diaphysis, demonstrating irregular cortex with periosteal lesion partly separated from underlying cortex. Some sediment is observed within the medullary cavity. Scale bar: 1 cm (photographs only). (Photos Jess E. Thompson; radiological images captured by L. Buck, Cambridge Biotomography Centre; processed by J. Magnussen & M. Pardey, Macquarie Medical Imaging).*

margins of the proximal aspect of the lesion present well-healed deposits of bone with microporosity and capillary impressions. The remainder of the lesion exhibits successive layers of plaque-like deposits of bone interspersed with micro- and macroporosity. The organization of the periosteal new bone varies across the lesion; striated plaque deposits overlie the interosseous surface while angular plaque deposits interspersed with capillary impressions are present on the antero-lateral aspect. The lesion differs in colour to the surrounding cortex and demonstrates increased rugosity and porosity.

Radiological observations:
The largest available fragment of the extant tibia, representing the distal diaphysis, displays widespread periosteal new bone for the full length of the fragment. The lesion is deposited in discrete zones and extends from the anterior aspect to the interosseous surface. The cortex presents slightly diffuse radiolucent holes, and it is trabeculated and thinner than expected (Fig. 8.40c). Radiologically, the margins of the lesion are clearer, and it is apparent that there are further extensions of the lesion onto the interosseous surface, where they may have been truncated by *postmortem* taphonomic damage. The lesion is observed to sit proud of the cortex in several areas, at the proximal and distal aspects of the extant fragment. The character of the periosteal new bone is not lamellated nor is any cortical thickness change evident as would be expected in association with chronic infectious processes.

All lesions are truncated because of *postmortem* fragmentation and, given that much of the element cannot be assessed, trauma and fracture must be considered in the differential diagnosis. Subperiosteal haematomata are commonly observed on the tibia secondary to trauma or scurvy, but exhibit microporotic ossification of the periosteum, as opposed to the diffuse nature of the lesions on the extant portion of this element (Ortner 2003, 88). Further potential aetiologies include chronic venous insufficiency, hypertrophic osteoarthropathy, and microtrauma because of tibial stress syndrome, commonly known as 'shin splints'. Chronic venous insufficiency (CVI) is microporosity by damage or weakness in the valves and/or venous walls of lower leg veins, resulting in increased blood pressure and stasis in the lower legs as blood is unable to flow upward to the heart. Periosteal reaction may form in response to chronic soft tissue inflammation because of CVI, and has been observed clinically at ulcer sites, at a distance from ulcer sites, or not in association with ulceration (Gensburg *et al.* 1988, 1280; Nicholls 2005). Periosteal new bone in CVI cases is noted to be thick and undulating, resembling lesions seen in cases of hypertrophic osteoarthropathy (Gensburg *et al.* 1988, 1280).

Hypertrophic osteoarthropathy (HOA) refers to either a primary or secondary syndrome; the primary form of the disease is pachydermoperiostosis and genetic in origin, while the secondary form arises in response to varied conditions including those of pulmonary, endocrine, gastrointestinal, haematological and inflammatory origin (Ortner 2003, 354). HOA is typically identified through clubbing and arthritis of the digits alongside symmetrical periosteal bone deposition on long bones (Ortner 2003, 354). Lesions are typically separated from the cortex by a fibrous layer in the early stages and may gradually progress to involve cortical and endosteal resorption as the lesion thickens (Ortner 2003, 354–6; Pineda *et al.* 1987). The largest fragment of the extant tibia is damaged by fragmentation and erosion, yet the extant portion of the lesion on the distal diaphysis exhibits a slightly coagulated and ropey appearance. This may be consistent with the early stages of HOA or HOA secondary to lung cancer (Pineda *et al.* 1987, 778). However, it is impossible to ascertain whether other long bones and/or the digits were affected, as would expected, or whether articular surfaces are involved, which would rule out HOA (Ortner 2003, 354). Tibial stress syndrome encompasses stress injuries and pain because of overloading and improper bone remodelling which may present as tibial periostitis and/or stress fractures (Couture & Karlson 2002; Gaeta *et al.* 2008; Mubarak *et al.* 1982), deep posterior compartment syndrome, or a shin splint. The lesion on the anterior aspect of the extant tibia appears to be in a more advanced stage of healing, suggesting it represents an earlier insult, and it is therefore possible that the distal diaphyseal lesion is unrelated and of differing aetiology.

Lesion type and healing status: Mixed; Mixed.
Lesion preservation: Excellent.
Differential diagnosis: Activity-Related Change; Trauma; Other.

8.6.1.5. FB0037: Fibula

Context:	(960)
Grid Ref:	99/112
Year of Excavation:	BR94
Other Details:	Unit 2, Spit 4

Element identification and preservation:
Fragmentary and incomplete left adult fibula represented by two fragments presenting a transverse and stepped fragmentation margin across the distal third of the diaphysis. The fragments are observed to

conjoin well. The distal diaphysis is fragmented in a stepped profile while a curved fragmentation margin transects the distal-most portion of the middle third of the diaphysis. Small areas of root etching are diffuse across the extant portion of the element, as well as focal erosion and minor longitudinal cracks emanating from the refitted fragmentation margins. Some red ochre flecks are observed on the middle third of diaphysis. Adult age estimation is based on the size of the extant element and the relative thickness of the cortex (White *et al.* 2012, 315). There are no current morphological or metric sex assessment methods engaged for isolated, fragmentary fibulae. The element is ~35% complete and the extant portions of the element are in fair condition. All damage is observed to be *postmortem*.

Macroscopic observations:
Periosteal woven bone encircles the extant portion of the element, traversing the re-fitted fragments (Fig. 8.41a-d). The lesion is truncated both proximally and distally and, combined with some *postmortem* erosion, this obfuscates full observation of pathology. On the anterior aspect, the lesion extends the length of the extant fragments, measuring 148.2 mm. The lesion is continuous across the medial surface, extending a maximum length of 190.2 mm. On the posterior aspect, the lesion extends the full length of the extant fragments for 168.2 mm. On the lateral aspect, the extant portion of the lesion extends for 81.8 mm from the proximal fragmentation margin. The maximum length of the extant portion of the lesion is 190.2 mm. The maximum width is 45.0 mm,

Figure 8.41. *Photographic and radiological images pertaining to fragmented adult left fibula (FB0037) from Context (960) of the Circle sample, depicting periosteal lesions traversing the refitted fragments, including: a) anterior view; b) medial view; c) lateral view; d) posterior view; e) transverse cross-section from CT data at mid-diaphysis showing globulated character of lesion, partially separated from underlying cortex which is slightly pockmarked; f) transverse cross-section at mid-point of extant element showing layered character of the lesion with vascularization on the medial surface; g) transverse cross-section at distal aspect of extant element, showing continued vascularization within the lesion and pockmarked cortex. Scale bar: 1 cm (photographs only). Photos Jess E. Thompson. (radiological images captured by L. Buck, Cambridge Biotomography Centre; processed by J. Magnussen & M. Pardey, Macquarie Medical Imaging.)*

taken inferior to the proximal fragmentation margin using a flexible paper tape.

The lesion exhibits mixed activity phases. The anterior and medial aspects of the lesion present a rugose topography of periosteal woven bone of mixed organization. Islands and layers of successive periosteal bone deposition contain bony nodules and billowing flows interspersed with extensive microporosity of single and coalescing pores, as well as diffuse microporosity. A vascular channel of 84.7 mm length is observed on the medial aspect, bordered by raised lamellar margins created by successive, chronic deposition of new periosteal bone. Sinuous impressions across the entire surface of the lesion indicate hypervascularity. The postero-medial aspect presents more recent osteoblastic activity, presenting as periosteal woven bone interspersed with microporosity. Here, islands of woven bone are observed but they are less rugose with finer microporosity. The antero-lateral and posterior margins of the lesion exhibit smooth deposits of well-healed bone with diffuse microporosity. On the lateral aspect, periosteal woven bone extends across the triangular subcutaneous area interspersed with micro- and microporosity. In this area, the lesion margins are sharply defined and directly correspond to the superior and lateral borders of the triangular subcutaneous area. Elsewhere, the margins of the extant portion of the lesion are diffuse and not well demarcated. The lesion is more rugose and porous than the surrounding cortex and is observed to differ in colour. When viewed from the fragmentation margin, the woven bone sits proud of the underlying cortex and no cortical change is observed. There are no indications of fracture, cloaca, or sequestra on the extant portion of the element.

Radiological observations:
The lesion is markedly more prolific on the anterior and medial surfaces on the extant portion of the element, where the new bone is dense and compact. Some separation is evident between the cortex and the periosteal new bone, and vascularity is observed within the lesion on the medial aspect (Fig. 8.41e-g). The character of the periosteal new bone is not as well-organized as the underlying cortex and presents an almost globular appearance. The underlying cortex appears pockmarked across almost the full extent of the extant fragment; approximately <10% of the extant element presents unaffected cortex, largely on the lateral surface. The new bone continues across the extant portion of the diaphysis on the lateral and posterior aspects. On the lateral surface, the cortex is in good condition and appears to be unaffected.

The lesion is truncated because of *postmortem* fragmentation, indicating that it extended onto at least the proximal metaphysis and distal diaphysis and was more widespread than is observable. Given that much of the element cannot be assessed, trauma and fracture must be considered in the differential diagnosis. The lesion is diffuse, extensive and associated with cortical change, suggesting a systemic process (Ortner 2003). Dense periosteal new bone formation on the fibula has been reported in cases of melorheostosis, hypertrophic osteoarthropathy (HOA) and chronic venous insufficiency (CVI) (Fennell & Trinkaus 1997; Gensburg *et al.* 1988; Kelley & Lytle 1995; Lester 1967; Martinez-Lavin *et al.* 1994; Yap *et al.* 2017). Melorheostosis is a rare condition which typically affects one, and occasionally several, bones of the lower limb, presenting dense and nodular new bone in a characteristic 'dripping candle wax' formation (Ortner 2003, 499 ff). Melorheostosis can be discounted in this case, as the lesion presents a layered, ropey and plaque-like expression. As mentioned before, HOA presents as symmetrical diaphyseal lesions on long bones, often alongside clubbing of the digits (Ortner 2003, 354). The location and expression of the lesion on the extant fibula resembles reported cases of HOA, although it cannot be ascertained whether the contralateral element or further long bones and/or digits were affected. As a result of the similar expression of periostitis because of HOA and CVI, CVI remains a possible aetiology in this case (Gensburg *et al.* 1988, 1280).

Lesion type and healing status: Mixed; Mixed.
Lesion preservation: Excellent.
Differential diagnosis: Trauma; Other.

8.6.1.6. FB0038: Fibula

Context:	(960)
Grid Ref:	99/112
Year of Excavation:	BR94
Other Details:	Unit 1, Spit 4

Element identification and preservation:
Fragment of right adult fibula which comprises the proximal metaphysis and approximately half of the proximal third of the diaphysis. A stepped fragmentation margin transects the fibular neck and an irregular fragmentation margin truncates the diaphysis. Minor areas of focal erosion are observed on the margins of the lesion. Adult age estimation is based on the size of the extant element and the relative thickness of the cortex (White *et al.* 2012, 315). As mentioned before, there are no current morphological or metric sex assessment methods engaged for isolated, fragmentary fibulae. The element is ~15% complete and the extant portion of the element is in fair condition. All damage is observed to be *postmortem*.

Figure 8.42. *Photographic and radiological images pertaining to fragmented adult right fibula (FB0038) from Context (960) of the Circle sample, depicting periosteal lesions traversing the refitted fragments of the proximal metaphysis and diaphysis, including: a) anterior view; b) medial view; c) lateral view; d) posterior view; e) transverse cross-section from CT data at proximal metaphysis showing sediment adhesion and pockmarked cortex; f) transverse cross-section toward the distal aspect of the extant element showing periosteal deposition on the medial aspect, perpendicular to the cortex. Scale bar: 1 cm (photographs only). Photos Jess E. Thompson; (radiological images captured by L. Buck, Cambridge Biotomography Centre; processed by J. Magnussen & M. Pardey, Macquarie Medical Imaging).*

Macroscopic observations:
Periosteal woven bone is observed on the extant portion of the element, although fragmentation of the proximal metaphysis and the diaphysis obfuscate full observation of pathology (Fig. 8.42a-d). On the anterior aspect, the lesion extends the full extent of the extant portion of the element along the interosseous crest, measuring 64.8 mm. From the proximal fragmentation margin, the lesion extends for 17.3 mm on the lateral aspect, 46.1 mm on the posterior aspect, and 11.4 mm on the medial aspect. The maximum length of the extant portion of the lesion is 64.8 mm along the interosseous crest; the maximum width measures 42.0 mm, encompassing the circumference of proximal metaphysis, inferior to the proximal fragmentation margin.

The lesion surrounds the metaphysis and exhibits mixed stages of activity. Woven bone exhibiting microporosity is present on the anterior and antero-lateral aspects. On the anterior aspect, the woven bone forms sheet-like deposits, while it is organized in approximately parallel lines of varying thickness along the interosseous crest, some of which coalesce towards the distal aspect of the extant portion of the diaphysis to become ropey and sit perpendicular to the cortex; these linear features extend onto the lateral aspect in two areas. Smooth plaque-like deposits of well-healed bone are present from the postero-lateral aspect to the medio-lateral aspect, interspersed with microporosity. On the antero-medial aspect, spicules are observed extending from the plaque deposit. The margins of the extant portion of the lesion are diffuse and not well-demarcated. With respect to the surrounding cortex, the woven bone is more rugose and porous and differs in colour. When viewed from the fragmentation margin, the woven bone sits proud of the underlying cortex and no cortical change is observed. There are no indications of fracture, cloaca, or sequestra.

Radiological observations:
Sediment is observed within the medullary cavity, particularly in the region of the proximal metaphysis, and therefore much trabecular bone has not been preserved. Some co-occurrence is observed with sediment adhesion and erosion of adjacent cortices, suggesting demineralization because of taphonomic processes (Fig. 8.42e). The cortex, particularly in the region of the proximal diaphysis, is irregular and pockmarked. Toward the distal end of the extant fragment, where sediment has not penetrated the element, the cortices underlying the periosteal lesions are observed to be slightly thicker and better preserved (Fig. 8.42f). Adjacent to the distal fragmentation margin, periosteal new

bone is observed on the anterior aspect and the underlying cortex is irregular. On the posterior aspect, the cortex is more regular and well-preserved, indicating that the lesions represent zonal deposits of new bone. The lesions are more apparent on the extant portion of the diaphysis than the metaphysis.

The lesion is truncated because of *postmortem* fragmentation, indicating that it extended further on the proximal metaphysis and diaphysis and was more widespread than is observable. As much of the element cannot be assessed, trauma and fracture must be considered in the differential diagnosis. The lesion occupies multiple surfaces and therefore does not represent a subperiosteal haematoma or ulcer (Ortner 2003, 84, 207). Although the extant portion of the lesion is damaged because of *postmortem* taphonomic processes, the expression of the periosteal new bone is ropey as opposed to nodular and therefore does not resemble that seen in cases of melorheostosis (Ortner 2003, 499 ff.). As outlined above, HOA and CVI are potential differential diagnoses. The character of the lesion on the extant fragment may be consistent with HOA, although we would expect the lesion to be more prolific on the mid-diaphysis, which is absent. Moreover, it cannot be ascertained whether the contralateral element or further long bones and/or digits were also affected. As a result of the similar expression of periostitis because of HOA and CVI, CVI again remains a possible aetiology in this case (Gensburg *et al.* 1988, 1280).

Lesion type and healing status: Mixed; Mixed.
Lesion preservation: Excellent.
Differential diagnosis: Trauma; Other.

8.6.1.7. Summary

Surprisingly, given their discrete depositional context, the adult elements described above exhibit periosteal lesions of widely varying expression. This presents a challenge to differential diagnosis. Research by Weston (2008, 2009) demonstrates that the morphology of periosteal lesions does not strongly correlate with their aetiology, but rather relates more closely to healing status and chronicity. Only some general conclusions can be made based on lesion type; for example, thick periosteal new bone deposits often indicate a chronic condition or osteomyelitis (Weston 2008, 55). Knowledge of the individual's age, sex, and health status (especially co-morbidities) are of key importance for differential diagnoses (Weston 2008, 56). Unfortunately, beyond broad adult age range, these factors cannot be addressed here, and caution must be exercised in attempts to identify aetiology/ies.

Nevertheless, through reference to bioarchaeological, clinical and palaeopathological literature, it is possible to exclude some potential aetiologies for each element. Significantly, there is no repetition of elements in this sample, as even the fibula fragments represent different sides and zones. The left ulna and radius present focal deposits of minor periosteal reaction on several muscle attachment sites; the character of the lesions, mixed healing stages, and muscles involved are similar across both elements. Furthermore, they are both observed to be of similar size and morphology (Fig. 8.43) and were excavated from the same level within this grid square. This may suggest that they originate from the same individual, who repetitively placed their left forearm under excessive strain. The

Figure 8.43. *Fragmented adult left radius (FB0033) and ulna (FB0034) from Context (960) of the Circle sample, both from grid square 99E/112N. While excavated in a disarticulated state, these elements are both of similar condition, size and morphology. Periosteal lesions are observed on contiguous muscle attachment sites on both elements, suggesting they precipitate from the same individual. Scale bar: 1 cm. (Photo Jess E. Thompson).*

lower limb elements provide different insights. The femoral fragment is likely osteoporotic, a factor which may relate to the aetiology of the periosteal lesions. Osteoporosis is not indicated in the lower leg elements, for which a small range of diagnoses are considered. Lesions on the extant portion of the right tibia, however, may represent multiple aetiologies and/or insults, and are distinct from those on the fibula fragments. In addition to the complexities of differential diagnosis when presented with disarticulated fragments, it is difficult to distinguish between prospective aetiologies for the lower leg elements. Many clinical reports highlight extreme cases and do not deal with dry bone specimens, while radiography is unlikely to register the early stages of periosteal bone formation (Weston 2012, 495). Altogether, we suggest that these elements originate from at least five individuals and demonstrate a range of pathological processes.

The high proportion of adult elements displaying periosteal lesions in this area is exceptional because of both their close spatial association and the relative under-representation of this category of lesions in all other contexts within the Circle. Context (960) is dated toward the end of the Circle's use, a period when declining environmental conditions and changing agricultural practices may have signaled restricted dietary diversity (§8.7.6). These elements may precipitate from individuals who lived through phases or cycles of resource instability and experienced heightened psychological, nutritional, metabolic and physical stress as a result.

8.6.2. Context (960) non-adult remains

8.6.2.1. FB0039: Frontal fragments

Context:	(960)
Grid Ref:	99/111
Year of Excavation:	BR94
Other Details:	Unit 1, Spit 3

Element identification and preservation:
Fragmentary non-adult frontal bone represented by three fragments which are observed to refit (Fig. 8.44a). The fragments comprise the left orbit, the frontonasal suture, the medial aspect of the right orbit, the left frontal eminence, and the left and medial portions of the frontal squama. On the supero-medial aspect of the frontal squama, an ovoid-shaped area of *postmortem* damage fully penetrating the cortex is observed. The margins of the defect are broader on the ectocranial surface, and they are rough, clean and differ in colour to the ecto- and endo-cranial surfaces. Minimal sediment is observed within the diploë. This damage therefore likely occurred during excavation. Taphonomic erosion and root etching interrupt the lesion in numerous locations. Although standards exist for estimating age based on measurements of the frontal bone (Young 1957; cf Scheuer & Black 2000, 108), it is not possible to apply metric analysis to this element because of its highly fragmentary and incomplete state. The metopic suture is in the process of closure and is only retained immediately superior to the frontonasal suture, suggesting the individual was in the range of 2–4 years of age at the time of death (Scheuer & Black 2000, 108). The extant element is in fair condition and represents ~60% of a complete frontal. All damage is assessed to be *postmortem*.

Macroscopic observations:
Periosteal lesions are observed on the ecto- and endocranial surfaces and within the left orbit and extant medial portion of the right orbit (Fig. 8.44b-e). *Postmortem* fragmentation truncates the lesion on all aspects; sediment has adhered to spicules in some areas, and root etching has interrupted the lesion. Full observation of pathology is therefore obfuscated. When viewed from the fragmentation margins, the lesions are observed to sit proud of the underlying cortex. Potential cortical involvement is only observed on a small area within the right and left supra-orbital margins. Since the lesion is truncated by fragmentation, its relationship to the surrounding cortex cannot be defined. There are no indications of fracture, cloaca or sequestra on the extant portion of the element.

On the ectocranial surface, the maximum length of the lesion is approximately 112.0 mm, measured with a flexible paper tape from the lateral border of the coronal suture to the most medial extent of the element; the maximum width of the lesion is approximately 130 mm on the sagittal plane. On the endocranial surface, the maximum length of the lesion is approximately 106.0 mm, from the most lateral border of the coronal suture to the medial extent of the element; the maximum width of the lesion is approximately 125.0 mm on the sagittal plane. On the infraorbital surface, the maximum length of the lesion is 38 mm along the centre of the orbit on the coronal plane; the maximum width of the lesion is approximately 40.0 mm along the centre of the orbit on the sagittal plane.

The lesion presents mixed activity phases. On the ectocranial surface, approximately 90% of the superior aspect of the frontal squama exhibits compact bone with hypervascular activity. Extensive branching capillary impressions are observed posterior to left frontal eminence and along the sagittal midline, interspersed with diffuse microporosity. Focal micrporosity with grooved exit channels is observed on the supero-medial aspect of both the right and left

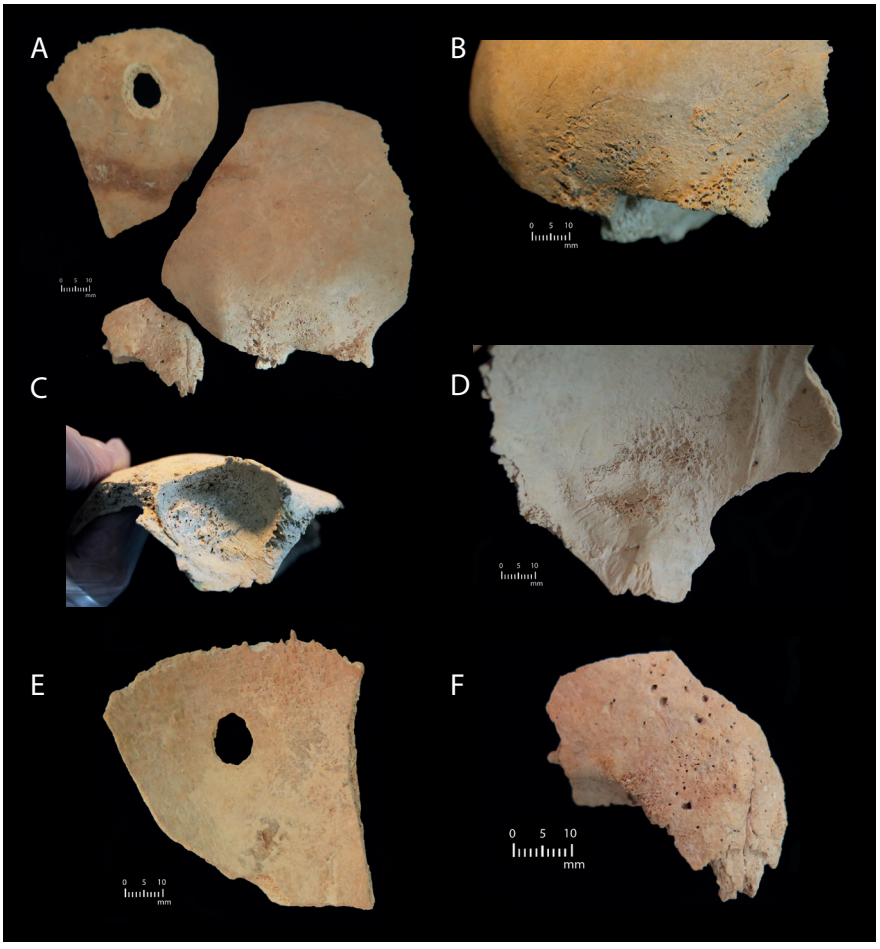

Figure 8.44. *Photographic images pertaining to fragmented non-adult frontal (FB0039) from Context (960) displaying extensive periosteal lesions, including: a) three re-fitting fragments of frontal bone; b) woven bone, capillary impressions and exit channels surrounding the left supraorbital margin on the ectocranial aspect; c) inferior view of left orbital roof presenting woven bone, macroporosity and extending spicules on the lateral aspect of the supraorbital margin; d) endocranial aspect of the frontal, displaying island of woven bone in the left frontal fossa; e) endocranial aspect of the central fragment of the frontal squama, presenting plaques of periosteal new bone; f) ectocranial aspect of the glabella and the extant portion of the right supraorbital margin displaying finely woven bone and macroporosity. Scale bar: 1 cm. (Photos Jess E. Thompson).*

supra-orbital margins, and on the lateral aspect of the left supra-orbital margin (Fig. 8.44b). Additionally, macroporosity with grooved exit channels is observed in this region. The margins of at least five micropores appear to have been eroded and enlarged *postmortem* because of taphonomic activity. A small area on the left frontal eminence differs in colour compared to the surrounding lesion; it is more yellow, glossy, and is most likely the original cortical surface. Extensive periosteal woven bone is observed in the glabella region and on the left supra-orbital margin. Perhaps as a result of *postmortem* truncation which may have eroded surrounding new bone, the woven bone appears to cluster in islands across this area. On the medial aspect of the left supra-orbital margin, supero-lateral to the metopic suture, and on the supero-lateral aspect of the right supra-orbital margin, these islands present as arrangements of fine, interconnected spicules perpendicular to the cortex, interspersed with micro- and macroporosity. The spicules on the left supra-orbital margin communicate with the lesion on the orbital roof. These islands are interspersed with micro- and macroporosity and bordered by capillary impressions. On the supero-lateral aspects of the left supra-orbital margins, the woven bone is extremely prolific and presents a more rugose topography of plates of bone organized perpendicular to the cortical surface, interspersed with micro- and macroporosity. On the left supraorbital margin, these plates of bone extend out from the margins, changing the anatomical profile of these features. The most supero-lateral aspects of the lesion in this region assume a more plaque-like deposit of woven bone and fine microporosity.

Extensive deposits of woven bone extend across the entire surface of the left orbital roof (Fig. 8.44c). The organization of woven bone is variable and interspersed with microporosity. The woven bone assumes a rugose topography within the anterior and medial aspects of the orbital roof, presenting as tall, perpendicular interconnected spicules assuming a trabecular-like organization. At the most medial aspect of the orbital roof, extensive osseous proliferation has produced sizeable, nodular projections, compromising the orbital space. On the postero-lateral aspect of the orbital roof, fine linear deposits of new bone overlie the cortex, often coalescing to form successive sheet-like plaques

resulting in raised platforms that compromise the orbital space. Postero-medial to this is a border of finely woven bone which assumes a trabecular-like organization. Posterior to this, an area of compact bone with diffuse capillary impressions is observed across the orbital wall, interrupted by a deposit of finely woven bone, bordered by capillary impressions at the most inferior extant margin.

On the endocranial surface, mixed activity phases are observed. In the region of the superior aspect of the frontal crest, branching capillary impressions are observed within the compact bone. Diffuse microporosity is observed on the inferior aspect of the frontal crest, bordered laterally by woven bone. Extensive woven bone deposits are observed on the endocranial aspects of the extant portions of the right orbital roof, the left orbital roof, and in the area immediately extending from and infero-medial to the midcoronal suture landmark, although these lesions are truncated by *postmortem* fragmentation. Extensive proliferation of woven bone is observed on the superficial and anterior endocranial aspects of the left orbital roof. A plaque-like deposit of finely woven bone is observed on the medial aspect of the left orbital roof superficial to the horizontal portion. This lesion exhibits increased rugosity as it extends laterally and superiorly onto the left frontal fossa, where the lesion projects from the cortical surface into the cerebral space (Fig. 8.44d). Here, the lesion presents as focal areas of interconnecting perpendicular spicules and plates of new bone, which in some places exhibit trabecular organization. *Postmortem* damage has compromised complete observations of this lesion. Deposits of fine woven bone, interspersed with capillary impressions, border the lesion on all sides. The maximum length of this lesion is 18.3 mm (medial-lateral) and the maximum width is 13.4 mm (anterior-posterior). On the supero-medial aspect, the lesion is interrupted by circular granular depressions approximately 2–3 mm Ø.

Extending supero-laterally from the frontal crest on both extant right and left sides, capillary impressions are observed within plaque-like deposits of bone, occasionally interspersed with small islands of finely woven bone. These capillary impressions extend to lesions adjacent to the coronal suture on both sides. On the left side, a plaque-like deposit of disorganized and rugose woven bone is present, exhibiting microporosity and capillary impressions; its maximum length is 28.3 mm (medial-lateral), and maximum width is 32.8 mm (superior to inferior). On the right side, the lesion presents similarly as a plaque of disorganized, rugose woven bone, although the extant portion of the lesion is smaller as it is truncated because of *postmortem* fragmentation. It occupies a maximum length of 28.6 mm (medial to lateral) and a maximum width of 30.3 mm (superior to inferior) (Fig. 8.44*e*). The character, healing stage and organization of the woven bone and hypervascularity suggests the lesions adjacent to the left and right coronal suture pre-date the lesion in the left frontal fossa. Furthermore, it is likely that the lesion occupied other elements of the calvarium, because of its close relationship to cranial sutures on the extant portion of the frontal.

Radiological observations:
On the largest fragment, encompassing the left orbit, left frontal eminence and lateral aspect of the frontal squama, the outer table appears irregular in the area of the supra-orbital margin (Figs 8.44f & 8.45a-b). The periosteal new bone deposition is pronounced toward the floor of the anterior cranial fossa and, here, the outer table is more well-defined and radiolucent than the inner table. Elsewhere, the cortices and diploë are in good condition on this fragment. The greatest degree of spiculation is observed closest to, and involving, the frontal sinus (Fig. 8.45c). At the cross-section of the frontal sinus, the cortices change from smooth and well-defined margins to develop a diffuse, poorly demarcated lesion characterized by small radiolucent holes. The diploë and trabecular bone are eroded and there appear to be multiple layers and pockmarks throughout the inner and outer tables of the sinus alongside pronounced spiculation. The outer table of the supra-orbital margin is markedly thin and the cortical bone has been stripped away as a result of pathological processes. The central frontal fragment with extant nasal bones also features some diffuse radiolucent holes on the outer table, however there are no spiculations and there is no obvious periosteal new bone formation in this area. On this fragment, the trabeculae are in good condition and well-preserved. There are small spicules on the medial margin of the left orbit, but the underlying cortex is well-preserved.

Pathogenically, the lesion on the extant frontal is widespread but not generalized. The inner and outer tables and diploë are mostly well-preserved and intact except where they directly underlie prolific lesions. Therefore, haematopoietic disorders, specifically haemolytic anaemia and beta thalassaemia (commonly found in central Mediterranean populations), can be discounted, as these conditions are characterized by hyperplasia as a result of expansion of the erythropoietic marrow (Lewis 2018, 200; Ortner 2003, 364–5). In this element, localized trabecular erosion with overall preservation of the bone architecture strongly indicates a metabolic or inflammatory process. A localized intra-cranial infection in the regions of greatest spiculation – the cone of the orbit, sinus and/or ethmoid – may be considered. Intra-cranial infections such as sinusitis rarely develop suppurative

complications, including meningitis and subdural empyema (Farmer & Wise 1973; Skelton *et al.* 1992). Childhood meningitis commonly develops following a bacterial infection, such as gastroenteritis, measles, mumps, *otitis media*, pneumonia, syphilis, tuberculosis, typhoid fever, and whooping cough (Lewis 2018, 144). Lesions involving the meninges on this element present as plaque-like deposits with capillary impressions and micropores, suggesting healing was underway at the time of death. Characteristic granulations associated with tubercular meningitis are absent (Lewis 2018, 144; Ortner 2003, 94). The proliferative lesions are reminiscent of metastasizing secondary bone tumours such as neuroblastoma; however, no osteoclastic activity is observed, and the new bone does not exhibit a radiating appearance (Ortner 2003, 536–7). Infantile cortical hyperostosis (ICH) occasionally reoccurs past infancy and has been reported in children of 2–4 years of age (Swerdloff *et al.* 1970). The condition sometimes involves the skull, provoking the deposition of pitted layered new bone, although most often affects the mandible, clavicle and long bones (Lewis 2018, 145; Lewis & Gowland 2009; Neuhauser 1970). The lesions on the extant frontal are distinct, presenting a more spiculated and hypervascular character without increased cortical thickening or involvement of the cortex.

Figure 8.45. *Radiological images pertaining to fragmented non-adult frontal (FB0039) from Context (960) displaying extensive periosteal lesions, including: a) sagittal cross-section from CT data displaying periosteal new bone in infraorbital surface, the endocranial aspect of the pars orbitalis and the frontal squama, and thinning of the outer table on the supraorbital margin; b) sagittal cross-section from CT data through the glabella displaying woven bone in the orbital vault and on the supraorbital margin; c) orthogonal plane cross-section from CT data displaying spicules of new bone within the left frontal sinus. (Radiological images captured by L.T. Buck, Cambridge Biotomography Centre; processed by J. Magnussen & M. Pardey, Macquarie Medical Imaging).*

The concentrations of reactive, woven and spiculated new bone on the supra-orbital margin, orbital roof and anterior cranial fossa are disorganized and were active at the time of death. These lesions are characteristic of subperiosteal and subdural haematomata, representing ossification following localized bleeding. In infants and children, such cranial lesions form part of the typical signature of trauma and abuse, alongside postcranial fractures of the ribs and long bones (Caffey 1946, 1974). No evidence of traumatic fracture is present on the extant frontal bone, and further periosteal reaction on the ecto- and endocranial surfaces of the frontal squama do not accord with a traumatic origin. As such, systemic metabolic disorders are the strongest candidates in this case. Vitamin C (scurvy) and vitamin D (rickets) deficiencies both stimulate periosteal new bone formation on the cranium in non-adult individuals (Brickley & Ives 2008; Lewis 2018, 211, 214; Ortner 2003, 386, 394). Rachitic features include osteopenia, bone thinning, frontal bossing, delayed fontanelle closure, and woven bone deposition which may eventually replace the inner and outer table (Brickley & Ives 2008, 103 ff.). On the extant frontal, the anterior fontanelle is observed to be closed (although this does not rule out the possibility that its closure was delayed), and there are no indications of osteopenia. Woven bone is zonally deposited on the ectocranial aspect of the frontal squama, and may indicate a phase of healing rickets with the commencement of osteoid mineralization. Scorbutic features include bilateral microporosity on the cranium and orbits and new bone formation in the orbits following haemorrhage because of weakened blood vessel walls (Brickley & Ives 2008, 57ff.; Lewis 2018, 214). Snoddy *et al.* (2018, 887) deem subperiosteal new bone and porosity on the endocranial surface suggestive markers of scurvy, while bilateral haemorrhage in the orbital roof is diagnostic. On the extant portion of the frontal bone assessed here, it is not possible to ascertain whether lesions are bilateral, although the

proliferative new bone observed on the extant medial aspect of the right orbit and supra-orbital margin provides a strong association. The proliferative lesion in the region of the anterior cranial fossa is consistent with subdural haematoma. The plaque-like lesions occupying the frontal squama may suggest this individual experienced chronic episodes of vitamin C deficiency, as they appear to be in a healing state. Diffuse capillary impressions and porotic lesions present across much of the frontal squama indicate an inflammatory response to extravasated blood (Snoddy *et al.* 2018, 878; Stark 2014, 19). The lesions on the extant frontal are therefore most consistent with scurvy but are not diagnostic in isolation.

Lesion type and healing status: Proliferative; Active.
Lesion preservation: Good.
Differential diagnosis: Metabolic.

8.6.2.2. FB0040: Frontal fragment

Context:	(960)
Grid Ref:	99/111
Year of Excavation:	BR94
Other Details:	Unit 1, Spit 3

Element identification and preservation:
Fragment of right non-adult frontal bone comprising the lateral three quarters of the orbit and right sphenofrontal suture. Although this fragment does not re-fit to the extant portion of frontal described in §8.6.2.1 above, the location and expression of the lesion corresponds to that seen on, and surrounding, the left orbit of fragment FB0039. Additionally, this fragment is consistent in size and morphology with the extant portion of the frontal. A quadrangular-shaped area of *postmortem* taphonomic erosion is observed on the supero-lateral aspect of the supraorbital margin and interrupts the lesion. Further *postmortem* erosion and sediment is observed adhering to the spicules on all aspects of the lesion. Although standards exist for estimating age based on measurements of the frontal bone (Young 1957; cf Scheuer & Black 2000, 108), it is not possible to apply metric analysis to this element because of its fragmentary and incomplete state. Given that this fragment is similar in size and morphology to the element described above, we can assign it to a similar age range (2–4 years of age). The extant element is in fair condition and represents ~10% of a complete frontal. All damage is assessed to be *postmortem*.

Macroscopic observations:
Periosteal new bone deposition is observed on the ecto- and endocranial surface and within the extant portion of the right orbit (Fig. 8.46a-c). *Postmortem* fragmentation truncates the lesion on all aspects, and full observation of pathology is therefore obfuscated. When viewed from the fragmentation margins, the lesion is observed to sit proud of the underlying cortex. Since the lesion is truncated by fragmentation, its relationship to the surrounding cortex cannot be defined. There are no indications of fracture, cloaca or sequestra on the extant portion of the element.

The lesion traverses the full extent of the extant portion of the element on all aspects. On the ectocranial surface, the maximum length of the lesion is 42.2 mm; the maximum width is 26.7 mm. On the endocranial surface, the maximum length of the lesion is 44.0 mm (measured with a flexible paper tape); the maximum width is 29.0 mm. On the infraorbital surface, the maximum length of the lesion is 27.6 mm; the maximum width is 27.0 mm (measured with a flexible paper tape. Mixed activity phases are observed. On the ectocranial surface, the superior and supero-medial margins of the lesion exhibit compact bone interspersed with capillary impressions (Fig. 8.46a). Capillary impressions including microporosity are extensive adjacent to the border of the medial fragmentation margin. The lateral and inferior portion of the lesion exhibits extensive periosteal woven bone. The supero-lateral aspect exhibits microporosity; here, the woven bone presents a diverse organization of narrow spicules which lie both parallel, and at an approximate 45° angle to, the original cortex. The infero-lateral aspect of the lesion is truncated because of the quadrangular area of *postmortem* erosion. Bordering the erosion, on the infero-medial aspect, a more rugose topography of extensive woven bone is observed. In the central portion, interconnecting plates of bone arranged perpendicular to the cortex and interspersed with macroporosity are observed. The medial aspect of this area displays a cluster of finer spicules arranged in trabecular-like organization interspersed with extensive microporosity. Adjacent to this, on the supero-medial aspect of the supra-orbital margin, discolouration is observed with respect to the surrounding lesion and may represent truncation of the lesion subsequent to post-excavation cleaning.

On the endocranial surface, sediment adhesion suggests that stages of *postmortem* taphonomic erosion and other processes have interrupted the lesion, truncating its original expression (Fig. 8.46b). The superior, lateral and inferior margins of the lesion present compact bone interspersed with capillary impressions, some of which are truncated by the fragmentation margins. Within the centre of the lesion, woven bone presents an arrangement of fine spicules perpendicular to the cortex arranged in trabecular-like organization, interspersed with microporosity. The woven bone is

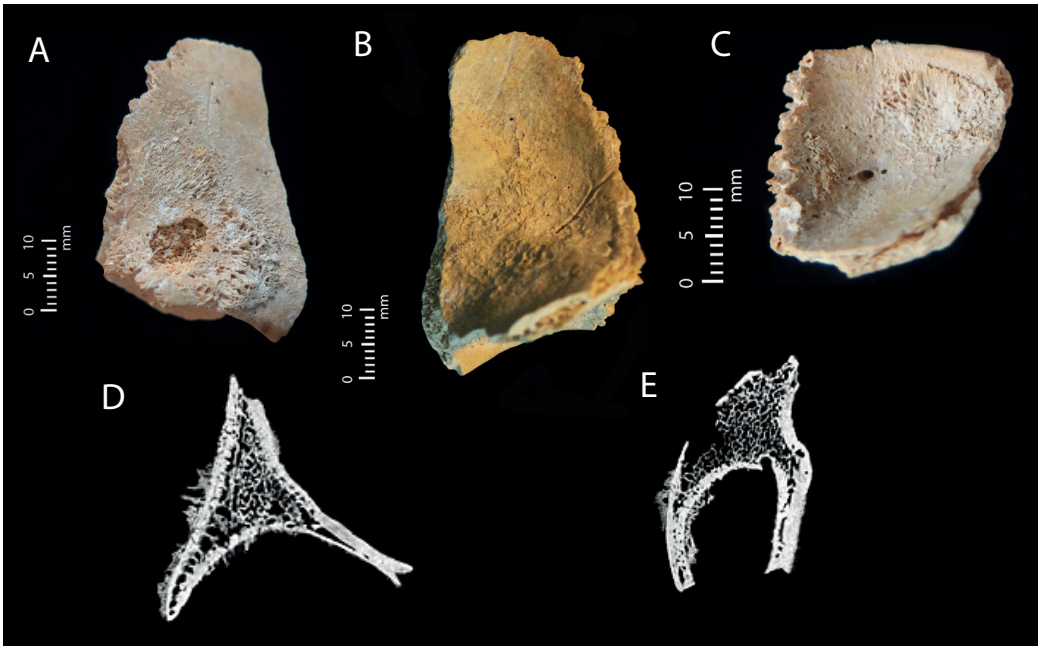

Figure 8.46. *Photographic and radiological images pertaining to fragment of non-adult frontal (FB0040) from Context (960) displaying extensive periosteal lesions, including: a) antero-lateral view of the ectocranial surface, with woven bone superior to the supraorbital margin and truncated by* postmortem *taphonomic erosion; b) endocranial view displaying woven bone and capillary impressions; c) inferior view of right orbital roof presenting islands of woven bone; d) sagittal cross-section from CT data through the mid-point of the orbit displaying spiculated new bone on the supraorbital margin, infraorbital surface and pars orbitalis; e) sagittal cross-section through the lateral aspect of the orbit, displaying woven bone on the supraorbital margin and infraorbital surface. Scale bar: 1 cm (photographs only). (Photos Jess E. Thompson; radiological images captured by L. Buck, Cambridge Biotomography Centre; processed by J. Magnussen & M. Pardey, Macquarie Medical Imaging).*

interrupted with small granular impressions on the infero-medial border.

On the infraorbital surface, the anterior border of the lesion along the supra-orbital margin presents compact bone. The antero-medial quadrant of the orbital roof exhibits woven bone interspersed with microporosity. The spicular organization varies; spicules overlying the cortex project anteriorly to the supra-orbital margin, while others are arranged at a sharply acute angle to the cortex. The postero-lateral quadrant of the orbital roof exhibits woven bone; fine spicules are arranged at an angle to the cortex, projecting medially, and interspersed with microporosity. Within the centre of the lesion, three distinct pores are observed. The posterior half of the lesion presents compact bone interspersed with capillary margins and microporosity.

Radiological observations:
The periosteal new bone is observed to be thicker than the cortex in most areas. Compared with the larger portion of the frontal, described above, there is more extant proliferative new bone formation on the ectocranial surface (Fig. 8.46d). On the lateral aspect of the extant portion of the right frontal, the cortices are in fair condition, but are observed to deteriorate progressively and are increasingly thinned approaching the medial aspect (Fig. 8.46d & e). The trabeculae are in fair condition. Given the similar expression and location of the lesion on this fragment when compared with the left orbital roof and supra-orbital margin, described above, it is highly probable that these fragments originate from the same individual and represent the same pathogenic process. As mentioned before, such proliferative lesions in the orbital roof indicate subperiosteal haematoma, usually attributed to trauma or scurvy (Brickley 2018; Brickley & Ives 2008, 58; Caffey 1974). As outlined above, reactive new bone formation along the supra-orbital margin is not consistent with trauma. The developmental stage, morphology, and lesion character on the extant right frontal are strongly compatible with the re-fitted fragments described above, and all were excavated from the same level and unit. Therefore, we argue that these fragments

all originate from the same young child. As such, the orbital lesions indicate bilateral orbital haemorrhage, diagnostic of scurvy (Brickley & Ives 2008, 57; Snoddy *et al.* 2018, 887; Thompson *et al*. 2021).

Lesion type and healing status: Proliferative; Active.
Lesion preservation: Good.
Differential diagnosis: Metabolic.

8.6.2.3. FB0041: Zygoma

Context:	(960)
Grid Ref:	99/111
Year of Excavation:	BR94
Other Details:	Unit 1, Spit 3

Element identification and preservation:
Left zygoma with frontal process fragmented. *Post-mortem* damage is observed on the infraorbital margin. The maximum length of the zygoma, measured from the maxillary process to the temporal process using digital callipers, is 34.3 mm. Postnatal age estimation through metric analyses for the zygoma is not provided; however, the element is observed to present adult proportions, with a serrated temporal process, characteristic of individuals at least 2–3 years of age (Scheuer & Black 2000, 124). The extant element is in fair condition and is ~95% complete. All damage is assessed to be *postmortem*.

Macroscopic observations:
Periosteal new bone deposition is observed on the anterior, posterior and superior aspects of the element, extending across the full extent of each surface (Fig. 8.47a-c). The maximum length of the lesion from the maxillary process to the temporal process on the anterior aspect is 34.2 mm. the maximum width of the lesion on the midpoint of the sagittal plane is 16.2 mm. On the posterior aspect, the maximum length of the lesion from the maxillary process to the temporal process is 34.4 mm; the maximum width of the lesion is 15.5 mm. On the infraorbital surface, the maximum length of the lesion is 21.5 mm and the width of the lesion is 9.6 mm.

The lesion presents mixed activity phases. On the anterior surface, the proximal half of the lesion presents woven bone arranged in plate-like formations, perpendicular to the cortex, interspersed with diffuse micro- and macroporosity (Fig. 8.47a). Capillary impressions are observed on the medial and lateral margins of the element. The distal half of the lesion presents well-healed bone with microporosity; the inferior border exhibits capillary impressions and one macropore. On the posterior surface, spicules

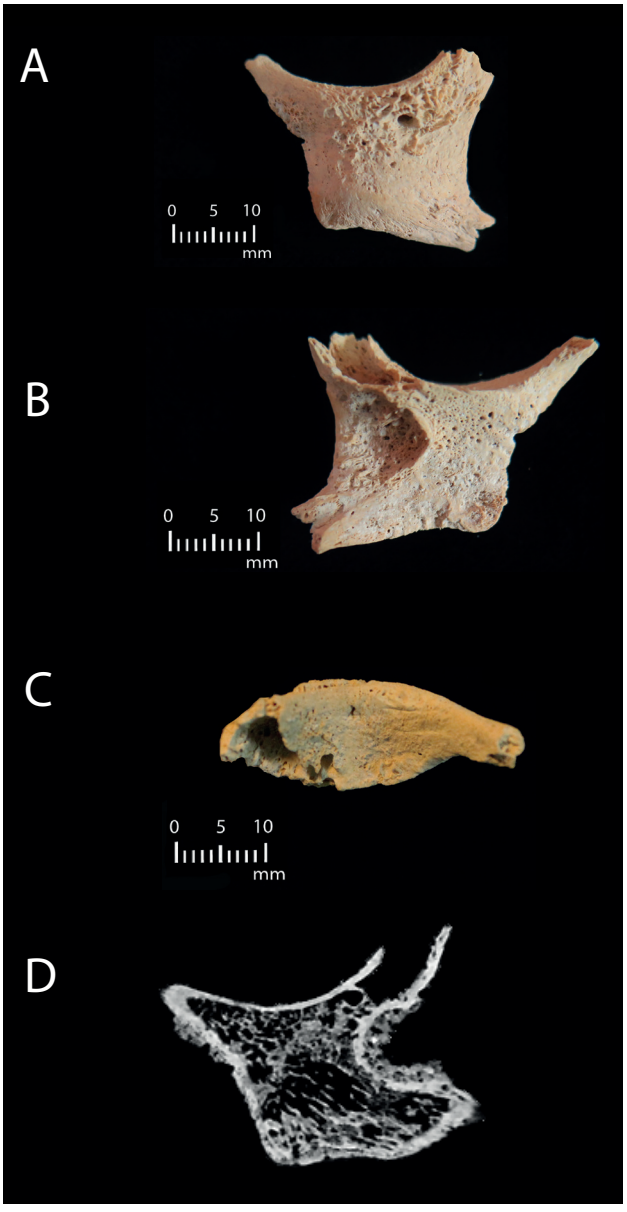

Figure 8.47. *Photographic and radiological images pertaining to non-adult left zygoma (FB0041) from Context (960) displaying extensive periosteal lesions, including: a) anterior view with woven bone concentrated on the proximal half of the element; b) posterior view presenting diffuse microporosity and woven bone; c) superior view displaying woven bone and microporosity on infraorbital surface, interrupted by excavation toolmarks; d) coronal cross-section from CT data presenting discontinuous cortex and periosteal new bone on the medial, lateral and inferior aspects. Scale bar: 1 cm (photographs only). (Photos Jess E. Thompson; radiological images captured by L. Buck, Cambridge Biotomography Centre; processed by J. Magnussen & M. Pardey, Macquarie Medical Imaging).*

perpendicular to the cortex are observed on the lateral portion interspersed with more diffuse woven bone deposition and micro- and macroporosity (Fig. 8.47b). On the medial and inferior aspect, smooth deposits of bone exhibit extensive microporosity. The infraorbital surface presents woven bone, becoming perpendicular in organization, interspersed with microporosity although some taphonomic damage, including excavation cutmarks, interrupts the lesion (Fig. 8.47c). Within the centre of the lesion, well-healed bone presenting microporosity is observed. The margins of the lesion cannot be defined and its relationship to the original cortex cannot be described. There are no indications of fracture, cloaca, or sequestra.

Radiological observations:
Considerable demineralization of the cortices is evident. The outer cortex underlying the lesion is both discontinuous and porotic (Fig. 8.47d). The trabeculae are relatively well-preserved, and the margins of nutrient foramina and vascular channels remain intact, indicating a minimal degree of internal bone loss. The new bone deposition is neither lamellated nor particularly spiculated on any aspects of the element, rather it is markedly disorganized and thick. The lesion does not resemble the typical lamellar new bone observed in cases of traumatic fracture.

Periosteal lesions on the zygoma are relatively uncommon, reported in association with tuberculosis (Meng & Wu 1942; Ortner 2003, 250), iron-deficiency anaemia (Ortner 203, 373), and scurvy (Buckley *et al.* 2014; Ortner *et al.* 1999, 2001; Snoddy *et al.* 2017). Tuberculous lesions on the cranium are most often observed in non-adult individuals (Lewis 2004, 150) and may involve the zygoma, especially the orbital margin (Ortner 2003, 250). Lesions are typically focal and destructive, however, in contrast to the extensive woven bone observed on this element. Ortner (2003, 373) presents a severe case of porotic hyperostosis and marrow hyperplasia indicating iron-deficiency anaemia in a young child; the zygomae exhibited porous lesions, expansion of the diploë and destruction of the outer table. Beta thalassaemia can cause more extensive changes, as trabecular expansion, cortical thinning and delayed sinus development lead to altered facial features, including 'bulging' zygomae (Lewis 2018, 200; Ortner 2003, 365). On the extant element, however, the trabeculae are well-preserved with no indication of enlargement, and porosity is mostly focussed on the internal aspect.

Scorbutic lesions on the zygoma are typically located on the internal/posterior aspect and the lateral orbital margin (Ortner *et al.* 2001, 346; Snoddy *et al.* 2018, 879). These locations are associated with *Mm. masseter*, *temporalis* and *orbicularis occuli* as well as branches of the masseteric, superficial temporal, zygomaticoorbital and zygomaticofacial arteries, all implicated in facial movement and expression (Snoddy *et al.* 2018, 879). The extant element presents extensive woven bone and porosity on the posterior surface, while the infraorbital and anterior surfaces exhibit islands of spiculated woven bone, suggestive of subperiosteal haematomas. The *Mm. zygomaticus minor* and *major* attach to the anterior aspect of the zygomae, essential for movement of the mouth. Brown and Ortner (2011, 200) present a case of scurvy in a Medieval two-year-old child, observing unilateral porosity inferior to the zygomaticofacial foramen. The lesions on the anterior aspect of the extant element appear to be rare in the presentation of scurvy. Snoddy *et al.* (2018, 888) note that porosity and subperiosteal new bone on the zygoma is suggestive of scurvy when observed bilaterally. Unfortunately, the contralateral zygoma is unavailable for assessment. However, the expression and location of the lesions are most consistent with a scorbutic aetiology.

Lesion type and healing status: Mixed; Mixed.
Lesion preservation: Excellent.
Differential diagnosis: Metabolic.

8.6.2.4. FB0042: Mandible fragments

Context:	(960)
Grid Ref:	99/111
Year of Excavation:	BR94
Other Details:	Unit 1, Spit 3

Element identification and preservation:
Two non-adult mandible fragments are observed to refit. The largest fragment comprises the right ramus, with right coronoid process almost complete and right mandibular condyle fragmented along the neck, and most of the mandibular corpus. The corpus is fragmented on the posterior aspect of the alveolus of the second left deciduous molar. The smaller fragment is observed to refit along the superior aspect of the corpus, completing the alveolus containing the second left deciduous molar, although the inferior portion of the mandibular corpus is fragmented and absent. The left coronoid process is almost complete, while the left mandibular condyle is fragmented along the neck. Focal areas of *postmortem* erosion are observed on the element, while a small triangular area of fragmentation on the lingual aspect of the right mandibular corpus exposes the crypt containing the developing germ of the right first permanent molar. The mandibular symphysis is fused. Mandibular dental eruption indicates

an age at death of 2 years (±8 months) because of the eruption of the deciduous right first molar (FDI 84), incomplete root development of the deciduous left second molar (FDI 74), and developing crown of the permanent right first molar (FDI 46; Ubelaker 1989). The extant portion of the element is in good condition and is ~90% complete. All damage is assessed to be *postmortem*.

Macroscopic observations:
Periosteal new bone deposition is observed on all aspects of the element. *Postmortem* fragmentation in the alveolus posterior to the second left deciduous molar obfuscates full observation of pathology. When viewed from the fragmentation margins, the lesions are observed to sit proud of the underlying cortex and no cortical change is discerned. All lesions differ in colour to the surrounding cortex, but present diffuse margins which are not well demarcated. There are no indications of fracture, cloaca or sequestra.

The lesion envelops the anterior and lateral aspects of the mandibular corpus, encompassing approximately 90% of the right ramus. The lesion commences approximately 6.9 mm from the superior-most projection of the right mandibular condyle and extends anteriorly for 20.5 mm to the coronoid process and 27.0 mm inferiorly to the gonial angle, where a small localized area of *postmortem* erosion truncates the lesion. From its most posterior extent on the right gonial angle, the lesion envelops the mandibular corpus for a maximum length of approximately 111.0 mm (measured with a flexible paper tape) and is truncated by the fragmentation margin (Fig. 8.48a & b). The maximum height of the lesion on the posterior border of the right ramus is 32.1 mm. The lesion demonstrates mixed activity phases. On the right ramus, capillary impressions are observed on the superior margins, on the condyle and coronoid process. Woven bone is observed on the margins of the lesion, interspersed with micro- and macroporosity. Postero-inferior to the oblique line, woven bone is arranged in conjoined spicules and plates perpendicular to the cortical surface, assuming a trabecular-like appearance, bordered inferiorly by fine capillary impressions on the gonial angle. *Postmortem* damage has removed portions of the new bone in this area. Macroporosity is observed on the posterior border of the oblique line. A small area of plaque-like bone is present in the centre of the ramus, interspersed with fine capillary impressions.

On the lingual aspect, periosteal new bone is observed in two focal areas: adjacent to the fragmentation margin associated with the crypt of the developing germ of the first permanent right mandibular molar (FDI 46), and on the right ramus extending to the submandibular fossa (Fig. 8.48c). The first lesion is truncated by the previously mentioned fragmentation margin, but is observed to commence within the posterior aspect of the left submandibular fossa 6.5 mm proximal to the fragmentation margin. The extant portion of the lesion encompasses a maximum length of 6.5 mm and a maximum height of 2.5 mm. The lesion presents mixed activity phases. The peripheral margins exhibit well-healed plaque deposits of bone interspersed with capillary impressions, while the centre exhibits extensive woven bone deposition with focal micro- and macroporosity. The margins of the lesion are diffuse and not well-demarcated. The second lesion commences 5.2 mm inferior to the fragmentation margin on the right coronoid process, extending 20.7 mm posteriorly to the mandibular condyle and inferiorly for 28.2 mm to the gonial angle. From the most posterior extent of the lesion on the gonial angle, its maximum length is 30.7 mm to the submandibular fossa. On the coronal plane, the maximum height of the lesion is 28.0 mm on the right ramus. The lesion demonstrates mixed activity phases. The superior and posterior margins of the lesion present compact bone with increased micro- and macroporosity. The central portion of the lesion, within and surrounding the mylohyoid groove, demonstrate periosteal woven bone. Capillary impressions surround the mylohyoid groove, particularly on the superior aspect, and extensive micro- and macroporosity is observed within the mylohyoid groove. Some islands of woven bone are observed posterior and inferior to the mylohyoid groove, interrupted by compact bone. Increased porosity is demonstrated across the lesion. On the inferior aspect of the right mandibular corpus, periosteal new bone deposition is observed anterior to the previously mentioned fragmentation margin, encompassing a maximum length of 4.2 mm and a maximum width of 2.8 mm. The extant portion of the lesion exhibits periosteal woven bone interspersed with microporosity; its margins are distinct from the surrounding cortex and the bone is observed to be more rugose and porous.

Woven bone interspersed with microporosity extends across the right side of the mandibular corpus on the distal half and on the left mandibular corpus. *Postmortem* erosion has damaged the lesion, however, and the margins are not well demarcated. A small island of woven bone is observed in the fossa between the right mental foramen and mental eminence, presenting microporosity. Extensive microporosity is present on the mental eminence, interspersed with patches of woven bone deposition and capillary impressions on the inferior border (Fig. 8.48b). Well-healed plaque deposits of bone are observed posterior to this, interspersed with microporosity. Across the

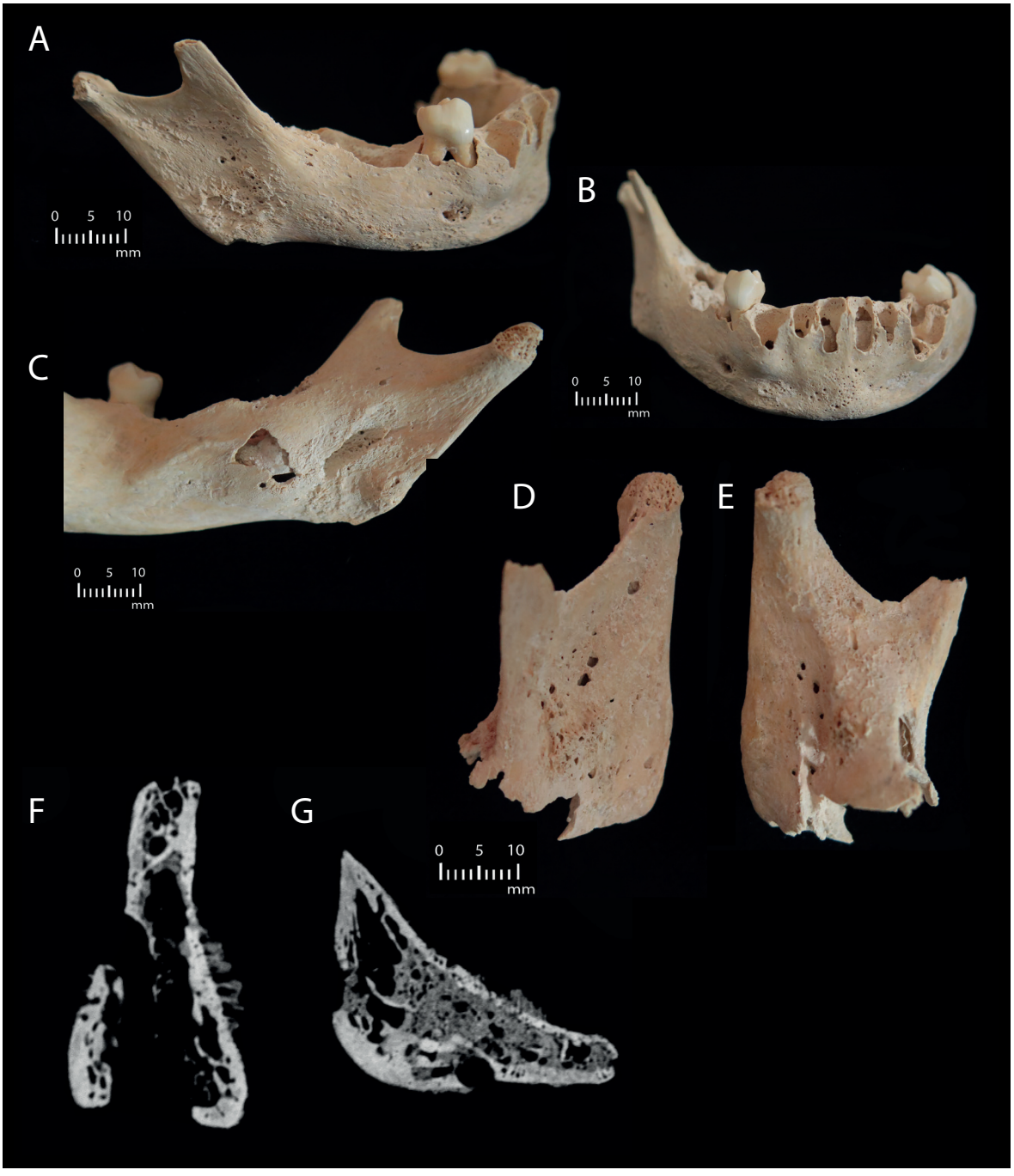

Figure 8.48. *Photographic and radiological images pertaining to fragmented non-adult mandible (FB0042) from Context (960) displaying focal periosteal lesions, including: a) lateral view of right ramus and corpus with woven bone concentrated on the ramus; b) anterior view presenting microporosity and finely woven bone on the mental eminence; c) medial view of right ramus with woven bone surrounding crypt containing developing right first permanent molar (FDI 46) and finely woven bone surrounding the mylohyoid groove; d) antero-lateral view of fragmented left ramus displaying woven bone and macro- and microporosity; e) medial view of fragmented left ramus with finely woven bone on anterior border of mylohyoid groove; f) transverse cross-section from CT data through left ramus vertical short axis displaying spicules on lateral aspect; g) sagittal cross-section through right ramus displaying spicules on medial aspect. Scale bar: 1 cm (photographs only). (Photos Jess E. Thompson; radiological images captured by L.T. Buck, Cambridge Biotomography Centre; processed by J. Magnussen & M. Pardey, Macquarie Medical Imaging).*

entire anterior surface of the mandible, the lesion demonstrates hypervascularity although the margins are diffuse and not well-demarcated. A small island of woven bone deposition is observed in the fossa between the right mental foramen and the mental eminence, presenting microporosity bordered by fine capillary impressions. Further capillary impressions and plaque-like bone deposition extend inferiorly and posteriorly along the corpus. Four micropores are observed inferior to the left mental foramen. Well-healed plaque deposits of bone are observed posterior to this, interspersed with microporosity.

On the lateral aspect of the left ramus, periosteal new bone deposition commences 7.2 mm inferior to the fragmentation margin on the coronoid process, extending 19.1 mm posteriorly and 20.3 mm inferiorly (Fig. 8.48d). The maximum height of the lesion on the coronal plane is 27.1 mm; the maximum width of the lesion is 20.8 mm. The lesion exhibits mixed activity phases. The posterior margins of the lesion exhibit well-healed lamellar bone interspersed with micro- and macroporosity and capillary impressions. Well-healed bone extends into the centre of the lesion with macroporosity on the oblique line. Islands of woven bone are observed on the anterior aspect inferior to the mandibular notch, on the most inferior aspect of the coronoid process and posterior to the oblique line. In the latter location, bony nodules are observed on the superior aspect and, inferior to this, clusters of spicules and conjoined bony plates are present at a perpendicular angle to the cortex, interspersed with microporosity. On the posterior aspect, the lesion commences 28.7 mm inferior to the mandibular condyle and extends for 8.1 mm. The maximum width of the lesion is 3.4 mm. The lesion presents smooth deposits of bone surrounding focal macroporosity.

On the medial aspect, the extant portion of the lesion commences inferior to the margins of *postmortem* erosion on the left condyle, extending inferiorly for 36.5 mm and anteriorly for 22.7 mm (Fig. 8.48e). The maximum height of the lesion is 36.7 mm on the posterior border and the maximum width of the lesion is 15.6 mm on the inferior aspect of the mandibular notch. The lesion presents mixed activity phases. Inferior to the mandibular condyle, small granular and capillary impressions are observed. Inferior to the mandibular notch, woven bone is interspersed with microporosity, continuing inferiorly onto the anterior and posterior border of the mylohyoid groove. Macroporosity is observed within the mylohyoid groove. On the anterior border of the mylohyoid groove, clusters of bony spicules and plates sit perpendicular to the cortex. Woven bone is observed on the margins of the lesion, interspersed with capillary impressions and micro- and macroporosity.

Radiological observations:
On the largest fragment, the cortices are smooth and well-defined on the lingual and buccal aspect of the mandibular corpus, particularly around the sagittal midline, representing healthy tissue. Some small spiculations are preserved on the anterior aspect of the mandibular corpus, superficial to the alveoli containing the developing permanent canines, presenting a bilateral expression on the labial aspect of the corpus. No lesions are observed on the lingual aspect. The mandible retains a 'normal' appearance until just posterior to the crypt containing the developing right first permanent molar, after which the lesion progressively worsens (Fig. 8.48f). On the right ramus, the degree of bone loss on the buccal surface around the area of the developing right first permanent molar is extensive. At the angle of the mandible on the right side, small areas of periosteal new bone are observed. Similarly, periosteal new bone is observed on the left mandibular angle, although the lesion is more widespread, especially on the buccal surface (Fig. 8.48g). On the left mandibular ramus, the cortices present diffuse poorly demarcated radiolucent holes and the trabeculae are observed to be pockmarked. Lesions are located close to the alveoli on the buccal aspect of the posterior teeth and are expressed bilaterally. No periosteal new bone is observed within the crypts.

As Lewis (2018, 3) notes, distinguishing new bone formation as a result of the normal growth process from infectious or traumatic new bone deposition is challenging. Focal areas of micro- and macro-porosity on the extant mandible may usually be attributed to growth, however, their association with finely woven new bone across much of the element, as well as the bilateral expression of the reactive new bone is suggestive of pathological processes. There is no evidence of fracture; the element is re-fitted along a *postmortem* fracture margin and a small portion of the lingual surface of the corpus is absent. Such extensive porosity and new bone deposition likely has either an infectious, neoplastic or metabolic origin.

As mentioned before, infantile cortical hyperostosis (ICH) has been reported past infancy, in children of 2–4 years of age (Swerdloff *et al.* 1970). The condition most often affects the mandible and clavicle and is characterized by extensive periosteal new bone formation (Lewis 2018, 145). In the early stages of inflammation, cortical hyperostosis is pronounced, while later remodelling is evident through widening of the medullary cavity (Lewis 2018, 145). On the extant element, the cortex is of expected

thickness and only demonstrates irregularity in the region of the periosteal lesions, and no expansion of the medullary space is observed. Such observations, alongside dental eruption in the expected sequence, also rule out beta thalassaemia (Lewis 2018, 200; Ortner 2003, 365). Primary or secondary tuberculosis may involve mandibular lesions, including osteomyelitis (Imamura *et al.* 2004) and lytic destruction in the region of the mandibular angle alongside new bone formation (Gupta & Singh 2007). Actinomycosis, a rare bacterial infection, can present similarly; *Actinomyces* bacteria commonly line the oral cavity and may provoke localized infection secondary to tissue damage, for example following injury, trauma or periodontal disease (Ortner 2003, 319). Inflammatory reactions on the mandible include periosteal new bone deposition, hypervascularity, and numerous focal lytic lesions alongside some cortical and trabecular erosion (Ortner 2003, 319-20). On the extant element, new bone deposition is observed, including on the mandibular angle, but there is minimal cortical erosion and no lytic foci are present. Leukemia, cancers of the myeloid and lymphoid hematopoetic cells, peaks in children from 2–5 years of age, presenting as periosteal new bone formation and extensive lytic pitting (Lewis 2018, 206). Rothschild *et al.* (1997) present a case of childhood leukemia in which periosteal new bone was observed on the external aspect of the mandibular ramus alongside lytic pitting on the cranium, scapula, long bones, pelvis and pedal elements. On the extant mandible, porosity is less frequent than woven new bone deposition and no lytic pitting is observed.

Therefore, a metabolic disorder is most likely. The concentrations of woven subperiosteal new bone bilaterally on the ascending ramus, between the mental foramen and mental eminence, and in the region of the mylohyoid groove were active at the time of death and are characteristic of subperiosteal haematomata. Scorbutic lesions on the mandible include extensive microporosity (Brickley & Ives 2008, 57; Ortner *et al.* 2001), new bone on the coronoid process, ramus, alveoli and mylohyoid line (Lewis 2018, 217; Ortner *et al.* 2001; Snoddy *et al.* 2018), and *antemortem* tooth loss (Lewis 2018, 217). The coronoid processes are fragmented on the extant mandible and cannot be assessed, however new bone is observed on the lateral and medial aspect of the rami, as well as on the mandibular corpus. There is no evidence of periodontal disease or alveolar resorption, indicative of *antemortem* tooth loss. Bilateral deposits of subperiosteal new bone on the rami are diagnostic of scurvy (Snoddy *et al.* 2018, 890). Significantly, the lesions on this element accord with attachment sites for the *Mm. mentalis*, *masseter*, and *medial* and *lateral pterygoid*, which are involved in movement of the lower lip, mastication and speech (Parkin & Logan 2007, 40, 42), indicating micro-trauma associated with these essential facial movements.

Lesion type and healing status: Mixed; Mixed.
Lesion preservation: Excellent.
Differential diagnosis: Metabolic.

8.6.2.5. FB0043: Rib fragment

Context:	(960)
Grid Ref:	99/111
Year of Excavation:	BR94
Other Details:	Unit 1, Spit 3

Element identification and preservation:
Fragment of left middle-lower order rib shaft. The head and the neck of the rib are fragmented and absent. A *postmortem* transverse fracture truncates the shaft of the rib at the approximate mid-point. Regression equations exist for age estimation according to the length of individual ribs in prenatal individuals (Fazekas & Kosa 1978; cf Scheuer & Black 2000, 243). Amongst infants and children however, the major factor affecting rib morphology is increased torsion in rib shafts as the ventral aspect of the thorax descends (Scheuer & Black 2000, 241). Although incomplete, the morphology of the extant portion of the rib shaft demonstrates torsion and may indicate that this individual was between the ages of at least 1–3 at the time of death (Scheuer & Black 2000, 241). The extant portion of the element is in good condition and represents ~50% of a complete rib. All damage is assessed to be *postmortem*.

Macroscopic observations:
Periosteal new bone deposition is observed almost circumferentially on the extant portion of the body of the rib, involving the external and pleural surfaces (Fig. 8.49a-b). The lesion is truncated medially and laterally, obfuscating full observation of pathology. There are no indications of fracture, cloaca, or sequestra on the extant portion of the element.

On the external aspect, the lesion commences 24.5 mm from the anterior fragmentation margin and extends for 67.0 mm. The lesion demonstrates mixed activity phases. On the pleural aspect, the extant portion of the lesion commences adjacent to the anterior fragmentation margin and extends for 77.0 mm (measured with a flexible paper tape). On the external aspect, partially healed plaque-like deposits of bone are observed, interspersed with diffuse capillary impressions (Fig. 8.49a). The margins of the extant portion of the lesion are diffuse and not well demarcated.

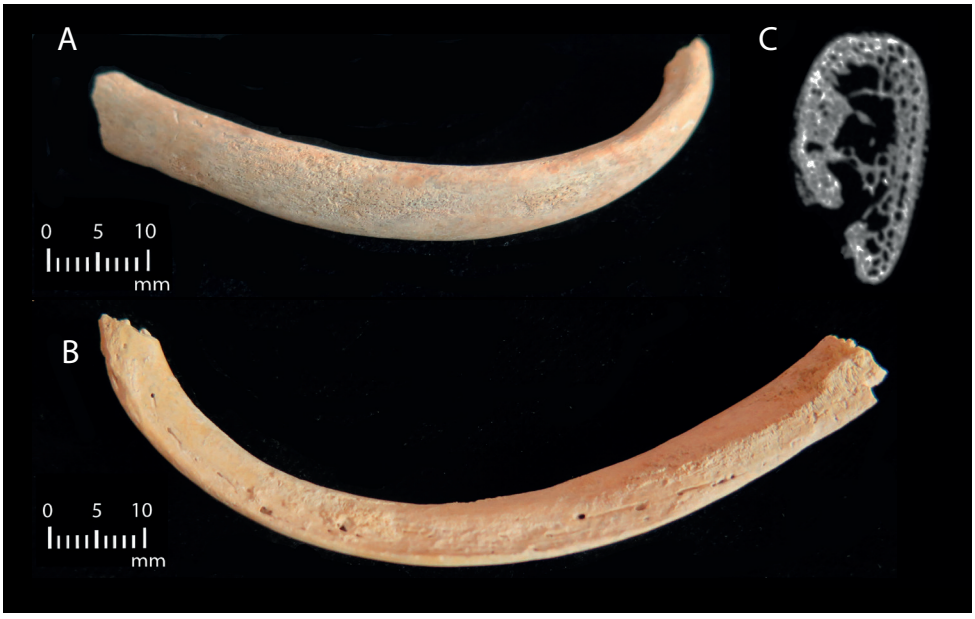

Figure 8.49. *Photographic and radiological images pertaining to fragmented non-adult left rib (FB0043) from Context (960) displaying focal periosteal lesions, including: a) posterior/external view displaying finely woven bone with capillary impressions; b) inferior view of pleural surface displaying focal lesions of woven bone; c) sagittal cross-section from CT data through distal aspect of extant portion of rib, displaying fine spiculation on superior, external and pleural aspects. Scale bar: 1 cm (photographs only). (Photos Jess E. Thompson; radiological images captured by L. Buck, Cambridge Biotomography Centre; processed by J. Magnussen & M. Pardey, Macquarie Medical Imaging).*

The lesion is taller than the surrounding cortex and is observed to differ in colour. When viewed from the lateral fragmentation margin, the lesion merges with the original cortex. On the pleural surface, the most medial and lateral portions of the extant lesion present clusters of bony spicules and plates, sitting perpendicular to the cortex in trabecular-like organization (Fig. 8.49b). The lesion is more severe on the anterior aspect. In the central aspect of the extant pleural surface, mild and partially healed periosteal new bone deposition is observed, interspersed with capillary impressions. Micro- and macroporosity is present along the costal groove on the extant portion of the element.

Radiological observations:
At the mid-point of the extant portion of the rib, fine periosteal lesions are observed on the external surface. Towards the medial aspect, periosteal new bone is also observed on the pleural surface, and patchy new bone deposition extends almost circumferentially. Towards the lateral end of the extant fragment, there are thicker spiculated lesions with separation evident in parts between the periosteum and the new bone, indicating subperiosteal haematoma (Fig. 8.49c). There are more widespread but subtle changes throughout much of the shaft toward the distal aspect.

There is no evidence of fracture on the extant portion of the element, suggesting the observed lesions are not associated with trauma. As Lewis (2018, 3) notes, distinguishing new bone formation as a result of the normal growth process from infectious or traumatic new bone deposition is challenging. The extant element presents focal lesions incorporating capillary impressions on the external aspect and diffuse finely woven new bone on the pleural aspect, suggestive of pathological processes. Lesions on the pleural rib surface suggest inflammation of the pleura, typically associated with respiratory infections, such as tuberculosis. Tuberculous rib lesions commonly affect the middle ribs, incorporating lytic foci, enlargement of the costochrondral joint and minimal periosteal new bone on the pleural surface (Ortner 2003, 246). Unfortunately, the sternal end of the rib is absent and cannot be assessed; however, lesions on the extant fragment are not observed to be lytic. The external lesions appear to be in a more advanced stage of the healing process, while the pleural lesions are more active, suggesting a chronic process. Subperiosteal new bone deposition on the ribs is occasionally noted in cases of non-adult scurvy (Buckley *et al.* 2014; Snoddy *et al.* 2017), and may be observed alongside fracture and/or enlargement of the costochrondral junction (the 'scorbutic rosary') (Brickley & Ives 2008, 57). The external

rib surface is associated with *Mm. serratus anterior* and *pectoralis major* (Snoddy *et al.* 2018, 880). Therefore, subperiosteal new bone on the external surface of the extant rib may be a result of micro-trauma associated with movements involving these muscles, while the pleural lesions indicate subperiosteal haemorrhage because of expansion and contraction of the lungs. These features are deemed suggestive of scurvy but should be observed bilaterally alongside further characteristic lesions (Snoddy *et al.* 2018, 891; Thompson *et al*. 2021).

Lesion type and healing status: Mixed; Mixed.
Lesion preservation: Excellent.
Differential diagnosis: Metabolic.

8.6.2.6. FB0044: Rib fragment

Context:	(960)
Grid Ref:	99/111
Year of Excavation:	BR94
Other Details:	Spit 3

Element identification and preservation:
Fragment of right lower order rib shaft. The head of the rib is fragmented and absent. A transverse fragmentation margin truncates the shaft of the rib at the approximate mid-point and *postmortem* taphonomic erosion is observed in several locations. As mentioned before, regression equations exist for age estimation according to the length of individual ribs in prenatal individuals (Fazekas & Kosa 1978; cf Scheuer & Black 2000, 243). Amongst infants and children however, the major factor affecting rib morphology is increased torsion in rib shafts as the ventral aspect of the thorax descends (Scheuer & Black 2000, 241). Although incomplete, the morphology of the extant portion of the rib shaft demonstrates torsion and may indicate that this individual was between the ages of at least 1–3 years old at the time of death (Scheuer & Black 2000, 241). The extant portion of the element is in fair condition and represents ~50% of a complete rib. All damage is assessed to be *postmortem*.

Macroscopic observations:
Periosteal new bone deposition is observed on the superior, pleural and posterior aspects of the extant portion of the body of the rib (Fig. 8.50a-c). *Postmortem* fragmentation truncates the lesion both medially and laterally, and *postmortem* taphonomic erosion has removed some of the periosteal new bone on the anterior surface. These factors obfuscate a full observation of pathology. There are no indications of fracture, cloaca, or sequestra on the extant portion of the element.

On the superior aspect, the lesion commences 16.9 mm from the anterior fragmentation margin and extends for 45.0 mm. On the pleural aspect, the lesion commences 16.5 mm from the anterior fragmentation margin and extends for 67.0 mm (measured with a flexible paper tape). On the posterior aspect, two lesions are observed. The most medial lesion commences adjacent to the medial fragmentation margin and extends for 28.0 mm. The second lesion commences approximately 42.0 mm from the medial fragmentation margin and extends for 18.4 mm. The maximum length of the extant portion of the lesion is 67.0 mm on the pleural aspect. Where apparent, the lesion is continuous across the pleural, cranial edge and external surfaces of the element.

The lesion exhibits mixed stages of activity. On the cranial edge, the lesion is interrupted by *postmortem* taphonomic erosion and small areas of sediment adhesion, although small spicules extend superiorly from the proximal lesion on the posterior aspect (Fig. 8.50a). The lesions are more rugose and porous than the surrounding cortex and are observed to differ in colour. On the pleural surface, the extant posterior portion of the lesion presents rugose deposits of periosteal woven bone interspersed with microporosity; spicules are observed on the neck of the rib on the superior and inferior aspects, perpendicular to the cortical surface (Fig. 8.50b). Moving anteriorly, the lesion exhibits fine woven bone deposition, interspersed with capillary impressions. Macroporosity is observed along the costal groove on the extant portion of the element. The margins of the extant portion of the lesion are diffuse and not well-demarcated. On the posterior aspect of the rib body, two lesions comprising healing plaque deposits of bone are observed (Fig. 8.50c). The most medial lesion exhibits microporosity on the peripheral margins and diffuse microporosity in the centre, along the angle of the rib. The second lesion exhibits extensive microporosity with both single and coalescing foramina.

Radiological observations:
The lesions on the extant portion of the rib present a similar expression radiologically as the rib described above. Circumferential spiculation is evident and is observed to be more widespread than the left rib although subtler in expression (Fig. 8.50d).

Once again, the absence of any fracture on the extant portion of the element suggests that the observed lesions are not associated with traumatic fracture. In non-adult material, it is difficult to distinguish new bone formation as a result of the normal growth process from infectious or traumatic new bone deposition (Lewis 2018, 3). The extant element presents diffuse lesions incorporating woven bone and microporosity

on the pleural and external surfaces and cranial edge, suggestive of pathological processes. Lesions on the pleural rib surface suggest inflammation of the pleura, typically associated with respiratory infections, such as tuberculosis. Tuberculous rib lesions commonly affect the middle ribs, incorporating lytic foci, enlargement of the costochrondral joint and minimal periosteal new bone on the pleural surface (Ortner 2003, 246). Unfortunately, the sternal end of the rib is absent and cannot be assessed; however, lesions on the extant fragment are not observed to be lytic. The external lesions appear to be slightly more advanced in healing, while the pleural lesions are more active, suggesting a chronic process. As mentioned before, subperiosteal new bone deposition on the ribs is occasionally noted in cases of non-adult scurvy (Buckley *et al.* 2014; Snoddy *et al.* 2017), and may be observed alongside fracture and/or enlargement of the costochrondral junction (the 'scorbutic rosary') (Brickley & Ives 2008, 57). The external rib surface is associated with *Mm. serratus anterior* and *pectoralis major* (Snoddy *et al.* 2018, 880). Therefore, subperiosteal new bone on the external surface of the extant rib may be a result of micro-trauma associated with movements involving these muscles, while the pleural lesions indicate subperiosteal haemorrhage because of expansion and contraction of the lungs associated with respiration. These features are deemed suggestive of scurvy, but should be observed bilaterally alongside further characteristic lesions (Snoddy *et al.* 2018, 891). Both this rib and the rib described above (§8.6.2.5) were excavated from the same level and are observed to be of similar size, morphology and developmental stage. The presentation and location of the lesions on both elements are strongly consistent with one another, suggesting they may derive from the same individual and demonstrate bilateral rib lesions attributable to scurvy.

Lesion type and healing status: Mixed; Mixed.
Lesion preservation: Excellent.
Differential diagnosis: Metabolic.

8.6.2.7. FB0045: Ulna fragment

Context:	(960)
Grid Ref:	99/111
Year of Excavation:	BR94
Other Details:	Unit 1, Spit 3

Element identification and preservation:
Fragment of non-adult ulna, representing the distal half of the diaphysis. *Postmortem* fragmentation truncates the element at the approximate midpoint of the diaphysis, while the distal metaphysis is eroded as a result of *postmortem* taphonomic processes. As a result of the severity of the lesion, no anatomical landmarks are visible and the element cannot be confidently assigned to side. Small areas of *postmortem* taphonomic erosion are observed on the fragment. Standards exist for age estimation based on ulnar length (Maresh 1970; cf Scheuer & Black 2000, 207). However, metric analyses cannot be applied because of the incomplete state of the element. The extant portion of the element is in fair condition and represents ~40% of a complete ulna. All damage is assessed to be *postmortem*.

Macroscopic observations:
Periosteal new bone deposition envelops the diaphysis for the extent of the fragment, obscuring anatomical features (notably the interosseous crest and pronator ridge) and no traces of the original cortex can be discerned (Fig. 8.51a-c). The new bone comprises perpendicular spicules which, in some areas, are bridged and appear 'frosted' and dense. The lesion is truncated by fragmentation, severe *postmortem* taphonomic erosion and sediment adhesion, obfuscating full observation of pathology. There are no indications of fracture, cloaca, or sequestra on the extant portion of the element.

The maximum length of the extant portion of the lesion is 55.5 mm. The maximum width of the lesion is approximately 28.0 mm encircling the diaphysis at the midpoint of the fragment, measured with a flexible paper tape. The lesion comprises woven bone tightly organized in trabecular-like formation. When viewed from the fragmentation margin, the lesion is observed to sit proud of the underlying cortex, extending approximately 0.9 mm in height. Post-depositional taphonomic processes have eroded most of the trabeculae, with only some trabeculae preserved at the area of the distal metaphysis. As such, the degree of trabecular involvement cannot be characterized. No lesion margins can be identified for this fragment.

Radiological observations:
No healthy cortex remains on the extant portion of this element; it is completely comprised of radiating spicules (Fig. 8.51d-f). There is marked cortical thickening alongside demineralization and a pock-marked appearance to the cortical bone. As a result of taphonomic erosion of the distal metaphysis, the element cannot be assessed for diagnostic radiological features, including Pelkan spurs, metaphyseal white lines ('white line of Frankel') and the Trümmerfeld zone. Within the medullary cavity, few trabeculae are retained; this is most likely an artefact of *postmortem* damage as some trabecular bone is preserved in the region of the distal diaphysis. On the distal third of the diaphysis, segments of periosteal new bone appear

Figure 8.50. *Photographic and radiological images pertaining to fragmented non-adult right rib (FB0044) from Context (960) displaying focal periosteal lesions, including: a) superior view of cranial edge displaying finely woven bone and spiculations; b) anterior view of pleural surface displaying rugose deposits of woven bone; c) posterior/external view displaying finely woven bone with capillary impressions; d) sagittal cross-section from CT data through mid-point of extant portion of rib, displaying almost circumferential fine spiculations. Scale bar: 1 cm (photographs only). (Photos Jess E. Thompson; radiological images captured by L. Buck, Cambridge Biotomography Centre; processed by J. Magnussen & M. Pardey, Macquarie Medical Imaging).*

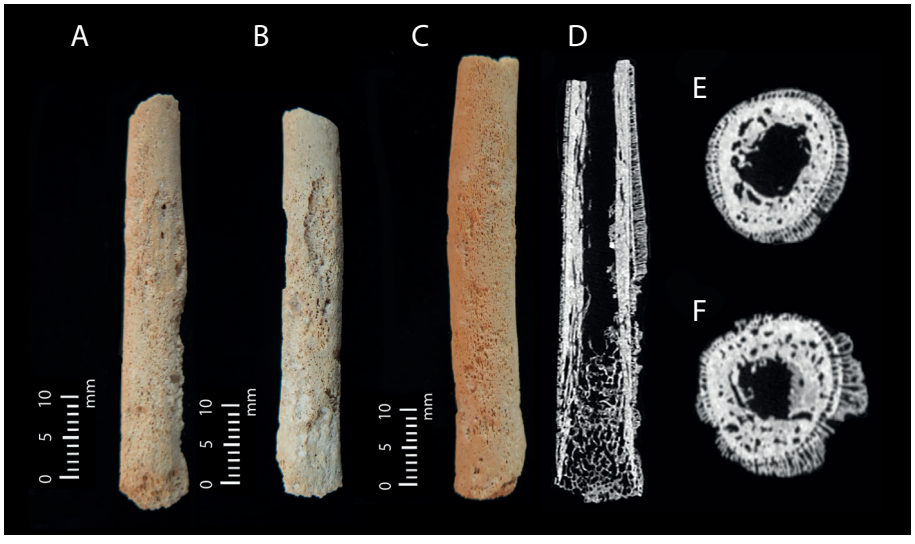

Figure 8.51. *Photographic and radiological images pertaining to fragmented non-adult ulna (FB0045) from Context (960) displaying circumferential periosteal new bone; all anatomical features are obscured: a)* postmortem *taphonomic erosion has removed the lesion in small areas, revealing the depth of new bone; b) microporosity underlying areas of erosion; c) spicules which are occasionally bridged or 'frosted' are evident; d) sagittal cross-section from CT data revealing extensive spiculation overlying cortex, and some separation between the cortex and lesion is evident; e) transverse cross-section at proximal aspect of extant element; f) transverse cross-section at mid-point of extant portion of element. Scale bar: 1 cm (photographs only). (Photos Jess E. Thompson; radiological images captured by L. Buck, Cambridge Biotomography Centre; processed by J. Magnussen & M. Pardey, Macquarie Medical Imaging).*

elevated from the underlying cortex, indicative of subperiosteal haematoma (Fig. 8.51e-f).

Such extensive bony change because of infection would lead to sequestra, cloaca, and/or significant cortical bone loss. Additionally, beta thalassaemia can be discounted because of the typical proportions of the medullary space and the evidence for osteoblastic activity (Lewis 2018, 2000; Ortner 2003, 365). Therefore, a metabolic disorder is the most likely differential diagnosis. Widespread and porous subperiosteal new bone deposition on long bone diaphyses and/or metaphyses are diagnostic of scurvy when observed alongside lesions on the cranium (Brickley & Ives 2008, 57; Snoddy *et al.* 2018, 891–2). Although this element appears to have been disarticulated when excavated, it was assigned the same unit number as the frontal fragments described above (FB0039 & FB0040; §8.6.2.1–2) and is observed to be of a similar developmental stage. It is therefore possible that these elements originate from the same individual, but this cannot be verified without further bimolecular analyses. Snoddy *et al.* (2018, 892) further note that periosteal lesions on the long bones are expected to be bilateral. As the contralateral ulna is absent, this cannot be ascertained. However, while microporosity and finely woven bone ought to be exhibited bilaterally, subperiosteal haemorrhage occurs as a result of trauma and is therefore unlikely to be symmetrical in location (Stark 2014, 19). On the extant portion of the ulna, new bone deposition covers the regions of several muscle attachment sites, including *Mm. flexor digitorum profundus, pronator quadratus, extensor carpi ulnaris,* and *extensor pollicis longus.*

The extent of proliferative, spiculated new bone on the extant element exceeds cases of subperiosteal new bone deposition on the long bones of scorbutic non-adults presented in the bioarchaeological literature (e.g. Brown & Ortner 2011; Buckley *et al.* 2014; Geber & Murphy 2012; Ortner *et al.* 2001; Snoddy *et al.* 2017). Klaus (2014) presents two cases of non-adult scurvy with more diffuse long bone lesions: woven bone and porosity on the upper limb bones of a 16–21 month old child, and cortical thickening alongside woven periosteal new bone on the ulna, femora and tibiae of a 1–1.5 year old child. On the latter individual, the ulna and tibia exhibit a very fine layer of woven bone which is clearly separated from the underlying cortex (Klaus 2014, 41). The extant ulna presents a distinctive case of long bone diaphyseal periosteal reaction alongside cortical thickening which, given its severity of expression, may indicate a chronic process.

Lesion type and healing status: Proliferative; Active.
Lesion preservation: Moderate.
Differential diagnosis: Metabolic.

8.6.2.8. Summary

All non-adult elements described above (except for FB0044, for which this information is lacking) were assigned the same unit number upon excavation, indicating their close spatial association. Mandibular dental eruption provides the narrowest estimated age range, of 2 years ±8 months, while all other elements are consistent with an estimated age of 2–4 years. In addition to their restricted depositional context and similar developmental stages, the extant elements present periosteal lesions which are remarkably consistent in both macroscopic and radiological presentations. Islands or extensive regions of thick, woven new bone extruding perpendicular to, and sitting on top of, the cortex, are observed on all elements. Additionally, hypervascularity and porosity are common and minimal cortical erosion is observed. The radiological presentation of the lesions on the left rib fragment (FB0043, §8.6.2.5), when viewed in cross-section were observed to be similar to all other non-adult elements, but especially the ulna fragment (FB0045, §8.6.2.7). It is therefore possible that these elements originate from one young child, but this cannot be definitively verified without further biomolecular analyses.

Differential diagnosis of individual elements is challenging, especially as periosteal lesions are frequently regarded to be of non-specific aetiology (although see Weston 2009 for critique). However, such proliferative lesions within non-adults are striking and sufficiently characteristic to aid differential diagnosis. For each element, traumatic fractures were not evident, and several pathological processes were considered. The expression and location of the lesions consistently indicated a metabolic disorder. Considered in isolation, the fragmented frontal bone might accord with an alternative aetiology of intra-cranial infection. However, the widespread periosteal new bone deposition and the likely bilateral nature of the orbital lesions indicates a severe progression that would not have been survivable in a prehistoric context in the absence of modern antibiotics. Furthermore, such an advanced infectious process would be expected to present cloaca or sequestra.

As the fragmented right frontal is consistent with the larger frontal bone fragments, a bilateral expression of orbital and supra-orbital lesions is observed. The zygoma further presents proliferative lesions, and bilateral lesion sites are observed on the mandible. Both ribs presented healing posterior/external surface lesions, with woven new bone on the pleural surface. The involvement of the external rib surface and lack of lytic lesions is not consistent with a diagnosis of pulmonary infection. The fragmented ulna presents the most severe proliferative new bone within this

sample, alongside subperiosteal haematoma, marking a rarely observed case of diaphyseal scorbutic lesions. Overall, when considered together, the distribution of lesions across these elements is diagnostic of scurvy, possibly co-morbid with vitamin D deficiency (rickets) and iron-deficiency anaemia (Brickley 2000; Brickley & Ives 2008, 57ff.; Ortner *et al.* 2001; Snoddy *et al.* 2018). This finding is significant as it may represent one of the earliest descriptions of scurvy for the central Mediterranean region.

Scurvy often occurs alongside other micro-nutrient deficiencies, resulting in a complicated disease presentation as each affects the pathophysiology of the other. Significantly, the biology of vitamin C, D and iron absorption and function are strongly linked. Extensive bleeding caused by the weakening of blood vessel walls in chronic scurvy can exacerbate or lead to iron-deficiency anaemia, which in turn may inhibit intestinal absorption of minerals such as vitamin D, potentially leading to rickets (Fain 2005; Brickley & Ives 2008, 113). Scurvy and rickets can lead to similar osseous changes, with characteristic and diagnostic features of each disease observed in similar locations (such as long bone metaphyses and costochrondral rib junctions). When scurvy and rickets co-occur, their presentation depends on the order in which they developed, healing status, and severity, with one disease usually dominating the other (Schattman *et al.* 2016). Clinical and bioarchaeological research has found that scurvy usually dominates in infants, with the skeletal features of rickets masked and requiring radiological and/or microscopic imaging to identify more confidently (Bromer & Harvey 1948; Schattman *et al.* 2016).

In addition to lesions preserved on suggestive and diagnostic locations for scurvy on the extant elements, described above, we have also presented lesions attributed to scurvy in locations which have received less attention in the palaeopathological literature. Of particular note are the bilateral proliferative lesions on the supero-lateral aspect of the supra-orbital margin, bilateral woven bone and porosity on the anterior margin of the mylohyoid groove and within the mandibular foramen, and circumferential spiculations on the ulna diaphysis. Similar mandibular lesions have been observed previously (Brickley 2000, 187; Brickley & Ives 2006, 166; Brown & Ortner 2011, 200), and lesions on the medial or internal aspect of the ramus are diagnostic when bilateral (Snoddy *et al.* 2018, 890). However, these cases do not demonstrate subperiosteal new bone extending as far inferiorly on the mylohyoid groove as the present example. These lesion sites provide greater insight into the pathogenesis of scurvy, as well as revealing the process experienced by this individual. This child experienced a severe and chronic case of vitamin C deficiency, resulting in more advanced proliferative lesions – especially on the zygoma and ulna – than many presented in the bioarchaeological literature. As a result, our research brings together pathognomic scorbutic lesions with those which indicate specific individual circumstances, demonstrating the extent to which periosteal lesions may develop in chronic cases.

Vitamin C, or ascorbic acid, is essential for collagen and osteoid formation because of its role in amino acid hydroxylation (Hodges *et al.* 1971). It is therefore critical for normal bone growth, as well as for blood formation and the metabolism of iron and folate (Lipschitz *et al.* 1971; Popovich *et al.* 2009). Furthermore, the role of ascorbic acid as a co-factor in 15 enzymes means that chronic dietary deficiency can lead to the failure of multiple physiological systems and, if untreated, is fatal (Padayatty & Levine 2016). Humans are unable to synthesize ascorbic acid and must consume vitamin C rich foods, in particular fresh produce, especially citrus fruits and dark green vegetables, as protein-rich foods such as milk, fish and meat contain lower levels of vitamin C; critically, however, the nutritional content of fresh produce is reduced when foods are cooked (Fain 2005, 124). Vitamin D is mostly synthesized through exposure of the skin to UVB rays in sunlight, with natural dietary sources limited to eggs and oily fish (Brickley & Ives 2006,83; Holick 2003).

Human breastmilk is high in vitamin C (Grewar 1965) but breastfeeding increases the daily metabolic requirements of vitamin C to an estimated 120 mg, almost double the amount required prior to pregnancy (NIH 2020). In contrast, breastmilk is low in vitamin D, and breastfeeding individuals must maintain healthy levels of vitamin D through exposure to sunlight (Pettifor 2004). If this child was breastfed by an individual who was deficient, and perhaps malnourished, they would have received insufficient nutrition in turn (Fain 2005, 126; Hirschmann & Raugi 1999, 899). Alternatively, weaning may have precipitated nutritional deficiency in this young child (Brickley & Ives 2008, 45). The process of weaning is often related to micro-nutrient deficiencies and weaning diets must be carefully considered (Davies & Hare 2004; Mosha *et al.* 2000; Tontisirin *et al.* 2002, 246) as nutritional status during the early years of life is strongly correlated with long–term health (Barker *et al.* 2002; Gluckman & Hanson 2006; Heijmans *et al.* 2008; Hoffman *et al.* 2017; Mandy & Nyirenda 2018; McFadden & Oxenham 2020; Roberts & Manchester 2005; Temple 2019). If appropriate animal–based dairy products were lacking or introduced too early, or dietary diversity was low because of resource scarcity, for example on a

seasonal basis (Cheung *et al.* 2003; Ianotti & Lesorogol 2014), this would have adversely affected the diet and health of vulnerable individuals. Importantly, it has been shown that cereal phytates can bind to calcium, reducing the overall intake of calcium, and this in turn affects vitamin D synthesis (Pettifor 2004). In Neolithic Malta, it is possible that infants and children were weaned onto diets either lacking in dairy or containing non–fermented dairy products, especially given the high rates of lactose intolerance which persist in the contemporary Maltese population (Burger *et al.* 2007; Storhaug *et al.* 2017). The potential for periodic resource scarcity cannot be excluded, and it is probable that weaning diets were cereal–rich, limiting the synthesis of vitamin D. In §8.7.6, we place this individual in chronological context to further evaluate the circumstances which lead to insufficient nutritional intake in this young child.

The current recommended daily amount of vitamin C for 1–3-year olds is 15 mg (NIH 2020). In non-adults, when the bodily pool of vitamin C is <300 mg, scorbutic symptoms are expected to commence at any time between 29–90 days (Brickley & Ives 2008, 45) and 6–10 months after the onset of dietary deficiency (Jaffe 1972). These include a suite of behavioural and soft tissue changes: failure to gain weight, loss of appetite, fatigue, irritability, depression, weakness, gingival bleeding and swollen gums (leading to periodontal disease and *antemortem* tooth loss), pinpoint bleeding in the skin (petechiae) and/or bruising (purpura) (Fain 2005; Hirschmann & Raugi 1999; Hodges *et al.* 1971). Chronic bleeding in response to muscular trauma, in subperiosteal and joint spaces, is especially painful and can result in restricted mobility (Hirschmann & Raugi 1999, 902). Such severe joint and muscle pain may be alleviated by the child assuming a 'frog position', lying on their back with limbs semi-flexed and externally rotated (Popovich *et al.* 2009). The deposition of periosteal new bone usually indicates that some vitamin C has been reintroduced to the diet, facilitating osteoblastic activity. We hypothesize that this individual may have experienced chronic, recurrent vitamin C deficiency or a consistently low dietary intake to provoke such extensive proliferative new bone deposition. Rickets, if present, may have been a late onset, possibly as the child became too ill to move independently and therefore spent less time outside.

This methodological case study provides an ambitious and rare example of detailed pathological analysis of fragmentary and disarticulated elements. The level of attention demonstrated here is uncommon in complex, commingled assemblages such as these, as the ability to carry out differential diagnosis is limited when discrete individuals cannot be recognized. Palaeopathological analysis is typically employed to characterize health on a population-wide scale, or to illustrate significant singular case studies. Rarely have pathological lesions provided the opportunity to unite the remains of disarticulated individuals (González-Reimers *et al.* 2015; Ortner 2003, 210). The approach employed herein supports appeals for the integration of macroscopic analyses and radiological imaging (Stark 2014) to aid differential diagnosis and, crucially, bring palaeopathological studies into alignment with the clinical literature. Radiological observation of these periosteal lesions reveals surprising variation in their character and architecture, a finding which may also be clinically significant, as they are typically not subject to radiological imaging in contemporary contexts. Although requiring significant investment of time and resources, this work highlights the utility and value of pathological analyses of highly fragmented and disarticulated assemblages. The benefits, exemplified here, include the potential for posthumous reunification of individuals, increased accuracy of differential diagnoses, and greater insights into the lived experiences of health and disease in communities such as those inhabiting the prehistoric Xagħra plateau (Thompson *et al.* 2021).

8.7. Discussion

8.7.1. Limitations of study

To echo our statements at the outset of this research, we underscore the awareness that the results and interpretations presented here should only be perceived as a minimum number of incidences, and not as overall statistical prevalence of a complete burial population. The Circle assemblage has not been fully excavated, nor has the excavated population been exhaustively analysed. For example, the six examples of vertebral pathology presented in §8.5.3.1–6 represent only 0.7% of the 922 isolated elements (or fragments thereof) from the curated burial population. Our objective here was to bring further clarity to the known spectrum of health and disease for the Circle population by focusing on case studies of 'extreme pathology', an approach first applied to this population by Stoddart *et al.* (2009a). Ongoing scientific studies by the current authors will seek to further elucidate all aspects of the pathology, anthropology, demographics, affinity and cultural engagement of the Neolithic community interred in this space.

We were fortunate to have received permission to subject some of the remains included in the case studies to radiological analyses via micro-CT. Undoubtedly, further scanning would have enhanced the pathological descriptions and differential diagnoses of those

elements that were subject to macroscopic analysis alone; however, the temporal, pecuniary and logistical parameters of the current project could not permit comprehensive inclusion for this component of the study. It is hoped that future extensions of the project will facilitate further radiological studies, ideally with local facilities and experts in Malta.

8.7.2. The Circle in context

As described in §4.6.2, less than two dozen late Neolithic funerary sites are known from across Malta and Gozo (Chapters 13 & 14; cf Malone *et al.* 2009d). Of these others, only the human skeletal remains from the Xemxija tombs have previously been subjected to osteological analysis and published (Pike 1971; Rodgers 1971). Although several publications refer to the human remains identified within the Ħal Saflieni Hypogeum (Zammit 1910, 1926a; Zammit *et al.* 1912), commentary pertains to cranial morphology and metrics, as was the prevailing focus of the emerging field of biological anthropology. Indeed, in alignment with contemporary archaeological praxes across the region, the disciplinary focus on architecture and material culture combined with the fragmentary and poorly preserved nature of many skeletal remains, precluded their analysis. This study therefore presents the largest and most fine-grained investigation of skeletal pathology from late Neolithic Maltese sites to date.

The excavation of Xemxija tombs 1–6 brought to light almost 15,000 fragments of human bone from similarly commingled and disarticulated contexts as the Circle rock-cut tomb and cave complex (Evans 1971, 112–6). An inventory and brief overview of the human skeletal and dental remains was provided (Pike 1971; Rodgers 1971), although their treatment was not exhaustive, and the descriptions are not supplemented by figures of the few elements discussed in detail. Pike (1971, 236) noted the presence of non-adult individuals of all age ranges but commented on the under-representation of older adults because of a lack of age-related osseous change. At least one old adult (50+ years) was recently identified through a fragment of right pubic symphysis displaying age-related degeneration (Thompson 2020, 138). However, the fragmented nature of the assemblage impedes identification of further older individuals.

As discussed above (§8.4.4), individuals of advanced age have primarily been identified at the Circle through well-preserved ossified cartilage, pubic symphyseal degeneration, rare observations of *hyperostosis frontalis interna* (§8.5.2.8–11) and potentially age- or diet-related osteoporosis (§8.7.6). In the Xemxija tombs, there were low incidences of skeletal pathology: one well-healed (non-reduced) clavicle fracture; one well-healed (non-reduced) tibia fracture; one healed non-reduced tibia fracture exhibiting misalignment with overlapping of the fractured segments by 1.2–1.9 cm, associated with possible infectious change; two healed fifth metatarsal fractures, one with callus; one tibia fragment presenting endosteal thickening perhaps because of haematoma; one talus with osteomyelitis and cloacae indicating local infection (Pike 1971, 236–7). These elements complement and extend the case studies offered above from the Circle, and further the evidence for the treatment and short-term care of injured individuals in Neolithic Malta, aligning with the 'bioarchaeology of care' approach, described below.

There has been a relatively long history of research documenting human pathological indicators of health associated with the transition from foraging to agriculture. The publication of the foundational volume '*Palaepathology at the Origins of Agriculture*' by Cohen & Armelagos (1984) provided the first systematic and global documentation of the impact of this dietary and cultural transition on human health. Multiple chapters in this volume provided evidence for a widespread deterioration in palaeopathological indicators of health across this transition, an interpretation that was later challenged by the publication of the 'Osteological Paradox' (Wood *et al.* 1992) which raised a range of reasons why it is difficult to interpret population frequencies of skeletal pathology in a straightforward manner. Despite the controversy over interpretation of palaeopathological data in Neolithic populations, the early observations of widespread increases in the frequency of lesions associated with infectious and metabolic diseases, as well as indicators of systemic stress such as enamel hypoplasia, have been broadly supported by more recent studies (Cohen 2009). The past few decades have seen quite significant changes in our understanding of the Neolithic. Among these are the acknowledgement that social and dietary changes occurred over a considerable timespan and were regionally variable. As a result, the implications of the Neolithic lifestyle on human health are also variable and locally contingent (Stock & Pinhasi 2011). Recent research has also demonstrated that there were strong selective pressures on human populations following the adoption of agriculture which have shaped genetic variation within our species (Richerson *et al.* 2010). Recently it has been proposed that agricultural societies also shift their energetic ecology and life-history strategies, resulting in a greater investment in immune function and reproduction at the expense of somatic growth (Wells & Stock 2020).

These perspectives on human ecology and health in the Neolithic have emphasized the importance of understanding regional variation and local impacts

of the Neolithic upon populations, as well as subtler analyses of how human impact on the environment changed and shaped health throughout the Neolithic as farming practices and land usage changed, and environmental impacts of human activity compounded (Stephens *et al.* 2019). The observations of pathology in the Neolithic populations of the Circle provide a unique opportunity to interpret the patterns of health and disease in an island Neolithic population. As resources are known to be limited in island environments, it also provides an opportunity to consider how local ecology, population dynamics and activities impacted human pathology during this period.

8.7.3. The bioarchaeology of care

The interpretative lens for the case studies detailed above aligns with the 'bioarchaeology of care'. The bioarchaeology of care is a conceptual framework which seeks to promote understanding of the lived experiences of disease, disability and physical impairment in the past. It applies social theoretical concepts to bioarchaeological evidence to study the indicators of health-related caregiving practice and psycho-social, emotionally supportive care (Tilley 2013, 2015; Tilley & Oxenham 2011; for the *Index of Care*, cf Tilley & Cameron 2014; Tilley 2017). The framework was developed to examine the broader implications of health-related care provision in past populations via case study-based research, including caregiving across the life course, emic attitudes towards illness, impairment and disability, and the role of animals as both recipients of and agents for care provisions (Powell *et al.* 2017). The bioarchaeology of care is founded on a combination of elements drawn from a range of sub-disciplines, such as post-processualism, social, cognitive and mortuary archaeologies, and palaeopathology (Tilley 2017, 12). Additional influence is drawn from other disciplines relevant to caregiving including nursing, clinical medicine, philosophy, sociology and psychology (Tilley 2017, 12). Originally focused on skeletal remains, the bioarchaeology of care has recently been repositioned to also incorporate naturally and artificially mummified human remains (Nystrom & Tilley 2019).

The first principle of the bioarchaeology of care is that the research of disease, disability and care in the past is 'quintessentially bioarchaeological' (Tilley 2017, 15; cf Buikstra & Beck 2006). Although the evidence-base of the bioarcheology of care is bioanthropological, it cannot be analysed without continuous reference to what is known regarding the associated socioeconomic, material, geographical, chronological and cultural contexts (Tilley 2017, 15). It argues that although some symptoms of pathology may be biologically evident, or even pathognomonic, health, disease and disability were perceived, addressed and understood very differently across cultures (Tilley 2015, 3). Moreover, the bioarchaeology of care advocates for the uniqueness of any lived experience, maintaining that 'everybody experiences disease in their own way, disability for one person may not be a dis-ability (or not the same disability) for another' (Tilley 2015, 3; cf Shakespeare 1999, 99).

The second principle is that agency is central to all features of health-related caregiving (Tilley 2017, 15). According to Tilley, any 'human remains bearing evidence of caregiving literally embodies the collective agency of those involved in providing care' (2015, 128). This agency should be contextualized temporally and geographically to the period in which care was provided. Human remains displaying evidence of pathology requiring care can be seen as both actor and artefact. Traditional palaeopathological study typically views remains as only 'artefact'; however, the person receiving care is also an actor or agent. Palaeopathology's tendency to concentrate on 'fossilised disease' (Cross 1999, 23) in the form of observable bodily variations risks objectifying the remains of sick and/or physically impaired individuals as purely material resources. Assumptions of dependency, exclusion, marginalization or disadvantage based solely on observed bodily variation risks misrepresenting and dehumanizing the lived experiences of people from the past (Cross 1999, 8).

The bioarchaeology of care rallies against the reconstruction of individuals receiving care as passive or deficient. To do so negates their agency in the 'negotiation of, contribution to, and cooperation with their care [as] integral to its design and its outcomes' (Tilley 2017, 15). The passivity and concomitant medicalized study of physical impairments, bodily difference and disability as a pathological 'deficit' is a key feature of much archaeological, palaeopathological and osteoarchaeological research. These fields have emerged from the so-called 'medical model', the origins of which may be traced to the Industrial Revolution (*circa* 1760–1840), developing alongside the professionalization and standardization of modern Western medicine (Byrnes & Muller 2017, 2; Davis 2013; Siebers 2008). The medical model pathologizes physical and mental impairments, and any other deviation from an idealized bodily 'norm', conceptualized by western medicine as functional limitations (Byrnes & Muller 2017, 2). The expression 'medical model' is used by many disability studies scholars as a synonym for the biased view of disease and disability that attributes an individual's biological 'deficits' to inadequate health practices, genetics or incidents (such as traumatic

accidents) (Vehmas *et al.* 2009, 2; cf Pfeiffer 2001, 30). The first wave of disability scholarship, and indeed the activist origins of the field, strongly reject medicalization, believing it to perpetuate modern dominance hierarchies of medical practices and experts (Vehmas *et al.* 2009, 2).

Palaeopathology has perhaps inadvertently played a role in the continuation of the medical model within historical and archaeological research. The study of disease in past populations originally developed as an interdisciplinary pursuit by historians, doctors, archaeologists and biologists, often with little examination of socio-cultural contexts (Živanović 1982, 2). While palaeopathology relies heavily upon the medicalized examination of human remains, this should not automatically result in the dominance of the medical model as it is problematic in a number of ways. Firstly, it supports a dualistic notion of health; namely, that healthy and unhealthy exist as binary opposites, rather than acknowledging that people move between these states throughout the life course, and may never be entirely one or the other. 'Health' is most often experienced as a spectrum rather than a binary status. Secondly, the dualism of health treats biological and psychological problems separately when they are in fact inextricably linked (Appleby 2015; Cole & Dendukuri 2003; Roberts & Manchester 2005; Taylor 1995). Thirdly, especially applied to past populations, the medical model can be deterministic. By interpreting bodily differences as 'deficits', the medical model suggests that a particular person's 'problem' – a disease/impairment *etcetera* – indicates that person could not have been an equal; they are assumed to be inherently disadvantaged. Additionally, the medical model risks implying that a person with a potential illness or disability was solely a passive recipient of treatment (or lack thereof). In this way, the medical model, and its application in palaeopathology is inclined towards disablist narratives as it defines health in terms of a 'modern' able-bodied norm. While acknowledging biological imperatives of health, it is important to recognize that perceptions of 'healthy' and 'functioning', and understandings of the aetiologies of disease, congenital variation and the implications of disease or trauma, were variable in past societies, as they remain in the present.

Bioarchaeology now routinely incorporates social theories to increase the biocultural and sociocultural investigation of multiple categories of evidence and more critically (re)interpret past embodied experiences and interpretations of corporeality and corporeal difference (Byrnes & Muller 2017, 3). The bioarchaeology of care offers a means to record, interpret and report palaeopathological analyses in an embodied and human-centred way (Boutin 2016; Byrnes & Muller 2017; Tilley 2014). When archaeologically derived remains indicate that a person experienced acute or chronic, congenital or acquired, resolved or unresolved disease during their lifetime (Tilley 2017, 11), it is justifiable to infer that this person received some degree of health-related care to manage the impacts of disease, and survive to their ultimate age of death. Considerations of the characteristics of caregiving, and even the willingness to give care, offers a range of opportunities for scholars to 'reflect not only the motivations and commitment of the carers themselves, but also the values, traditions, experience, knowledge, beliefs, skills, resources, politics, economy and organization of the society in which care occurs' (Tilley 2017, 12; cf Hofrichter 2003; Pol & Thomas 2001). The bioarchaeology of care offers a means of analysis that overcomes many of the issues that arise from the medical model and its dominance in palaeopathology, facilitating insights into the lived experiences of individuals in our archaeological narratives that have been hitherto inaccessible or ignored.

From this perspective, the individuals encountered through our studies of the Circle population contribute a great deal to the global discourse surrounding the bioarchaeology of care. Particularly considering the severe fractures described for a mandible (FB0002, Context (951); §8.5.1.1, above), humerus (FB0007, Context (951); §8.5.3.7, above) and femur (FB0001, Context (1241); §8.5.3.15), it is clear that the individuals who sustained these injuries would have required significant and enduring care from other members of their communities. Initially, care would have been required to survive the biological shock associated with such serious physical trauma (Britt *et al.* 1996; Eastridge *et al.* 2019; Hardaway 2006; Kahl *et al.* 2013). In clinical studies, after brain injury, shock is the second leading cause of death after trauma (Siegel 1995). Assistance would have also been required in the procurement, preparation and consumption of food and drink, as well as securing other basic human needs (such as safe shelter and warmth) while incapacitated (Pittman & Zeigler 2007). Further to this, affected individuals would have required varying levels of support and care during recuperation and rehabilitation, as they healed from their injuries and learned to integrate the associated changes in mobility and/or function. It is important to acknowledge that the cases presented here precipitate from the earliest and middle use-phases of the Circle (from approximately 2900–2500 BC), making these findings even more significant. The survival of these individuals beyond the initial trauma and resumed effective use of their affected elements is evidence for many combined months of successful

care extended to them by their communities, without which in a prehistoric context would almost certainly have resulted in the loss of their lives.

8.7.4. Hyperostosis frontalis interna

Above, we have demonstrated the presence of *Hyperostosis frontalis interna* (HFI) in four individuals from the Circle, two possible females and two possible males deriving from Contexts (1268), (960) and (979), dated from the Early to the Late use-phase of the site (FB0023, FB0024, FB0025 and FB0026; §8.5.2.10–13, above). *Hyperostosis frontalis interna* describes the growth of thick, irregular and undulating nodules on the endocranial surface of the frontal bone (Ortner 2003, 416). It is distinct from *hyperostosis calvaria diffusa* (HCD) or *hyperostosis cranii interna* (HCI) because of discrete involvement of the frontal bone; whereas HCI is often observed in association with severe HFI, HCD is determined to be a separate phenomenon (Hershkovitz *et al.* 1999; Talarico *et al.* 2008). HFI is usually observed bilaterally and spares the midline, resembling a butterfly in appearance (Mann & Hunt 2012, 57; She & Szakacs 2004). The nodular lesions are contained within the region bordered by the superior sagittal sinus and the middle meningeal artery and these features, as well as sutures, are not involved (May *et al.* 2011b). Although appearing macroscopically as dense lamellar bone, histological and radiological analysis reveal that the inner table is remodelled with cancellous bone and the diploic space is preserved (Bracanovic *et al.* 2016; Cvetković *et al.* 2019; Hershkovitz *et al.* 1999, 310; Ortner 2003, 416). As a result, the frontal bone is noticeably thickened but the ectocranial surface retains a normal appearance. HFI is categorized morphologically based on its extent and appearance into four types (Types A-D) (Hershkovitz *et al.* 1999); more recently, a fifth type has been introduced following recognition of the involvement of the *falx cerebri* in cadavers (Raikos *et al.* 2011). However, analysis of the microstructure of HFI only identified significant differences between two types, moderate (Types A-C) and severe (Type D) (Bracanovic *et al.* 2016).

This pathology was first reported in the 18th century as part of the triad defining Morgagni's syndrome, alongside virilism (the development of male secondary sexual characteristics in women, such as hirsutism) and obesity (Morgagni 1719). This syndrome, combining metabolic and endocrine disorders, is sometimes linked with neuropsychiatric symptoms and termed Morgagni-Stewart-Morel syndrome (Morel 1929; Stewart 1928). HFI has also been reported in Troell-Junet syndrome, other characteristics of which include acromegaly, toxic goitre, and diabetes mellitus (Moore 1953). Several studies have found that HFI is not strongly correlated with these syndromes and it is widely accepted to be an independent and benign phenomenon (Dann 1951; Gershon-Cohen *et al.* 1955; Hershkovitz *et al.* 1999; Schneeberg *et al.* 1947; Smith & Hemphill 1956). However, the increased bone thickness and endocranial outgrowths consistent with HFI can cause compression of the brain tissue and, in exceptional cases, cerebral atrophy leading to cognitive impairment, neuropsychiatric symptoms, frontal headaches and epilepsy (Attanasio *et al.* 2013; Hasegawa *et al.* 1983). A recent study does not support an association between HFI and reduction in cranial vault size (Cvetković *et al.* 2019), although profuse cases of HFI may affect the soft tissues and thereby precipitate behavioural changes (Chaljub *et al.* 1999; Talarico *et al.* 2008).

HFI is idiopathic but given its common occurrence in post-menopausal individuals and low prevalence in males and young females, it is most likely related to endocrine imbalance and hormone dysregulation. The ratio of androgen, oestrogen and IGF-1 (insulin-like growth factor) are commonly cited as central to its pathogenesis (Hershkovitz *et al.* 1999; May *et al.* 2010; Talarico *et al.* 2008; Western & Bekvalac 2017), although the role of parathyroid hormones, calcium metabolism, neuropeptides, leptin and dietary phytoestrogens are also questioned (Raikos *et al.* 2011; Talarico *et al.* 2008). The extent to which HFI is a genetic or hereditary condition is debated (Hershkovitz *et al.* 1999, 323), although at least two cases of HFI in individuals with potential biological affiliation have been reported (Glab *et al.* 2006; Hajdu *et al.* 2009). When present in male individuals, HFI co-occurs with hormonal irregularities disrupting the androgen/oestrogen ratio (Belcastro *et al.* 2011; May *et al.* 2010; Ramchandren & Liebeskind 2007; Yamakawa *et al.* 2006). Menopause seems key to the pathogenesis of HFI, marking a decline in oestrogen production and, post-menopause, the conversion of androgens into oestrogen via aromatization; further, the age of onset of menopause appears to be genetically determined and usually occurs in the mid-40s to mid-50s (Lamberts *et al.* 1997). Hershkovitz *et al.* (1999, 322-3) note that the correlation between HFI progression and age may vary in ancient populations because of differing ages at menarche and menopause. The increase in HFI prevalence in modern populations indicates that environment and lifestyle are also critical factors, namely where the risk of diabetes and obesity are heightened, and where exposure to oestrogen is increased during the lifespan (Hershkovitz *et al.* 1999; May *et al.* 2011a; Western & Bekvalac 2017). However, a lower average life expectancy may explain the under-representation of HFI in pre-modern populations.

The prevalence of HFI is debated, with estimates ranging from 5–12% of the population (Moore 1955; Jaffe 1972), to 5% of males and 25% of females affected (Hershkovitz *et al.* 1999). The demographic most consistently presenting HFI are post-menopausal individuals, at rates of 40–60% (Gershon-Cohen *et al.* 1955). The prevalence and extent of HFI increases with age in female individuals (although plateaus past 50 years of age; Western & Bekvelac 2017), while only the likelihood of HFI increases with age in males, as its expression is typically limited to the minor Type A and B forms (Cvetković *et al.* 2019; Hershkovitz *et al.* 1999; May *et al.* 2011b). It therefore provides an exceptional opportunity to explore the presence of older individuals in past populations and can be a strong diagnostic tool for sex and age determination (Cvetković *et al.* 2019; Hershkovitz *et al.* 1999; Moore 1955; May *et al.* 2011b). When HFI is minor in expression, age and sex cannot be predicted; however, severe HFI in an isolated cranium or skull likely signifies an older female individual (Cvetković *et al.* 2019; May *et al.* 2011b). Here, we seek to be inclusive in our terminology and distinguish the prevalence of HFI in biological females from its links with the menopause, recognizing that menstruation (and its cessation) and does not directly map onto either past or present understandings of gender (Chrisler *et al.* 2016; Farikullah *et al.* 2012).

In a sample of 2,019 archaeological skeletal remains, Hershkovitz *et al.* (1999) did not find any evidence of HFI, and it is a relatively rare finding in archaeological assemblages (Flohr & Witzel 2011; Shahin *et al.* 2014; Szeniczey *et al.* 2019). Nevertheless, it has been reported in *H. erectus* and *H. neanderthalensis* remains and is evidently not a modern phenomenon (Antón 1997; Garralda *et al.* 2014). There are few contemporary later prehistoric cases for this pathology. Outside of Europe, HFI has been reported in several ancient Egyptians, including a young adult male from Tarkhan dated to 2890–2650 BC (Shahin *et al.* 2014), two males and a female from the 2300 mastaba group of the Western Cemetery at Giza (*c.* 2630–2350 BC) and one female from Naga-ed-Deir (*c.* 2200-–1800 BC; Watrous *et al.* 1993). To date, four cases of HFI within Neolithic Europe have been presented. At Les Boileau hypogeum (France), where successive deposition was practised over several centuries from the early to mid-3rd millennium BC, two individuals (from a minimum of 294) presented mild cases of HFI, both identified as females >50 years of age (Devriendt *et al.* 2004). When published, these cases were potentially the first incidences of this pathology reported in Neolithic Europe. We have only been able to locate two other cases. From the La Varde passage grave (Guernsey) likely dating between the 4th–3rd millennium BC, one fragmented probable frontal bone presented either mild HFI or osteoma (Cataroche & Gowland 2015, 30). In Sumburgh (Shetland), a cist containing at least 20 individuals dating from 3510–2660 cal. BC, presented evidence of a frontal bone with HFI although no age or sex determination was given for this individual (Walsh *et al.* 2011, 13).

Our findings of HFI from the Circle assemblage are significant insofar as they are the first to be reported for Malta, and supplement existing early cases for Neolithic Europe. Moreover, as a group of four cases, they equal in number all published evidence for this phenomenon to date for prehistoric Europe, therefore representing a significant addition to knowledge of this category of cranial lesions for the region and period. However, the real significance of these cases arises through considerations of their demographic and cultural meaning. As mentioned before, HFI is most strongly associated with increased age, and thus presents an excellent opportunity to consider the presence of older individuals in archaeological assemblages. There are widespread assumptions regarding low life expectancies in preindustrial societies (Appleby 2015; Cave & Oxenham 2016; Cox 2000), despite the fact that ethnographic research on the mortality profiles of modern hunter-gatherers and forager-horticulturalists from across the Americas, Australia, Africa, Europe and Island South East Asia indicates that the modal age of adult death is approximately 70, with survivorship variability applicable to either side of that estimate (Gurven & Kaplan 2007, 322; Walter & DeWitt 2017; cf Laslett 1991). This research has been supported as a feasible platform from which to infer demographic profiles of archaeological populations (Cave & Oxenham 2016; Hoppa 2002; Milner *et al.* 1989; Paine 1989; Weiss 1973; White 2014).

These observations from the Circle suggest that some members of the Neolithic communities of Gozo lived to a relatively advanced age. Our diagnoses of HFI are supported and extended by the observations tabled in §8.4.4, above, regarding further evidence for individuals of advanced age, including public symphysis degeneration and ossified cartilage (Fig. 8.5a-g). We have also reported other conditions for which age may be a contributing factor, such as osteoporosis (§8.5.3.2–7, §8.6.1.3, & §8.7.6). These discoveries call for a consideration of the bioarchaeology of caregiving across the life course for Neolithic Malta, particularly as shared with, offered and experienced by community members of advanced age.

In agreement with Appleby (2010, 2011, 2015; cf Fahlander 2013), we argue that discussions of old age in past populations have been neglected within

archaeological discourse. Despite the deserved focus apportioned to infants and children in archaeological narratives (Bacvarov 2008; Baxter 2005; Lillehammer 1989, 2000, 2010; Moore & Scott 1997; Power 2012, 2016; Schwartzman 2006; Scott 1999; Sofaer-Derevenski 2000), those at the other end of the life course have, for the most part, remained invisible to critical discussions of age and identity. However, as stated by Appleby, if we do not explore the 'actions, intentions and meanings associated with the oldest members of prehistoric communities, we risk significantly misunderstanding those communities' (2011, 146; cf Appleby 2010, 2015). This observation becomes particularly poignant when we consider the role of elders in certain cultures and pre-literate societies as leaders, caretakers and repositories of cultural and social knowledge (Goody 1976; Hazan 1994; Simmons 1945; Sokolovsky 1983; Press & McCool 1972).

The *status quo* of old age in archaeology perhaps reflects a modern Western lens through which the elderly are often viewed, where they are removed from socioeconomic significance through forced retirement, isolated through placement in nursing homes, and regarded as mentally and physically vulnerable and burdensome (Anderson 1972; Appleby 2011, 2015; Cumming & Henry 1961; Smith *et al.* 2017; Townsend 1981). It is often also attributed to the difficulties in assigning an accurate chronological age to older individuals by osteological assessment (Buckberry 2015; Cave & Oxenham 2016; Cox 2000; Hoppa & Vaupel 2002; Mays 2015; Ross & Oxenham 2015; Smith *et al.* 2017). In contrast to the relatively stable rate at which the younger members of the population grow (notwithstanding genetic and environmental variation), the rate at which humans senesce is profoundly variable. This is not only because of similar genetic and environmental influences faced by the younger members of the community, but amplified by other factors including lifestyle, health and disease and significant life events (Aykroyd *et al.* 1999; Buckberry 2015; Cox 2000; Kemkes-Grottenthaler 2002; Márquez Grant 2015; Mays 2015; Roksandic & Armstrong 2011; Tayles & Halcrow 2015). As such, the accuracy with which skeletal age determination can be effectively attributed diminishes following the fusion of the medial clavicular epiphysis between 20–30 years of age (White & Folkens 2005, 195, 372). The reliability of skeletal ageing methods beyond this physiological milestone, such as cranial suture closure, are considered controversial, at best (Appleby 2011; Aykroyd *et al.* 1999; Cox 2000; Molleson *et al.* 1993; White & Folkens 2005).

However, to reduce the concept of age to purely chronological or biological factors is to misunderstand and underestimate grossly the importance of the social aspects of the ageing process in both individual and community identity dynamics. Such considerations have been promoted by Arber and Ginn (1995) as a threefold division of age which encompasses contextualized considerations of chronological, biological and social processes of ageing, an approach which has also been embraced in some archaeological analyses (Appleby 2010, 2011, 2015; Gowland 2002, 2007, 2015, 2016; Sofaer 2006, 2011). Particularly important for prehistoric populations, this approach acknowledges that there is no universal relationship between chronological age, social identity and physiological status (Appleby 2011; Cox 2000; Ginn & Arber 1995), and that understanding of identities later in life should be culturally situated (La Fontaine 1986; Riley 1984; Thompson 1990).

We understand that an 'archaeology of age' for Neolithic Malta is beyond the scope of the current project, considering that its prerequisite negotiations of complex interrelated characteristics includes biological sex, gender, health, kinship, social status, geographical affinity and power amongst myriad other factors (Appleby 2011; Arber & Ginn 1995; Bury 1995; Lock 1993; McMullin 1995), and may prescribe, proscribe or permit various social roles (Appleby 2011; Blaikie 1999; Hazan 1994; Neugarten & Hagestad 1977). What we offer here, however, is an initial attestation of the presence of individuals of advanced age within the Circle from which further study may proceed. As discussed by Thompson *et al.* in Chapter 12 of this volume, the identification of individuals from across the life course in this highly significant cultural space implies a rich picture of inclusion and integration within the lived communities of Neolithic Malta, too.

8.7.5. Endocranial lesions

Our analyses of palaepathological lesions from the Circle assemblage revealed numerous examples of endocranial lesions in crania representing a multitude of individuals, demonstrating relatively widespread prevalence within the population. The endocranium is separated from the brain by the meninges, comprising the outer dura mater (pachymeninges), covering the arachnoid and pia mater (leptomeninges). The dura mater is a highly vascularized fibrous tissue which forms the endocranial periosteum and provides blood supply to the cranial bones (Lewis 2004, 84). In children, the dura adheres strongly to the sutures; this lessens throughout the process of cranial suture closure but the dura again firmly attaches to the endocranium in older adults (Weller *et al.* 2018). Inflammation and/or haemorrhage of the meninges can stimulate an osseous response on the endocranial surface in the form of 'diffuse or isolated layers of new bone on the original

cortical surface, expanding around meningeal vessels, as "hair-on-end" extensions of the diploë, or as "capillary" impressions extending into the inner lamina of the cranium' (Lewis 2004, 82; cf Roberts & Manchester 2005, 178–9). As has been commented upon (Hershkovitz *et al.* 2002, 201; Lewis 2004, 83), research into the variation, expression and aetiology of endocranial lesions has been limited. Such lesions have previously been referred to as *cribra cranii* (Koganei 1912; Henschen 1961) or *cribra cranii interna* (Møller-Christensen 1961) and were often observed in association with *cribra orbitalia* and porotic hyperostosis. Analyses of their location, form, and comorbidities in adults (Gomez *et al.* 2018; Hershkovitz *et al.* 2002; Janovic *et al.* 2015) and non-adults (Lewis 2004; Mensforth *et al.* 1978; Schultz 1993) have suggested a range of possible aetiologies including anaemia, meningitis, neoplasia, epidural or subdural haemorrhage, trauma, tuberculosis, venous drainage disorders, vascular malformations, vitamin deficiencies, and non-specific inflammation.

As reported by Lewis (2004), the first description of endocranial lesions was carried out by Koganei (1912), who observed endocranial lesions more frequently in adults than non-adults. Subsequent research has found endocranial lesions in association with porotic hyperostosis (Henschen 1961; Møller-Christensen 1961), intrathoracic infections such as tuberculosis and pneumonia (Hershkovitz *et al.* 2002), non-specific inflammation (Mensforth *et al.* 1978), and vascular malformation (Janovic *et al.* 2015). Endocranial lesions as a result of trauma or chronic Vitamin A, C or D deficiencies are more typically found in non-adults (Brickley & Ives 2006, 2008; Caffey 1974; Ortner & Ericksen 1997). Ortner (2003, 84) distinguishes between 'endocranial meningeal reactions' produced following haemorrhage, inflammation and tumorous processes. Haematomata overlie the inner table, and progress from small branching impressions to porotic new bone deposition which eventually remodels; inflammatory and tumorous processes involve the inner table and may penetrate the diploë, but while inflammation can produce plate-like new bone, neoplasms stimulate remarkably dense and proliferative new bone deposition (Ortner 2003, 84).

Comprehensive study of the distribution and expression of endocranial lesions has so far only been attempted in non-adult remains from Medieval and post-Medieval sites in England (Lewis 2004). In 528 individuals from neonatal to 17 years of age, Lewis (2004) distinguished between four types of endocranial lesions: (1) pitted; (2) fibrous; (3) capillary formations; (4) hair-on-end formations (these may become 'frosted' or thickened as they remodel). It was further noted that the lytic and granular endocranial lesions pathognomic of tuberculous meningitis represent a fifth type, which was rarely observed in the collections studied (Lewis 2004, 91). In contrast to their distribution in adults, in non-adult individuals endocranial lesions were most often found on the occipital, followed by the parietal and frontal, and often followed regions of venous drainage (Lewis 2004). Through analysis of their expression and relationship to age, it was found that porous and fibrous endocranial lesions in individuals younger than 6 months of age were most likely not pathological but rather the result of new bone production from the osteogenic dura (Lewis 2004, 94). Capillary and vascular impressions were often found on multiple cranial elements in the same individual and are suggested to represent healed lesions, supporting Schultz's (1993) earlier findings in adult individuals. Finally, hair-on-end lesions, whether spiculated or frosted, were deemed most likely to be secondary to infection (Lewis 2004, 95). Although developed for non-adult skeletons, Lewis' classification of endocranial lesions is largely applicable to adult individuals, with the caveat that aetiologies and differential diagnoses may not be directly comparable.

The relationship between endocranial lesions and meningeal and vascular anatomy, as well as their expression (for example, osteoblastic new bone formation, osteoclastic erosive lesions, or a combination of the two), is critical for differential diagnosis. In their study of the Hamann-Todd collection, Hershkovitz *et al.* (2002) defined a distinct form of endocranial lesion characterized by snaking canal-like erosions of the inner table with occasional marginal pitting, which they termed *serpens endocrania symmetrica* (SES). These lesions were distinct from tuberculous granular lesions, or 'sharply demarcated erosive defects' (SDED). SES were often bilateral, multifocal and located on the frontal, parietal and occipital bones, typically in the region of the sinuses or bosses (Hershkovitz *et al.* 2002, 204–5). They were observed in 32 adults, most of whom died as a result of tuberculosis (78.1%) and often also presented HOA, although myocarditis, syphilis, pneumonia, and gastric carcinoma were also reported. Therefore, SES is primarily argued to indicate intracranial infection, but may occasionally be congenital or age-related (Hershkovitz *et al.* 2002, 210).

There are two main types of endocranial lesions described within the Circle study sample; the first type is characterized as capillary impressions extending into the inner lamina extending from or surrounding meningeal vessels (see cases described in §8.5.2.3–9); the second type is characterized as the exuberant proliferation of the diploë within the frontal fossa, identified as *hyperostosis frontalis interna* (see cases described in §8.5.2.10–13, and contextualized in §8.7.4, above). The

previously mentioned vagaries associated with attributing aetiologies of the first type of endocranial lesion are compounded in the Circle burial population because of the high levels of fragmentation and commingling – we are unable to understand these osseous responses in relation to any of the required biocultural frameworks of age, biological sex or broader health statuses of any of the affected individuals. Although the preceding text presents many differential diagnoses which have been apportioned to these types of hypervascular lesions, in the absence of further osteological evidence we are restricted to describing these observed in the Circle as non-specific infectious or inflammatory meningeal responses (Mensforth *et al.* 1978; Ortner 2003), the severity of which enabled the affected individuals to survive long enough to produce an osseous response.

Notwithstanding this wide diagnostic bracket, the parentheses tighten when we consider lesion distribution according to chronology. Five of the seven cases identified amongst the sample precipitate from Context (951), one of the earliest use phases of the burial space. The remaining two derive from contexts (518), one of the final burial deposits dating to around 2350 BC, and (838), an undated Tarxien phase deposit to the north of the site. The former case presents more as macroporosity than hypervascularity. Considering that the cases presented above in §8.5.2.3–9 feature a substantial amount of element repetition it is likely that the cranial fragments are representative of ≥5 individuals, all of whom experienced some form of meningeal illness in Neolithic Malta, which (according to Schultz 1993, 2001) they survived. At least one individual also featured porotic hyperostosis on the ectocranial surface (also reported by Henschen 1961 and Møller-Christensen 1961), indicating that they had been subject to chronic nutritional, environmental or psychological stress. For such a cluster to be identified within one context of the Circle and be relatively absent elsewhere, we must consider the possibility of some form of infectious disease being present in Neolithic Gozo, such as meningitis (Patterson 1993). Meningitis is usually a result of a bacterial or viral infection, some of which are mildly to moderately contagious, but may also derive from non-infectious comorbidities such as neoplastic disease (Roberts & Manchester 2005). There is much debate about whether meningitis would have been survivable in pre-industrial populations prior to the development of antibiotics, however, according to Roberts (2000), this would depend on the virulence of the organism, which may have been lower in past populations. If these lesions are attributed to some form of infectious disease, we may then consider broader biocultural questions such as the vector from which the infection arose in an otherwise ostensibly isolated island environment; the population density required to support and/or transmit infection; the seasonality of infection (meningitis, for example, is most commonly observed clinically in winter and spring (Patterson 1993); and the care required to nurse affected individuals through the worst of the infection back to health.

8.7.6. Nutrition

The statement 'you are what you eat' is axiomatic for the human condition. Nutrition is one of the most important factors to influence our health and well-being, applying equally to prehistoric and contemporary populations. Numerous archaeometric approaches explore this universal concept for individuals and groups from the past, including isotopic analyses (Chapter 10), zooarchaeology (Volume 2, Chapter 9), palaeobotany (Volume 1, Chapter 3; Volume 2, Chapter 9), dental calculus analyses and coprology, to name only a few. However, equally important for nutrition (albeit less frequently discussed) is that 'you are what you *don't* eat', too. This consideration is extremely important in palaeopathology, as many of the most commonly diagnosed conditions including *cribra orbitalia*, porotic hyperostosis and enamel hypoplasia all include nutritional deficiencies amongst their differential diagnoses (Aufderheide & Rodríguez-Martín 1998; Ortner 2003; Roberts & Manchester 2005). Diet has critical bearing on many other factors that influence the lived experiences of past individuals, including but not limited to stature and body composition, fertility, immunity (Roberts & Manchester 2005; Steckel 1995) and dental health (Cook 1984; Goodman *et al.* 1980, 1984a, 1984b; Hillson 2005; Larsen 1995; Ortner 2003; Sciulli 1977, 1978; Smith *et al.* 1984; cf Chapter 4). Considerations of nutritional status are particularly important for many Neolithic cultures across the world in light of the transition to agricultural subsistence strategies and increasingly sedentary lifestyles that characterize this phase. The Maltese Islands are no exception to these developments; thus, any discussions of population health, behaviour and culture should include reference to food.

As stated in §8.4.3, above, observations by both the current study and Stoddart *et al.* (2009a) indicate that the previously mentioned characteristic indicators of nutritional and environmental stress, including *cribra orbitalia*, porotic hyperostosis and enamel hypoplasia, have very low incidence and prevalence rates within the Circle burial population. Power *et al.* reported in Chapter 4 specifically on enamel hypoplasia, revealing that although enamel hypoplasia was noted at a generally low rate throughout the use-life of the Circle, it had highest population incidence in the Late use phase of interments. This observation of increasing biological

and/or nutritional stress around 2550–2500 BC aligns with a trend observed in isotopic analyses towards lower enrichment of dietary $\delta^{15}N$ in samples of human bone from the site (Chapter 10). This trend was itself caused by palaeodietary shifts or changes in the balance of the nitrogen cycle in agricultural practices across the Xagħra plateau. Apart from the indicators outlined above, we may consider how these subsistence challenges might have physically manifest in other ways within the prehistoric population.

Extending the present study's biocultural focus, our research strategy embraces the inclusion of individual case studies to illuminate the lived experiences of 'real people' amongst archaeological assemblages, above and beyond requisite population-based reporting. As such, several of the pathologies described for the individuals above are relevant to discussions of compromised nutritional status in Neolithic Gozo. We presented several cases of vertebral crush fractures (§8.5.3.2–6), a proximal humerus fracture (§8.5.3.7), and a femoral fragment (§8.6.1.3) all of which demonstrated characteristic signs of severe osteopenia indicative of osteoporosis under radiological examination, including generalized demineralization and cortical bone loss. It is noteworthy that these elements precipitate from contexts that span from Early to Late interment phases of the site. There have been several investigations of osteoporosis in archaeological populations across Europe and more broadly (for example, Agarwal 2016; Agarwal & Grynpas 1996, 2009; Agarwal & Stout 2003; Beauchesne & Agarwal 2014; Mays 1996, 1999, 2016; Mays *et al.* 2006; Sansilbano-Collilieux *et al.* 1994; Spinek *et al.* 2016; Turner-Walker & Mays 2001; cf Brickley 2002; Brickley & Ives 2008). As noted in §8.7.4, above, osteoporosis is most commonly associated with age-related changes, particularly in biological females, because of physiological stressors imposed by short birth intervals, prolonged lactation and hormonal changes following the menopause (Ortner 2003; Turner-Walker & Mays 2001, 265), but it is also experienced by some biological males (Lorkiewicz *et al.* 2019). However, nutritional factors must be considered when attributing aetiologies to these cases, especially dietary deficiency of calcium (Brickley 2000; Martin *et al.* 1985, 1987; Ortner 2003; Roberts & Manchester 2005, 242ff.; Stini 1995). As the most abundant mineral in the body, calcium is essential for the healthy formation, growth and maintenance of bones and teeth. Calcium is available in dairy foods and certain vegetables (including broccoli, cabbage, beans and leafy green vegetables), and modern studies recommend an intake of between 230–1000 mg per day (Stini 1995).

While milk-producing animals were certainly present in Neolithic Gozo, and the archaeozoological evidence is consistent with their use as such, (Volume 2, Chapter 9), we cannot be certain of the extent to which all community members were able to access their products regularly. Similarly, further research is required to determine if the vegetal matter and crops grown and consumed on the prehistoric Xagħra plateau had sufficient bioavailable calcium. Another source of calcium is fish consumed whole with bones (Stini 1995), however isotopic analyses reveal that marine protein was not a major component of the Neolithic Maltese diet (Chapter 10). Over and above dietary deprivation, other factors may compromise the body's ability to absorb calcium, including dietary deficiency of vitamin D – essential for the absorption of calcium and phosphorous – or a high-protein diet, which may increase calcium excretion (Breslau *et al.* 1988; Orwall 1991; Stini 1990; Yuen *et al.* 1984). The latter is potentially supported by the enriched Nitrogen-15 results from the site, consistent with a high-protein diet, although environmental factors could also be driving this signal (Chapter 9). Coincidentally, studies have shown that fluoride may provide some protection against osteoporosis (Boivin *et al.* 1993; Stini 1995), which would theoretically stand the prehistoric Gozitan community in good stead considering the high endemic fluoride levels, cited by Stoddart *et al.* (2009a) and Power *et al.* in Chapter 4. However, for some individuals, this geological boon did not appear to deliver such benefits.

Regardless of the aetiology, the biocultural implications of osteoporosis for individuals and communities past and present can be profound. As we have seen in the Circle population, vertebral crush and compression fractures significantly alter the architecture of individual vertebral bodies, and therefore the physiology of the spine (Foldes *et al.* 1995; Frigo & Lang 1995; Mays 1996; Roberts & Wakely 1992). Depending on the number and severity of fractures sustained, an individual may develop a pronounced kyphosis (so-called 'Dowager's hump'; Aufderheide & Rodríguez-Martín 1998). In addition to compromised mobility, kyphosis may reduce the volume and efficacy of the pulmonary and abdominal cavities and lead to serious (and even fatal) respiratory and/or digestive complications (Shane 1998; Stini 1995). Although not yet noted within the Circle assemblage, osteoporosis is a well-known cause of other fractures within the body, especially those of the femoral neck, *ossa coxae* (pelvis) and radius (Aufderheide & Rodríguez-Martín 1998; Brickley 2000; Dequeker *et al.* 1997; Ortner 2003; Roberts & Manchester 2005; Stini 1995). Considering the present study's call for greater focus on the identification and inclusion of more senior members of ancient populations, these discussions offer another opportunity to highlight their significance within bioarchaeologies

of care. After all, in both the past and the present, it is this group for whom osteoporosis poses the greatest risk (Aufderheide & Rodríguez-Martín 1998; Roberts & Manchester 2005; Stini 1995; Woolf & St John Dixon 1988). Our current under-representation of this important demographic group undermines our understanding of the incidence and prevalence of this disease and its effects on morbidity and mortality in past populations.

Our methodological case study, presented in §8.6.2, above, enables us to consider dietary deficiency at the opposite end of the life course via a rare and compelling diagnosis of scurvy on a non-adult individual of approximately 2–4 years of age. This child experienced severe and chronic vitamin C deficiency. Considering the young age of this individual, we must consider whether their condition is indicative of their own direct dietary insufficiency, perhaps associated with a lack of dietary diversity or seasonal/cyclical famine (Brickley 2000); or whether we are witnessing the complications of weaning, such as the lack of availability of appropriate foods or digestive maladaptation (Brickley & Ives 2008, 45); or if the diagnosis represents malnourishment of the mother or wet nurse if the child was still breastfeeding. In any case, our findings indicate that at least one individual suffered considerably as a result of this specific form of malnutrition. In our summary above (§8.6.2), the osteological evidence is paired with clinical accounts of the lived experience of scurvy, producing evocative imagery of how this disease might have been experienced by this individual – harrowing for anyone, but especially for such a small child. Aligning with the principles of the bioarchaeology of care, we also must consider how this illness and eventual death may have impacted the community surrounding this very sick, very young individual (Thompson *et al*. 2021).

The chronology of this case aligns with the declining phase of the 'Temple Culture' in the Maltese Islands. Considering the unique nature of these lesions within the assemblage, it would be inappropriate to extrapolate the experience of this individual to a population level. Notwithstanding this, we note the wide acknowledgement that studies of mortality and morbidity during infancy and childhood provide the most accurate barometer by which the overall health of past populations may be measured (Adler & Ostrove 1999; Hewlett 1991; Lewis 2007; Lewis & Gowland 2007; Murray & Frenk 2002; Perry 2005; Power 2007, 2012; Saunders & Barrans 1999; Schutkowski & Power 2010). By occupying the most sensitive and dependent phase of the human lifecycle (Roth 1992), children and infants readily reflect a population's ambient living conditions and local socio-ecology (Saunders *et al.* 1995; Saunders & Barrans 1999). From this perspective, this small child is a sentinel for the final years of the temple building period, offering a biological translation of the lived experience of the prevailing natural and cultural environments – at least for some members of the population. Though much remains to be understood about synchronic and diachronic nutrition and dietary diversity in prehistoric Malta, this case provides the impetus for further interdisciplinary studies to explore the corporeality of cultural change across the archipelago.

8.7.7. Interpersonal violence

Our case studies include reports of healed fractures to the head and face (nasal bone, FB0014, §8.5.1.2; mandible, FB0002, §8.5.1.1) as well as the upper limb, including two humeri (FB0007, §8.5.3.7; FB0015, §8.5.3.8), and five ulnae (FB0008-FB0012, §8.5.3.9–13). Reports of interpersonal violence (IPV), including domestic violence, frequently cite injuries to these regions of the body, although male victims may experience more upper limb trauma compared with females (Redfern 2015, 19). Differential diagnosis of the mechanisms responsible for the fractures observed on these elements (i.e. accidental or intentional) is complex even in undisturbed burials, becoming more so in a disarticulated depositional context such as the Circle. Post-cranial elements associated with the fractured cranial bone and mandible are unobservable, as are further upper limb elements. As such, patterns of trauma and injury recidivism across discrete individuals cannot be traced within this burial population. Another consequence of this mode of funerary behaviour, in the absence of further biomolecular analyses, is our inability to determine the sex of the individuals from whom these elements derived. Only the nasal bone (FB0014) displaying traumatic fractures precipitated from a cranium with extant sexually-dimorphic characteristics and was assessed as a possible male. All the cases discussed here present a minimum incidence rate of trauma to isolated elements, impeding biocultural interpretations which account for factors such as age and sex.

The head and face are easy and common targets in violent encounters, at a convenient height for a raised arm, and with the potential to harm a victim's self-esteem through disfigurement (Brink *et al.* 1998; Rangel Goulart *et al.* 2014). Nasal bones are the most frequently fractured facial element, usually followed by the mandible, and a major cause of fractures in both regions is assault (Brickley & Smith 2006; Hershkovitz *et al.* 1996; King *et al.* 2004; Ogundare *et al.* 2003; Shepherd *et al.* 1990; Yabe *et al.* 2012). As a result of right-handed dominance, fractures resulting from IPV

are expected to be found on the left side, as observed on the mandible FB0002 (§8.5.1.1; Lovell 1997, 156; Novak 2000, 96). In the case of FB0014 (§8.5.1.2), the insult is observed on the right nasal bone. This, however, does not exclude the possibility of an assault with the left hand. It must also be remembered that the nose is the most prominent facial feature, and nasal bones are particularly fragile, increasing the potential for accidental injuries to the nose. Alternative aetiologies for nasal and mandibular fractures observed in clinical studies include falls either of significant force or from a height and sporting injuries (Hwang *et al.* 2017; King *et al.* 2004). Violent combat or duelling may be sporting and recreational, but can also be symbolic, ritualized, or otherwise socially sanctioned, as noted in numerous cultures, although Hershkovitz *et al.* (1996) demonstrate that regular combat is expected to produce a suite of lesions, including robust muscular attachments, as well as numerous rib and hand fractures.

The humerus fractures presented above may have arisen from accidental falls or direct trauma; as discussed in §8.5.3.7, fractures of the surgical neck of the humerus are often seen in osteoporotic women, while mid-diaphyseal humerus fractures (such as FB0015, §8.5.3.8) may be caused by overuse and weight-bearing straining the *M. Biceps brachii* and rotator cuff muscles (Brukner 1998, 416–8). Transverse fractures to the distal third of the ulna diaphysis, without involvement of the radius, are usually diagnosed as 'parry' or 'nightstick' fractures, although this eponym dictates that the injury was sustained as a result of fending off a blow (Judd 2008; Lovell 1997, 165). Clinical assessment reveals that ulna fractures are rarely caused by alternative mechanisms, although stress fractures must be considered in the differential diagnosis (Brukner 1998, 419–21; Richards & Nicole Deal 2014). Ulnar stress fractures as a result of repetitive muscular strain and athletic activity present well-aligned segments, smooth periosteal fusiform swelling and often occur at the junction of the mid-to-distal diaphysis (Judd 2008; Morris & Blickenstaff 1967). Parry fractures, in contrast, are located more distally, displacement of ≤10° may be observed and up to 50% of the fractured segment may be horizontally apposed (Judd 2008; Richards & Corley 1996). Notwithstanding the absence of ipsilateral radii, we observed at least four possible parry fractures in the current study of the Circle burial population (FB0008-FB0011, §8.5.3.9–12). Ulnar styloid fractures (such as FB0012 and FB0013, §8.5.3.13–14) are often caused by a fall onto an outstretched hand or sudden force applied to the wrist (for example, object thrown with momentum at wrist; Jurmain 1999). While the common differential diagnosis of many arm fractures is an accidental trip or fall, routine pushing is a recognized form of domestic abuse. For this reason, falls as a result of accidental injury (for example, sustained while quarrying, erecting large limestone megaliths in the Neolithic Maltese context, or walking over slippery or uneven surfaces) or violence are difficult to distinguish in the archaeological record.

Redfern (2015, 20) provides an important cautionary note for the interpretation of violent trauma in archaeological assemblages: IPV is not always the cause of blunt force trauma or facial fractures and there is no cross-cultural pattern of injuries which signify such altercations. It is also important to remember that traumatic insults more commonly result in soft tissue as opposed to skeletal injuries (Shepherd *et al.* 1990). Nevertheless, where sufficient data are present, patterns of injury in past populations are informative of a host of social phenomena, including inter- and intra-group relations, structural inequality, scales of violence, occupational and habitual activities, gendered behaviour, and even medical knowledge and care (Judd 2002b; Knüsel & Smith 2014; Redfern 2015).

Research on European Neolithic skeletal assemblages, until more recently, has tended to focus on cranial trauma as an indicator of close-range violence. Ante- and peri-mortem cranial trauma, often depressed fractures caused by blunt force, is usually evident in <15% of the assessed skeletal sample (Lorkiewicz 2012; Papathanasiou 2012; Robb 2007, 39; Schulting & Wysocki 2005; Silva *et al.* 2012). These figures indicate minimal (cf Stoddart *et al.* 2019, 329), but regular interpersonal conflict, often seemingly without lethal intent. The apparent absence of cranial trauma in the present sample from the Circle is therefore noteworthy, prompting us to consider whether violent encounters really were infrequent during the late Neolithic in Gozo, whether injuries were more often limited to the soft tissue, or if alternative means of resolving or de-escalating conflict were commonly practised. Alternatively, individuals who transgressed may have been deposited at other burial sites or by other – less enduring – means. Importantly, however, the bioarchaeological evidence corresponds with a similar paucity of weaponry in the lithic culture of the islands. The obsidian arrowhead from Santa Verna (Volume 2, Chapter 4), for example, counts as one of a very small number of such items known.

In contrast, post-cranial trauma is generally less prevalent (Lorkiewicz 2012; Papathanasiou 2012; Silva *et al.* 2012; Smith 2014). However, peri-mortem trauma from projectile weapons - often indicated by arrowheads still embedded in bone – demonstrates that attacks were sometimes planned and carried out over a greater distance (Beyneix 2012; Lahr *et al.* 2016; Pernter *et al.* 2007; Silva & Marques 2010; Smith 2014,

115; Vegas *et al.* 2012). The picture across much of Neolithic Europe is of occasional to regular incidences of interpersonal conflict as well as collective violence, perhaps equivalent to inter-group raids and feuding, which – especially in central Europe – could result in mass graves containing entire executed families or villages (Loison 1998; Meyer *et al.* 2015, 2018; Teschler-Nicola *et al.* 1999; Wahl & Trautmann 2012). In nearby Italy, conflict was usually small-scale, but may have been greater in the more densely settled lowland villages and appears to have decreased during the Copper Age (Robb 1997, 2007, 259). There are two potential mass burial sites in Italy, at Diga di Occhito (Puglia) and Grotta Pavolella (Calabria), yet the circumstances of these individuals' deaths remain to be known (Carancini & Guerzani 1987; Tunzi Sisto 1999; cf Robb 2007, 259).

Overall, ulna fractures are relatively rare in both large archaeological and clinical studies (Judd 2008, 1665), occasionally a single example is present (Lorkiewicz 2012; Smith 2014), although five possible parry fractures to right ulnae were reported at late Neolithic San Juan ante Portam Latinam (Spain) (Vegas *et al.* 2012, 288). The presence of several distal ulna fractures within the Circle sample is significant, especially given the low overall prevalence of long bone fractures. These examples of cranial and post-cranial fractures present a picture of exceptionally low incidences of conflict and violence which resulted in skeletal trauma in late Neolithic Malta. All fractures are healed; in each case, this would have taken at least several months, during which time the individuals' capacity to participate in expected routine tasks which would have been hindered, attesting to post-traumatic treatment (Lovell 1997, 144–5). While violence may increase as a consequence of economic hardship (Papathanasiou *et al.* 2000; Torres-Rouff & Junqueira 2006), there is so far minimal evidence to indicate that this was the case in the declining environment of the Maltese archipelago in the late 3rd millennium BC. Nonetheless, it is important to acknowledge that violence was part of the lived experience of some individuals interred within the Circle – as recipients or perpetrators. These cases offer a sobering indication that for some members of Gozo's prehistoric communities, island life was far from idyllic.

8.8. Conclusion

The report by Stoddart *et al.* (2009a) offered extensive observations of pathology for the excavated portion of the Circle burial population. These observations included the frequency and severity of spinal degenerative joint disease across the cervical, thoracic and lumbar regions. Cited diagnostic criteria included joint contour change, porosity and subchondral cysts, extension of joint margins and eburnation, as well as other indicators of chronic activity-related changes such as osteophytosis and Schmorl's nodes. Similarly, observations were made regarding the presence of osteoarthritis and entheseal changes across the manual and pedal elements, also indicative of chronic activity-related change, plus an observation of temporomandibular joint disease. Notations were made regarding the presence of healed fractures on ribs, a humerus, metatarsals, manual and pedal phalanges, clavicle, an 'arm', 'leg', 'knee', 'nose' (Stoddart *et al.* 2009a, 329) and unnamed elements. Further notes pertained to observations of sinusitis, osteomyelitis, neoplasia, periostitis, myositis, cholesteatoma (chronic ear infection) and meningitis. Congenital variations were also reported, including notes on *spina bifida occulta*. As with our own findings, Stoddart *et al.* (2009a) reported that the overall presentation of skeletal pathology is very low across the Circle, including low site-wide representations of the classic indicators of nutritional, environmental or psychological stress, such as *cribra orbitalia*, porotic hyperostosis or enamel hypoplasia.

The present study has employed several analytical approaches to build upon this foundational reporting on general pathology in the Circle. Our inclusion of radiological analyses for select pathological elements significantly enhanced our capacity to develop more comprehensive differential diagnoses than that possible through macroscopic observations alone. Further to this, the extensive radiocarbon dating programme described by Parkinson *et al.* in Chapter 3 of this volume provides a sturdy chronological platform from which the experiences of health, disease and trauma may be viewed for the Neolithic people interred within this burial space. Moreover, our commitment to representing the lived experiences of these individuals and communities through the interpretative lens of the bioarchaeology of care has facilitated an opportunity to engage more deeply with individual case studies as opposed to the broader population-based reporting presented in the 2009 volume.

Our research argues that the therapeutic accomplishments of the Neolithic Circle population are amongst the most significant discoveries for the bioarchaeology of care in prehistoric Europe, and perhaps the world. The examples presented above for the stabilization, treatment, rehabilitation and recovery of life-threatening fractures (even in modern clinical contexts) testify to the efficacy of therapeutic intervention practices in prehistoric Malta. The case of therapeutic dental intervention presented by Power *et al.* in Chapter 4 extends and secures this claim.

Considerations of care must also extend to our studies of certain forms of nutritional deficiencies and potentially infectious illnesses across the Neolithic Xagħra plateau. Foremost amongst these is the case of scurvy described for a 2–4-year-old child within the Late use phase of the Circle. The case is significant for a number of reasons: i) it is the earliest attestation of scurvy for Malta and is amongst the earliest for the central Mediterranean region; ii) non-adult scurvy is extremely rare in known global archaeological assemblages; iii) the case is a sentinel for the prevailing natural and cultural environments of the final years of the temple culture; and iv) perhaps most importantly, it provides further insight into the capacity for care within these ancient communities. Considering the length of time required for osseous responses to manifest, the extensive skeletal lesions described for this case are powerful biological evidence for the substantial efforts invested to try and keep this very young child alive. Despite the ultimate failure of their efforts, care for this child persisted after their death, as evidenced by their inclusion in this communal burial space and the continued engagement with their remains for many years afterwards. Similar testimonies emerge from our descriptions of endocranial lesions for a small number of adult individuals amongst the population, indicative of non-specific infection or inflammation, possibly meningitis. Here again, any determination of aetiology is equaled in significance by Schultz's (1993) argument that these kinds of capillary and vascular impressions represent *healed* lesions in adult individuals – thus, they are echoes of survival and care.

Despite these evocative biocultural narratives of the presence of the most favourable aspects of the human condition in Neolithic Gozo, it is important to note that our research suggests that some of our species' less-favourable qualities were also present. The patterning of certain healed fractures within the burial population, particularly those of the distal ulna, urge us to consider that some individuals were subject to interpersonal violence within their lived experiences on the Xagħra plateau. Therefore, it is axiomatic that perpetrators of violence lived amongst these communities, too. While differential diagnoses for these injuries must include accidental falls or impacts, the location and transverse nature of the fracture dynamics are strongly indicative of blows to the forearm sustained during self-defence. Although there is no evidence at this stage to indicate that interpersonal violence was widespread amongst the prehistoric Maltese population, especially compared with some other prehistoric communities, these case studies provide a strong indication that it did occur, at least occasionally. Although unsettling, it is important to report these findings, as they attest to the entire spectrum of human behaviour as it was undoubtedly expressed and experienced in past populations.

Similarly, we have aligned with contemporary voices in bioarchaeology to call for greater granularity regarding the entire spectrum of demographic experience in past populations, particularly concerning indicators of advanced age. Our findings of four cases of *hyperostosis frontalis interna* within the Circle burial population greatly enhance our understanding of this rarely noted condition for archaeological assemblages of human remains, as they equal the total number of published cases for prehistoric Europe and are the first described for the Maltese Islands. In combination with our descriptions of well-preserved ossified cartilage, pubic symphyseal degeneration and potentially age- or diet-related osteoporosis among the sample, this study has made substantial contributions to clearer characterization of the latter phase of the life course for some individuals in Neolithic Malta. In so doing, we have extended the discourse surrounding demography and culture in these ancient communities, thereby inviting further considerations of social inclusion, integration and knowledge exchange through an 'archaeology of age' across the archipelago.

Within a burial population of this size and complexity, there are myriad opportunities for further study to extend on the findings tabled here. Several of the phenomena described by Stoddart *et al.* were beyond the scope of our temporal and pecuniary research parameters to address within the current project, such as further analyses of the nature and significance of mastoiditis and chronic ear infections within the population, and dedicated comprehensive studies of the spinal, manual and pedal pathology observed by both Stoddart *et al.* (2009a) and the current authors. Perhaps the greatest opportunity for better understanding of population health for Neolithic Malta lies in a comprehensive analysis of non-adult pathology, considering the innate biological imperative for children to reflect ambient living conditions and local socio-ecologies. From methodological perspectives, additional detailed studies of particular contexts associated with key chronological phases would serve to illuminate the spectrum of health, disease and trauma in prehistoric Gozo beyond the singular or 'extreme' analyses carried out thus far. Moreover, the present study attests to the profound utility of partnering radiological analyses with any macroscopic palaeopathological project. A more comprehensive micro-CT-scanning regime would enhance our insights of the incidence, prevalence and experience of those conditions which are significantly aided in differential diagnoses through radiological techniques. Similarly,

histomorphometric analyses would greatly benefit our understanding of osteoporosis amongst the burial population.

Over and above palaeopathological analyses, additional opportunities exist for osteological studies to further characterize the relationships and affinities of those interred within the Circle. Such studies might address our observations of non-metric trait representations in discrete contexts, such as the vastus notch of patella, parietal emissary foramina and mandibular tori. We also observed a significant amount of cranial and postcranial morphological variation within the population, which would benefit from multiproxy analyses including CT/surface scanning, 3D geometric morphometrics and isotopic analysis.

Our research has demonstrated the benefits of biocultural approaches to archaeological assemblages of human remains. While building on population-level observations regarding the health, disease and trauma of those interred within the Circle, our biocultural focus necessitated that we consider them as individual people, with as much intellectual energy dedicated to understanding the experience and meaning of their lives as that devoted to diagnosing their pathologies. Our analyses have stepped beyond the 'medical model' that predominates in palaeopathological analyses which risks implying that those suffering illness or disability were passive in the processes of treatment, rehabilitation and recovery. By focusing on individual case studies contextualized within their cultural framework, this research has restored agency to both those receiving and giving care. Our research has argued that human remains displaying evidence of pathology are much more than 'artefacts' – they are the agents of their own lived experiences, and further are the literal embodiment of the collective agency of all involved in care provision within their communities (Tilley 2015). The ethical and interpretative benefits of this approach are clear. We have assumed this as a particularly important objective for a mixed collective funerary ritual assemblage such as the Circle, where many might expect that the levels of fragmentation and commingling would render such individual testimonies inaccessible. Considering that the cultural impetus behind this form of funerary behaviour appears to encourage the individual to reflect the collective, and the collective to reflect the individual, our approach is more than beneficial – it is appropriate.

Note

1. These analyses were carried out in two tranches with the approval of Heritage Malta and the Superintendence of Cultural Heritage, Malta, the first in July 2015 and the second in July 2017. Transport was carried out by Bernardette Mercieca-Spiteri, Officer of the Superintendence of Cultural Heritage, Malta, with the agreement of Heritage Malta. On both occasions, radiographic analyses (micro-CT scans) were carried out by Jay Stock, Laura Buck and Jaap Saers at the Cambridge Biotomography Centre, University of Cambridge, UK, with a Nikon Metrology XT H 225 ST. Scans were created with voxel sizes ranging from 0.06 to 0.12µm3 (to two decimal places) as appropriate for the region of interest and specimen size. Further processing of individual files was carried out by Jaap Saers in the Department of Biological Anthropology, University of Cambridge, UK. Radiological examination and description of the micro-CT scans was carried out by John Magnussen, Ronika K. Power and Jess E. Thompson, using 3D Slicer (BWH, slicer.org), RaDiant DICOM Viewer (Medixant, radiantviewer.com) and AW Server (GE Medical Systems, Milwaukee, USA) software at Macquarie Medical Imaging, Macquarie University Hospital, Sydney, Australia. Radiological images were processed for publication by John Magnussen and Margery Pardey at Macquarie Medical Imaging.